Table of Contents

List of Abbreviations

Antisense-CA	an antisense probe of the progesterone aptamer, P4-CA designed by Neoventures Biotechnology Inc.
AI	artificial insemination
CL	corpus luteum
BS3	bis(sulfosuccinimidyl)suberate
BSA	bovine serum albumin
b-mAb-str-MB	conjugates of biotinylated *anti*-progesterone monoclonal antibody and streptavidin coated magnetic bead
DBS	dried blood spot
DCC	*N,N*-dicyclohexylcarbodiimide
DCU	*N,N*-dicyclohexylurea
DMF	*N,N*-dimethylformamide
DSL	Digital Sensing Limited, New Zealand
E2	estradiol
EDC	1-ethyl-3-(3-dimethylaminopropyl) carbodiimide
EIS	electrochemical impedance spectroscopy
ELISA	enzyme-linked immunosorbent assay
FSH	follicle stimulating hormone
F-sAb	fluorescent conjugates of cy3 and *anti*-mouse IgG secondary antibody
F-streptavidin	fluorescent conjugates of cy3 and streptavidin
GNP	gold nanoparticle
GnRH	gonadotropin releasing hormone
HBS-EP	10 mM HEPES, 150 mM NaCl, 3 mM EDTA with 0.005% v/v P20
HRP	horseradish peroxide
HRP-avidin	conjugates of horseradish peroxide and avidin
KD	dissociation constant
LFA	lateral flow assay
LH	luteinizing hormone

LIC	Livestock Improvement Corporation, New Zealand
LOD	limit of detection
mAb	*anti*-progesterone monoclonal antibody
mAb-sAb-MB	conjugates of *anti*-progesterone monoclonal antibody and magnetic bead linked by *anti*-mouse-IgG secondary antibody
mAb-SMCC-MB	conjugates of *anti*-progesterone monoclonal antibody and magnetic bead linked by sulfo-SMCC
MALDI-TOF	matrix-assisted laser desorption/ionization mass spectrometry with time-of-flights
MB	magnetic bead
MIP	molecular imprinting polymer
MP	magnetic nanoparticle
MST	microscale thermophoresis
MW	molecular weight
Neoventures	Neoventures Biotechnology Inc., Canada
NHS	*N*-hydroxysuccinimide
OD	optical density
OEG	oligoethylene glycol
OVA	ovalbumin
P4	progesterone
P4 3-CMO	4-pregnen-3, 20-dione 3-O-carboxymethyloxime
P4-CA	P4 aptamer developed by Neoventures Biotechnology Inc.
P4-CA-HRP	conjugates of biotinylated P4-CA and HRP-avidin
P4-CA-MB	conjugates of biotinylated P4-CA and magnetic bead coated with streptavidin
P4-NH$_2$-MB	conjugates of progesterone and magnetic bead functionalized with PEG-NH$_2$
P4-OVA	conjugates of progesterone and ovalbumin
P4-OVA-COOH-MB	conjugates of P4-OVA and magnetic bead coated with PEG 600-COOH
P4-OVA-NH2-MB	conjugates of P4-OVA and magnetic bead functionalized with PEG 600-NH$_2$
PBS	phosphate buffered saline
PBS-EDTA	phosphate buffered saline with 2mM EDTA

PBST	phosphate buffered saline with 0.005% Tween 20
PEG	poly(ethylene glycol)
PEG-COOH-MB	magnetic bead functionalized with PEG-COOH
PEG-NH$_2$-MB	magnetic bead functionalized with PEG-NH$_2$
PGF$_{2\alpha}$	prostaglandin F$_{2\alpha}$
PMT	photomultiplier tubes
RU	resonation unit
RIE	reactive ion etching
sAb	*anti*-mouse IgG secondary antibody
sAb-MB	conjugates of *anti*-mouse IgG secondary antibody and magnetic bead
SAM	self-assembled monolayer
SELEX	systematic evolution of ligands by exponential enrichment
SD	standard deviation
SMCC-MB	sulfo-SMCC activated magnetic bead
SPR	surface plasmon resonance
SPRi	surface plasmon resonance imaging
ssDNA	single strand DNA
streptavidin-MB	magnetic bead coated with streptavidin
sulfo-SMCC	succinimidyl-4-[*N*-maleimidomethyl]cyclohexane-1-carboxylate
T3	terthiophene
T3C	a carboxylated terthiophene
Tm	melting temperature
TMB	3,3',5,5'-Tetramethylbenzidine

List of Figures

XIII

List of Tables

List of Schemes

1 Chapter 1: Introduction to Progesterone (P4) Tests in the Reproductive Management of Dairy Cows and Biosensors

1.1 The Reproductive Management of Dairy Cows

1.1.1 The importance of reproductive management and estrus detection

Reproduction management is one of the keys to the sustainability and profitability of the dairy industry. The milk production of a cow increases shortly after calving and typically reaches its peak during the breeding period. However, over the postpartum periods, the production of milk decreases, so the postpartum intervals to first ovulation, cyclicity and overall fertility of cows are important for milk production and profitability of the farm [1]. A report in the US suggested that a dairy farm loses USD $1 to $3 daily on a cow that does not succeed in conceiving within 90 days of post-calving [2] and another report in the Netherlands suggested a loss of €34-231 per cow, per year, depending on the reproductive performances [3].

The modern farms often use artificial insemination (AI) for breeding and the correct detection of estrus is important for the success of AI. Estrus can be detected in several ways including monitoring activity change, observing mounting behavior, using tail paint, measuring vaginal resistance and monitoring body temperature. These methods are usually used by farm staff manually, though some automatic activity monitors and mounting behavior detectors have been developed [4-6]. Low estrus detection rates and low detection accuracy based on these methods were reported, as well as large variations in the performance of these methods among different farms. A study conducted in over 400 farms in the US found the error rates were between 5% to 60%, with nearly one third of the participating farms having error rates over 10% including missed estrus or faulty detection [2]. A survey in Northern Ireland reported the average detection rate of estrus was 71%, with a range from 53% to 92% in 19 farms [7]. A survey of 14 farms in New South Wales, Australia reported a range of estrus detection accuracy of 88.9% to 100% by farm personnel but no data on detection rate was reported [8]. Further, nowadays cows show reduced duration and less intense behavior signs of estrus [5], which may increase the difficulty in detecting estrus by farmers based on cows' behaviors. As correct detection of estrus is important for successful conception when using AI to save both labor and cost of AI, other methods to improve the detection rate and accuracy are necessary.

1.1.2   The use of P4 tests for the reproductive management

It is known that P4 levels in cow's milk are low when cows are near estrus, so P4 tests were suggested for predicting or verifying the onset of estrus from the 1970s [9]. Particularly when combining P4 tests and other methods mentioned above, the estrus and cyclicity of cows can be detected accurately and cost-effectively [8, 10, 11], although there were limitations of using P4 tests alone such as the cost of P4 tests [8], the accuracy (sensitivity and specificity) of prediction [12, 13] and the ineffectiveness in anestrous cows [8].

Besides estrus detection, P4 levels can be used to identify non-pregnant cows, monitor postpartum ovarian status, differentiate various types of ovarian cysts, and evaluate responses to various hormone treatments, all of which are related to the management of cows' fertility [2, 14]. In particular, re-insemination of pregnant cows may cause the loss of fetus, so using P4 tests to verify pregnancy is very useful. However, caution should be taken for verifying pregnancy using P4 tests which are ineffective in phantom cows that do not return to heat within 35 days post insemination but are not pregnant as well [8].

1.2   P4 in Cows

1.2.1   P4 profiles in the estrous cycle of a cow

P4 is a hormone secreted by the corpus luteum (CL) and cleared by the liver. It is one of the essential hormones for conception and pregnancy. There is a positive association between P4 levels of cows or P4 supplementation before blastocyst hatching and subsequent pregnancy success [15]. P4 also plays an important role in regulating estrous cycles together with other sexual hormones (Figure 1.1).

The estrous cycle of a cow is typically around 21 days. When the Graafian follicle forms on the ovary, it releases estradiol (E2). E2 triggers the release of the gonadotropin releasing hormone (GnRH) from the hypothalamus and GnRH signals the release of the follicle stimulating hormone (FSH) and luteinizing hormone (LH) from the pituitary gland. FSH stimulates the growth and function of the follicle while LH stimulates the rupture of it. On the day of estrus (Day 0), LH surges and the Graafian follicle ruptures and ovulates. LH also stimulates the development of CL from the luteinized follicle and CL releases P4. CL keeps growing and reaches its maximum growth and function around Day 10 when

P4 also reaches its peak. CL does not regress till Day 16, nor does the P4 level decrease. After Day 16, if a cow is not pregnant, CL gradually regresses due to prostaglandin (PGF$_{2\alpha}$) released by the uterus and thus the P4 level starts to decrease. During Days 18-20, CL is almost non-functional and the P4 level decreases rapidly to a minimum, while a new Graafian follicle develops on the ovary and releases E2 followed by the increase of GnRH and the other hormones, proceeding to the next estrous cycle. However, if a cow is pregnant, the release of PGF$_{2\alpha}$ is blocked by the fertilized embryo in the uterus and CL does not regress and keeps secreting P4, so that P4 remains at a high level, which prevents the cow from ovulating again [16, 17].

Thus, for pregnancy prediction, P4 levels of cows are tested around day 23 after breeding, a high level of P4 suggests that the cow is pregnant and a low level of P4 suggests that the cow is not pregnant and may be bred again [18]. For estrus detection, P4 testing after calving shows the cyclic P4 levels and suggests that the cow returns to estrous cycles with a low P4 level indicating that the cow is near estrus.
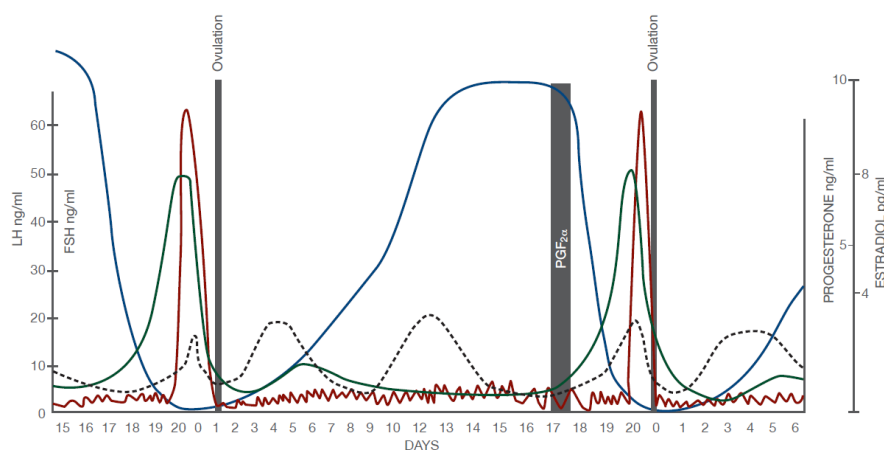
Figure 1.1 Bovine hormones during estrous cycles: the red line represents the levels of LH, the blue line represents P4, the dashed line represents FSH, and the green represents E2 [17].

Meanwhile, although there is a typical shape of P4 profiles of cows, there are some variations such as the cycle length and steepness of the slopes among individual cows, which are related to breeds, energy balance, milk yield [19] and change of seasons [20].

1.2.2 P4 in cow's blood plasma and cow's milk

P4 is present in multiple biofluids of cows such as cow's blood, milk, urine and saliva [16, 21]. Most commonly, P4 concentrations are measured in blood plasma or milk. In plasma, P4 concentrations are about 0.1-0.4 ng/ml near estrus (Day 0) at the lowest level and about 3-6 ng/ml around Day 11-13 of estrous cycles at its highest level; during early pregnancy, P4 concentrations are similar to the peak levels in estrous cycles. P4 levels are kept at high levels during pregnancy and drop before parturition. Within 20 to 60 days after parturition, P4 concentrations in blood plasma return to less than 0.5 ng/ml until estrous cycles occur again [22]. It is found that P4 levels in milk correlate to those in plasma, but they are of higher concentrations due to the presence of P4 metabolites in milk, selective uptake of P4 by the mammary gland and the fat content of milk [9, 23, 24]. In raw milk, P4 concentrations are around 1-2 ng/ml near estrus at the bottom level and more than 20 ng/ml in the middle of an estrous cycle at the peak level; around Day 20-24, milk P4 concentrations are less than 5 ng/ml in non-pregnant cows and around 15-20 ng/ml in pregnant cows [14, 19, 25-29].

Since P4 concentrations in milk are higher than those in plasma, and milk samples are more accessible than blood plasma, it is ideal to measure P4 in cow's milk for a dairy farm's reproductive management. Meanwhile, as the fat content in milk samples affects P4 concentrations in milk due to the higher solubility of P4 in fat than in aqueous solutions, care should be taken on the types of milk samples such as foremilk, milk fat, skimmed milk and the thresholds of P4 levels for the detection of estrus or pregnancy which differ among different milk samples [13].

Except for the purpose of reproductive management, monitoring P4 levels in milk and dairy products may also be interesting by health-related research. It was estimated that the ingestion of P4 from dairy products is around 3-7 μg/day by young children in western counties, which exceeds 1% of the production rate of P4 of pre-pubertal boys and girls, over the limit of the accepted daily intake defined by the U.S. Food and Drug Administration's guidelines. Also, there are studies suggesting a correlation between milk consumption and poor sperm quality, and an increased risk of prostate and testicular cancers. Therefore, monitoring P4 levels in commercial milk may help in understanding more about such issues [30].

1.2.3   The effects of milk matrix on P4 tests and the methods of reducing matrix effects

While using milk samples for P4 tests is ideal for dairy farms, the complex composition of milk makes testing problematic. Milk is composed of at least three physical states including: a solution of whey protein, a colloidal suspension of an emulsion of fat (Figure1.2), and casein micelles (Figure 1.3) [31, 32]. These proteins and fat contents together with lactose, minerals, hormones and other metabolic contents interfere in the measurement of target molecules in milk. Several studies showed a decrease in sensitivities or even failure in measurement when converting P4 tests developed in the buffer to milk sample [33-35]. Therefore, it is critical to reduce the milk matrix effect.
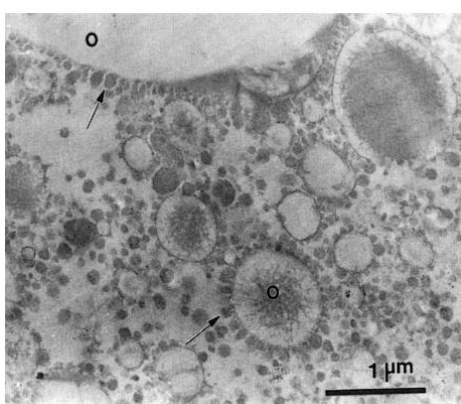
Figure 1.2 Milk fat droplets in casein micelles of homogenized milk, observed by thin-sectioning electron microscope [32].
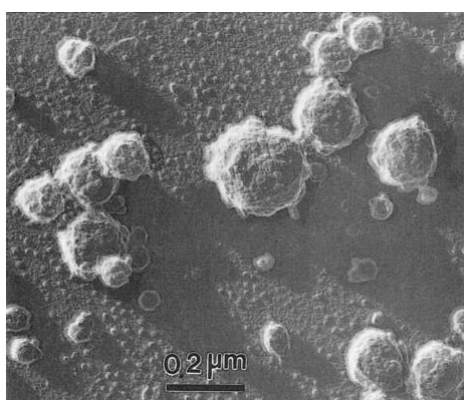
Figure 1.3 Casein micelles in raw milk present in the form of colloidal particles (diameter= ~ 0.1 um), observed by thin-sectioning transmission electron microscope [32].

As early as the 1970s, efforts were made to develop reagents to clarify milk and dairy products for chemical or enzymatic analysis. These reagents are mostly organic solvents, detergents and pH

reagents or their combination, which remove proteins or fat contents of milk by disrupting disulphide bonds and hydrogen bonds, hydrolyzing polypeptide chains, or solvating hydrophobic and lipophilic components [31]. These reagents are typically used at the end of analysis to clarify milk before photometric detection rather than before analysis, as such reagents disrupt analysis reactions. Thus, they are limited when used for reducing milk matrix effects.

Meanwhile, methods were developed to extract target analytes out of milk before analysis based on chromatography such as high performance liquid chromatography, and mass spectrum and gas chromatography. Such extraction methods includes liquid-liquid extraction [36], solid-phase extraction or solid-phase microextraction [37], matrix solid-phase dispersion [38, 39], and molecularly imprinted polymers [40] and their combination [41]. However, they are often time-consuming, inefficient at low analyte concentrations, and non-specific and expensive; and some of them use a large amount of organic solvents which are not environmentally-friendly. Although some of these methods could be implemented into on-line or automated forms [42, 43], they may not be suitable for the tests on dairy farms in terms of turnaround times and cost.

Magnetic particles (MPs) have been used to separate and concentrate target analytes from milk samples prior to analysis. With certain modifications, MPs can specifically bind to target analytes in milk and then separate together with the bound target analytes from milk by the application of magnetic fields. Superparamagnetic particles are widely used, because: (1) they have versatile surface modification chemistry that allows conjugation of capture agents; (2) they have good suspension in aqueous solutions suitable for analysis reactions such as biological interaction; (3) they present large mobile contact surfaces for sufficient interaction with target analytes; (4) a small amount of magnetic particles may be used in relatively large sample volumes to concentrate target analytes; (5) the separation of these particles is easy with magnets, which is possible to be applied in automatic systems or unattended on-line systems; and (6) they may be reused once the captured targets are properly eluted. Magnetic beads (MBs) have been used to isolate nutrients [44], trace chemicals residue, antibiotics, toxin M1, and estrogen [48] and bacteria [49-51] in milk and milk products. An ELISA assay using MP-antibody conjugates was reported with a detection limit of 0.09 ng/ml of milk P4 [52]. In this thesis, MB-antibody conjugates were used to separate P4 from milk before P4 detection on a surface

plasmon resonance (SPR) instrument to reduce the milk matrix effect. This was the first SPR P4 test using MB-antibody conjugates to our knowledge.

1.3   The Methods of Measuring P4

1.3.1   Physical-chemical methods

P4 measurement was first demonstrated on analytical instruments based on physical-chemical methods such as thin layer chromatography [53], gas chromatography [54], mass spectrometry [55] and high-performance liquid chromatography [56]. Sensitive detection can be achieved at a limit of detection (LOD) of 0.4 ng/ml of P4 [57]. However, these methods usually require expensive and delicate instruments and highly trained technicians; and as such detection of P4 is not specific, the sample preparation is often complicated, time consuming and expensive, as discussed in *Section 1.2.3*. Thus, they are not suitable for routine P4 tests on dairy farms.

1.3.2   Biological methods

Compared to the physical-chemical methods, biological methods detect P4 using biological reactions. Such biological reactions as the binding between P4 and *anti*-P4 antibodies are specific, so they can tolerate relatively more 'impurity' in samples. In other words, increasing the specificity of analysis reduces the interference by non-target substances during analysis, and thus sample preparation and P4 detection using biological methods are relatively easy and cheap compared to those physical-chemical methods. Therefore, biological methods are preferred for milk P4 tests on dairy farms. Detection using biological methods are called biosensing, and a biosensor refers to an ensemble or a device that realizes biosensing by using biologically-derived components and physicochemical transduction.

The first biosensor for milk P4 was a radioimmunoassay developed in 1973 [29]. The radioimmunoassays make use of radioactive compounds labeled *anti*-P4 antibodies to detect P4. They are relatively fast and easy to perform compared to the physical-chemical methods, but they can only be performed in special laboratories due to the use of radioactive compounds.

The first enzyme-linked immunoassays for P4 detection were developed in a laboratory in 1984 [58] and later some commercial enzyme-linked immunosorbent assays (ELISAs) became available [59].

The ELISAs use enzymes to label antibodies instead of radioactive compounds, so that they can be performed outside laboratories, possibly on dairy farms, and thus they are regarded as 'cow-side' tests. Until today, most commercial milk P4 tests are ELISAs, *e.g.* the milk P4 tests from Ridgeway Science (Gloucestershire, UK), EuroProxima (Arnhem, The Netherlands), Biovet (Saint-Hyacinthe, Canada), Biometallics (New Jersey, USA) and Abraxis (Pennsylvania, USA). However, these commercial ELISA kits are often available in the format of the 96-well plates and involve several experimental steps, so that they are commonly performed in laboratories by technicians rather than on farms. This raises the issue of milk sample transfer and storage and the cost related to it. Commonly, fresh milk samples collected on the farm are transferred chilled for immediate testing, or frozen for delayed testing, which requires special devices or facilities to transfer and store milk samples. Interestingly, inspired by the dried blood spot (DBS) technology, a study compared the ELISAs using dried milk samples on DBS cards and frozen samples, and found good correlation between the two types of samples [60]. Portable devices have been developed for measuring ELISA results to replace laboratory instruments, but ELISA procedures are complicated and difficult to be fully automated.

In 1996 the first lab-based lateral flow assay (LFA) for milk P4 was developed [61]. LFAs are similar to ELISAs, but are performed by simply dropping samples onto test strips or dipping test strips into samples. They are easy for farm staff to use on farms. However, the results of LFAs are most commonly based on color changes estimated visually by farm staff and they are at best semi-quantitative [62] with the aid of some devices, so such tests can be ambiguous and may lead to mis-interpretation. There are commercial LFAs available such as the P4 Rapid Test from Ridgway Science (Gloucestershire, UK). Also, there is a fully automated LFA integrated into an on-line herd management system, as in the Herd Navigator from DeLaval (Denmark) to detect milk P4 for verifying estrus. This on-line P4 test improved estrus detection but it is not cost-effective for routine use [63-65].

Fluorescent dye labeled antibodies have also been used to replace radioactive labeled antibodies in immunoassays. A direct time-resolved fluoroimmunoassay was developed to measure milk P4 [11]. At the same time, attempts have been made to perform label free immunoassays.

Label free immunoassays for P4 in milk have been developed on quartz crystal oscillators [66] and SPR platforms. Gillis *et al.* developed an SPR immunoassay for detecting P4 with LODs of 60 pg/ml of P4 in

a buffer and 0.6 ng/ml in bovine milk respectively [33, 67]. Utilizing secondary antibody and gold nanoparticles (GNPs) conjugates to enhance SPR signals – Mitchell and Wu improved the sensitivity of SPR immunoassays to an LOD of 8.6 pg/ml of P4 in a buffer [68]. Later, Yuan and Oliver improved SPR signals by using a mixed self-assembled monolayer (SAM) surface and attained an LOD of 4.9 pg/ml P4 in buffer solutions [69]. In addition, some portable SPR instruments were developed for P4 tests. A miniaturized SPR sensor was demonstrated but the detection was based on integrated molecular imprinting polymer (MIP) films rather an immunoassay [70]. A fiber optic SPR biosensor was developed to measure milk P4 and showed an LOD of 0.6 ng/ml with a detection range of 1-10 ng/ml and good correlation to the results from a commercial ELISA kit [71].

Other groups have developed electrochemical immunoassays for P4 tests [35, 72-76]. The devices of electrochemical detection are easier to be miniaturized and the disposable electrodes can be made cheaply, so they are more suitable for developing portable devices at low costs. A miniaturized biosensor using glassy carbon electrodes was developed to detect P4 in bovine serum [77].

1.3.3 Indirect measurement

P4 is released by CL. The ultrasonography of CL areas was used to estimate cow P4 levels. However, this method is not as accurate as physical-chemical methods and biological methods. Advances in the knowledge and technique on the ultrasonography of CL are required to improve the prediction of cow's P4 concentrations based on the size of the CL area [78].

1.3.4 Limitations of current methods and perspectives of new P4 tests

As discussed above, neither physical-chemical methods using chromatography nor indirect measurements using ultrasonography are practical for cow's P4 measurements for dairy farms. Biological methods appear more suitable, as they are relatively easy to perform and cheap in instrument costs, with enough sensitivity and accuracy remaining in P4 measurements.

Currently, the gold standard for milk P4 measurement is ELISAs. ELISA procedures include two main parts: P4 detection using antibodies, and signal transduction using enzymatic reactions. Using antibodies to detect P4 provides specificity in detection, but the cost, stability and batch variance of antibodies are of concern if ELISAs are adopted as routine tests. Using enzymatic reactions to

transduce signals for detection amplifies signals to achieve sensitive detection, but it also increases the assay time and reagent cost, while the instability of enzymes limits the shelf-life of kits and the variation of enzymatic reaction affects the repeatability of results. To achieve the cost-effectiveness of ELISAs, milk samples are often processed in batches using 96 well plates by lab technicians in testing laboratories rather than on farms. This requires the transfer of milk samples to laboratories, which increases tests' lead time and cost due to sample transportation and storage. Till now, they are not yet cost-effective enough for routine use. Therefore, interest remains in developing new biosensors to replace ELISAs.

Ideally, milk P4 is measured immediately after milking on farms. Fully automated P4 tests performed by farmers using handheld devices or integrated into robotic milking systems are ideal. Labor and transportation costs as well as tests' lead times will be reduced, compared to ELISAs performed in laboratories. Miniaturizing devices and lab-on-chip microfluidic systems will reduce instrument costs as well as reaction volumes that will further reduce the amounts of reagents required and lower reagent costs, compared to tests performed in 96 well plates. Using signal transduction methods other than enzymatic reactions (e.g. SPR and electrochemical impedance spectroscopy) may reduce reagent costs and assay times as well as improve repeatability of results. Substituting antibodies with other bio-recognition molecules (e.g. aptamers) may lower reagent costs, extend reagent shelf-life and reduce batch variance. With a lower cost of tests and devices, and a simpler operation and shorter lead time, milk P4 tests may become routine tests to provide more accurate estrus detection and prediction, as well as insights into luteal cycles and postpartum ovarian status of individual cows for improved breeding outcome and fertility management. However, all these modifications from ELISAs should not sacrifice accuracy and sensitivity of P4 tests.

1.4   Biosensors and Development of a P4 Biosensor

1.4.1   Definition and key components of biosensors

As discussed above, it is preferable to detect milk P4 by using biological methods or biosensing. Biosensing is a process that recognizes target analytes such as chemical compounds, DNAs, proteins, microorganisms *via* biological reactions, which then transduces a signal that can be detected. A biosensor is a device or ensemble that realizes and integrates each step of biosensing for the detection

and measurement of target analytes [79]. More than fifty years have passed since the definition of biosensor was first described by Clark and Lyons in 1962, who invented an electrochemical biosensor to measure oxygen and carbon dioxide *via* an enzymatic reaction [80].

The key components of a biosensor (Figure 1.4) include:

- Sensor surfaces
- Immobilization of bioreceptors
- Biosensing assays to detect target analytes
- Transduction and detection of signals

Bioreceptors are immobilized onto biosensor surfaces to recognize target analytes *via* biological interactions. Upon recognition, optical, electrical or thermal signals are transduced. The detection or measurement of these signals indicates the presence or concentrations of target analytes. Biosensing assays define the processes on how bioreceptors interact with target analytes, and how signals are transduced to detect or measure target analytes. The development of a biosensor involves developing and optimizing each component.
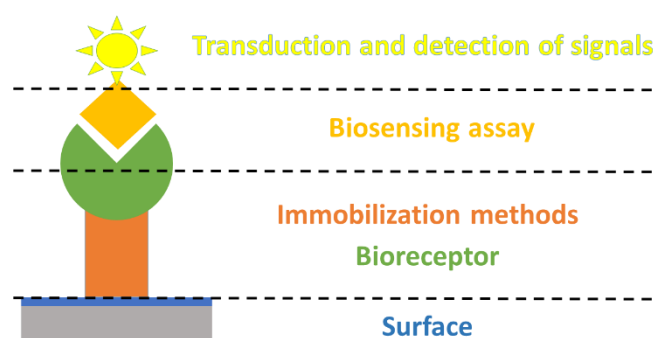
Figure 1.4 The key components of a biosensor.

1.4.2   Biosensing assays

1.4.2.1   Assay format

The biosensing assay is the most important component of a biosensor, as it describes how the target analyte interacts with the bioreceptor, and how a detectable signal is transduced and related to the

target analyte. The biosensing assays are generally classified as direct or indirect assays, as shown in Figure 1.5.

In a direct assay, the bioreceptor immobilized on the sensor surface is usually a ligand of the target analyte and it binds the target analyte specifically based on its biological function. The binding of the bioreceptor and the target analyte transduces physicochemical signals, or a signal is transduced by a second ligand of the target analyte that binds to the target analyte bounded to the bioreceptor on the sensor surface, which is referred to as a sandwich assay. In both cases, the strength of the signal has a positive correlation with the amount of the bounded target analyte.

In an indirect assay, the transduced signal does not result from the binding of the target analyte and the bioreceptor, and the signal strength is inversely proportional to the amount of the target analyte. There are two forms of indirect assays, namely inhibition assays and competition assays. In a competition assay, a ligand of the target analyte is immobilized as the bioreceptor on the sensor surface. When the sample containing the target analyte is mixed with an analog or derivative of the target analyte and added to the sensor surface, the target analyte in the sample competes with its analog or derivative in binding the bioreceptor on the sensor surface. A signal is transduced by the binding of the analog or derivative of the target analyte and the bioreceptor, rather than the binding of the target analyte and the bioreceptor. In an inhibition assay, the analog or derivative to the target analyte is used as the bioreceptor on the sensor surface. The sample containing the target analyte is first mixed with its ligand to allow the binding, then the mixture is added to the sensor surface. The binding of the ligand to the bioreceptor (the analog or derivative to the target analyte) is inhibited by the target analyte. The binding of the ligand to the bioreceptor transduces a signal. Thus, in both indirect assay formats, the signal is not transduced due to the binding of the target analyte itself and the strength of the signals has a negative correlation to the amount of the target analyte.

The choice of assay types and formats depends on the characteristics of target analytes and the required sensitivity of detection. P4 is a small molecule which makes its direct detection difficult, so P4 detection is often carried out *via* an indirect assay, which is common for small molecules detection and also achieves higher sensitivity than a direct assay [81].

In this thesis, P4 were detected using inhibition assays, where P4 derivatives were immobilized on the sensor surfaces as the bioreceptors. When the mixtures of the samples containing P4 and P4 ligands (antibody or aptamer) were applied to the sensor surfaces, the bindings of the ligands with the bioreceptors (P4 derivatives) on the sensor surfaces were inhibited by P4 in the samples. The signals triggered by the bindings of the ligands to the bioreceptors are reversely proportional to the amount of P4 in the samples. The development of inhibition assays involves the choice of P4 ligands and P4 derivatives, and the optimization of assay procedures and conditions.
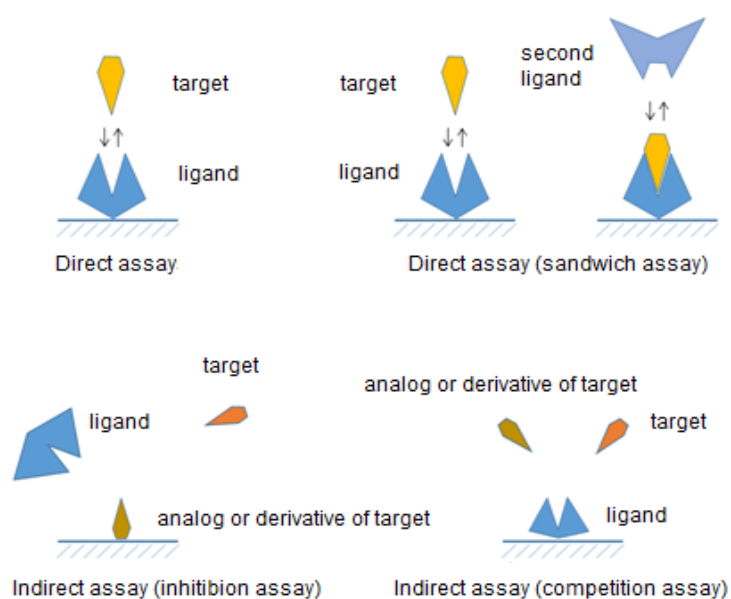
Figure 1.5 Different assay formats adopted from [82].

1.4.2.2 Ligands of P4

In biosensing assays, a ligand refers to a biomolecule that binds the target analyte specifically *via* biological interactions. Ligands can be enzymes, antibodies, antigens, aptamers, DNAs, organelles, tissues or even whole cells and microorganisms. The specificity, affinity and kinetics of the binding between target analytes and the ligands used in the assays affect the specificity and sensitivity of the assays.

1.4.2.2.1   Antibody

Antibodies are often used in biosensing, as they bind target analytes *via* highly specific antibody-antigen interaction. Biosensing assays using antibodies to recognize target analytes are called immunoassays, which were first demonstrated for measuring human plasma insulin [83]. Most biosensing assays for P4 tests are indirect immunoassays.

During the development of an immunoassay, it is necessary to consider the binding affinity and specificity of the antibody to the target analyte, the concentration of the antibody to be used in the assay, and the steric hindrance due to attaching the antibody to some particles, molecules or surfaces etc. Both reducing the amount of antibody and improving the antibody orientation were shown to increase the sensitivity of the assays [68, 84, 85].

1.4.2.2.2   Aptamer

Aptamers are short single-stranded DNA or RNAs which were selected from a pool of random nucleic acid sequences to specifically bind target analytes, including proteins, small organic molecules, viruses, tissues or even whole cells or microorganisms [86, 87]. The smallest target of aptamers is ethanolamine [88], while large targets such as tumor cells [89] or even tissues [90] have been used to select aptamers. The aptamers form 3D structures to interact with target analytes. Some of them can bind to their targets with high affinities and specificities, comparable to the binding between antibodies and their antigens [91, 92]. Some targets preferentially bind to DNA aptamers than RNA aptamers and vice versa, and the sequence motif of DNA and RNA aptamers to the same target analytes can be completely different [87].

There are several advantages in using aptamers as ligands when comparing antibodies, including: (1) oligo-nucleotides are less susceptible to biodegradation and cheaper and easier for mass production than antibodies; (2) aptamers can be easily labeled with enzymes, nanoparticles, quantum dots or redox molecules, as standard methods have been developed to synthesis nucleic acid with functional groups to covalently bind report molecules or particles; (3) the folding of aptamers and the binding of aptamers to target analytes are both reversible, which make the regeneration of biosensor surfaces relatively easy, hence the surfaces can be reused to lower the cost of tests; and (4) aptamers are much smaller than antibodies so they are more penetrable to be delivered *in vivo* and have low immunogenicity, which

is beneficial for *in vivo* applications. Therefore, aptamers have potential in pharmaceutical, diagnostic, biotechnology, biosensor applications and biological research [92]. Yet, the research and application of aptamers are still relatively new compared to antibodies. For example, so far there is only one approved therapeutical aptamer drug available, Macugen® for the treatment of neovascular age-related macular degeneration [93].

Conventionally the aptamers are selected from a library of oligonucleotides using a Systematic Evolution of Ligands by Exponential Enrichment (SELEX) protocol [92], and recently several modified SELEX approaches have been reported with improved efficiency in aptamer selections [94, 95]. The *in vitro* selection procedures can be carried out under the same conditions as how the aptamers are to be used in the assays. This enables the identification of aptamers with specific features, which is not possible in the development of antibodies. Thus, the selection process of aptamers provides an additional advantage over antibodies [92]. Chemical modification of aptamers before or after selection is used to add new structural features for interaction with targets, to stabilize aptamers in a biological environment, to improve the affinity of aptamers to anionic target molecules and prepare for downstream applications [92, 96].

Aptasensors are the biosensors utilizing aptamers in the recognition of target analytes, and the signals transduced by aptasensors are similar to immunosensors including electrochemical [97], fluorescent [98, 99], colorimetric [100, 101], SPR [102] and microchannel cantilever signals [95, 103].

With regards to P4 aptamers, only a limited number of papers have been published and P4 aptasensors were developed using electrochemical impedance spectroscopy (EIS) [97], GNPs [100, 101], fluorescent probes , surface plasmon resonance imaging (SPRi) [102] and luminescent nanoparticles [105] . More details on these aptamers and aptasensors are available in Section 5.1 of Chapter 5.

1.4.2.3 Derivatives of P4

In the inhibition assays for P4 detection, P4 and protein conjugates are commonly used as the bioreceptors on the surfaces. Direct immobilization of P4 on sensor surfaces leads to a low binding affinity between P4 and its ligands due to steric hindrance. Protein conjugates of P4 extend P4 away

from the surfaces, reduce steric hindrance and improve the binding between P4 and its ligands. Yet, the choice of protein conjugates affects the assay sensitivity and specificity.

The characteristics of the linkers between P4 moieties and proteins in the conjugates affect the binding of P4 with its ligands. The length, hydrophilicity and flexibility of the linker as well as the attaching position on the P4 molecule all have some effect on the binding [81, 106, 107]. Also, the conjugation degree, the number of P4 molecules per protein conjugate, affects the assay performance. In general, P4-protein conjugates with long flexible hydrophilic linkers (e.g. long linkers made of poly(ethylene glycol)) and high conjugation degrees are preferred, as: (1) long lengths and flexibility of linkers reduce the steric hindrance of binding between P4 moiety in the conjugates and P4 ligands; (2) hydrophilic linkers help P4 moiety to penetrate aqueous media to reach P4 ligands in aqueous buffer and reduce the non-specific binding of sensor surface due to hydrophobic interactions; and (3) high conjugation degrees increase the surface density of P4 to increase antibody binding. However, the synthesis and the immobilization of such P4 protein conjugates with long flexible hydrophilic linkers can be complicated and problematic, which is discussed in *Section 1.4.4*.

1.4.3   Sensor surfaces

Various materials are used for making sensor surfaces such as glass, silicon, polymer and metal. The gold surfaces are widely used, as they are relatively easy to functionalize and are inert in most physiological buffer conditions during biosensing [108]. In this thesis, mainly gold surfaces for SPR detection were investigated with a focus on the materials and methods used to coat gold surfaces and further functionalize them with P4-protein conjugates as the bioreceptors.

The simplest way to functionalize a surface with bioreceptors is *via* physical adsorption. However, there are limitations of direct adsorption on the metal surfaces [109]: (1) some proteins denature and lose their function in contact with metal surfaces; (2) some molecules, especially small molecules, are difficult to bind to metal directly; (3) undesired or non-specific interaction of bare gold surfaces can affect the accuracy of detection; (4) the binding of biomolecules can be loose; and (5) the orientation of molecules is uncontrolled. Therefore, often a gold surface is functionalized with a monolayer of synthetic molecules to reduce the non-specific binding of bare gold, and to provide chemical groups such as amine and carboxyl groups for covalent binding of bioreceptors.

There are two methods to deposit molecular layers on gold surfaces: Langmuir-Blodgett transfer and self-assembly. Langmuir-Blodgett deposition is generally more arduous and restricts the types of bifunctional molecules to those containing only one polar group [111]. Self-assembly based on the strong adsorption of disulfides, sulfides and thiols on metal surfaces are more widely used. These sulfur-containing species are well known to coordinate strongly onto metal surfaces due to sulfur donor atoms and Van der Waals forces, which can result in oriented and stable monolayers. Thiols form the highest ordered and oriented monolayers among sulfur-containing species. Uncontaminated gold surfaces are important, but not essential, for thiols monolayer formation as they display high affinity for gold even with contaminants [112]. The formation of a densely packed alkanethiol monolayer is observed in a few hours, but well-ordered monolayers take days to form. Alkanethiols usually stop at the monolayer level, but a multilayer of alkanethiols can be formed after immersion for longer periods.

Alternatively, a hydrogel matrix was proposed for gold surfaces used in SPR sensors [109]. The matrix is composed of a self-assembled alkanethiol monolayer for coating and protecting metal, and a carboxymethylated dextran hydrogel for covalent binding of ligands. This matrix provides [108]: (1) a hydrophilic environment favoured by biomolecular interaction; (2) a chemical basis for covalent binding of ligands; (3) a negative charged surface for electrostatic concentration of positive-charged molecules from the solution; (4) higher surface capacity for ligand immobilization; (5) an extension of interaction spaces and flexibility of surface-attached biomolecules; and (6) an inert surface in most contexts of biomolecular interaction. Also, the hydrogel surface is highly stable, allows reuse of the surface, and has a higher capacity of ligand immobilization compared to the SAM. However, regarding SPR detection, the hydrogel matrix is relatively thick compared to SAMs, which decrease the effectiveness of SPR signal stimulation and sensitivity of SPR detection, as the evanescent wave of SPR decreases with the distance from gold surface. SPR detection of P4 using SAM surfaces achieved higher sensitivity than the hydrogel surface [69]. Also, SAMs are relatively cheap in fabrication and therefore cost-effective. In this thesis, a new SAM gold surface is to be compared with a well-established commercial hydrogel matrix on the sensitivity of P4 SPR detection.

Gold surfaces can also be functionalized by MIP films. MIP films are made by first forming polymer films containing the templates of target analytes and then extracting the templates out of the films. MIP films are specific in trapping targets are robust, low cost, stable and have a long-shelf life [70]. However, the

specificity of detection is based more on the structure similarity other than the inter-molecule interaction; and its use in detecting small molecules is also limited due to the lack of sensitivity.

1.4.4 Immobilization methods

As discussed in *Section 1.4.2.3*, in the inhibition assays for P4 detection, typically protein conjugates of P4 are immobilized on the sensor surface as bioreceptors.

The small molecule and protein conjugates are usually synthesized in solution and then immobilized onto the biosensor surface. Most commonly, small molecules are covalently bounded to the lysine residues of proteins *via* amide bonds, as the lysines are of high prevalence on the surfaces of most proteins [113]. During synthesis processes, excess reagents are used to increase reaction conversion rates, but need to be removed together with the by-products afterwards from the reactions by gel filtration or dialysis. Such purification methods are time-consuming and may cause loss of products [114]. Limited by the purification techniques available, the final products from synthesis processes are often a mixture of conjugation products [113]. Further, some small molecules such as P4 have limited solubility in aqueous buffers, which affects the efficiency of conjugation reaction performed in aqueous protein solutions [115]. In contrast to conjugation in solution, solid-phase conjugation first immobilizes carrier proteins on solid supports before small molecules are conjugated to immobilized proteins; and in the end the synthesized conjugates are cleaved and eluted from solid supports for further application [116]. Solid-phase conjugation allows fast reactions and efficient washing, avoids product loss during intermediate steps and the problems of solvation of intermediate products and improves synthesis efficiency [117], but the final yield is dependent on elution efficiency.

In this thesis, a new approach of synthesizing and immobilizing P4 and protein conjugates on the sensor surfaces was used. The new approach applied solid-phase conjugation directly on the sensor surfaces; and the sensor surface where the conjugates are *in situ* synthesized can be used for biosensing directly. Thus, the elution of synthesized conjugates in solid-phase conjugation is omitted as well as the immobilization experiments after synthesis.

1.4.5 Transduction and detection methods

Optical or electrical signals are most often used in biosensors. This thesis focuses on developing optical biosensors, more specifically, sensors based on SPR and fluorescent signals.

1.4.5.1 SPR

SPR utilizes resonant oscillation of plasmons and photons which occurs at the interface between two media of different dielectric constants (e.g. metal and dielectrics). Kretschmann geometry (Figure 1.6) is the most common configuration to excite SPR for biosensing. In this setup, a thin layer of metal such as gold is coated on a glass slide which is coupled to a prism. The incident light is set up under the condition of total internal reflection. On the metal surface, free conduction electrons form periodic oscillation – a plasma wave. The amplitude of this wave decreases exponentially with the distance from the interface and thus it is an evanescent wave field. At a certain incident angle, the photons of incident light of a certain wavelength have the same momentum as the plasmons of the plasma wave. Thus, the surface plasmon can absorb the energy of photons and be excited. This results in a drop in the intensity of reflected light. Experimentally, a very sharp minimum of light reflectance is observed at a certain angle which is referred to the SPR angle [108, 118].

The SPR angle is affected by the refractive index of the medium outside the metal film and within the range where the evanescent wave field penetrates. The evanescent wave only penetrates a few thousands of Ångstroms. Thus, the SPR angle is sensitive to the change of refractive index close to the thin film surface, which is caused by solute concentration changes at the surface, regardless of the type of molecules. Therefore, the total concentration changes of different solutes or sequential events can be measured together by the changes of SPR angle, as resonation unit (RU) on an SPR instrument.

The labeling of reagents with detection tags is omitted in SPR analysis as the changes of reagent concentrations on the metal surface (due to the binding to immobilized bioreceptors in the case of biosensing) result in the changes of SPR angles in real time. The concentration analysis can be completed in a few minutes. Recently, SPR imaging (SPRi) has been developed allowing real-time visualization of binding events on SPR surfaces in two dimensions.
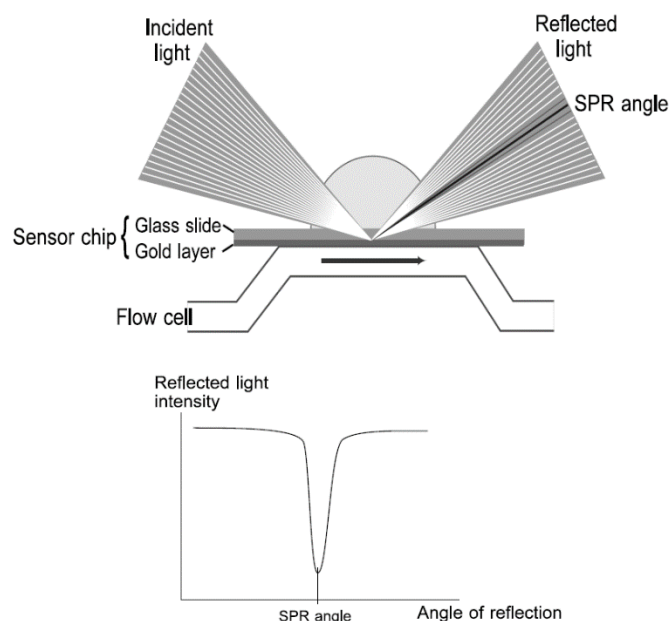
Figure 1.6 Kretschmann geometry configuration to excite an SPR and principle of SPR detection [108].

1.4.5.2 Fluorescence

Fluorescence is a phenomenon in which a substrate emits light as the result of photon absorption. Fluorescent substrates are excited from ground states to excited states due to photon absorption, and then light is emitted when the substrates return to their ground states.

Fluorescent signals are widely used in biosensing. Fluorescent substrates include small organic fluorescent molecules such as fluorophores [119], naturally fluorescent proteins like green fluorescent proteins [120] and large fluorescent particles like quantum dots [121]. These three different types of fluorescence species have different characteristics and advantages. Fluorophores are of 20-100 atoms, the smallest in size. They are less likely to cause steric hindrance in molecular interactions. Fluorescent proteins are of 26-240 kDa and can be co-expressed with the proteins of interest by genetic engineering as a way to label the proteins of interest. Quantum dots are fluorescent particles of 2-10 nm in diameter and contain 100-100,000 atoms. Their excitation bands are broad, but their emission wavelengths are narrow and tunable based on the sizes of particles, which makes them suitable for multi-color imaging and barcoding. Also, they are resistant to degradation and photo bleaching, which enables continuous illumination.

In biosensors, these fluorescent substrates are introduced as tags attached to biomolecules so that those biomolecules can be detected. The devices to detect fluorescence mainly composed of a light source such as mercury lamps, LEDs and lasers to excite fluorescent substrates and a photon detector such as CCD cameras, photometers with photomultiplier tubes (PMT) and photodiodes. In laboratories, fluorescence is detected by fluorescent microscopes, fluorescent plate readers, DNA microarray scanners and flow cytometry.

Fluorescent detection is sometimes problematic due to background noises including autofluorescence of non-target substance in the detection system. Biomolecules such as flavin, polyphenol, NADPH, amino acids and collagen, and non-biological material like some polymers, exhibit autofluorescence. The autofluorescence from non-target substances increases background noises and affects the detection sensitivity and specificity [122].

1.5   Research Aims and Thesis Outlines

As discussed in Section 1.3.4, ELISAs as the current gold standard for milk P4 tests are not adapted as routine tests on dairy farms due to their cost and operation. Therefore, there remains interest in developing new biosensors to detect milk P4. The aim of this thesis was to develop a new biosensor to detect/measure P4 in milk samples, which has the potential use in cow's estrus detection. In the future, the developed biosensors will ultimately be transferred to a low cost sensor platform to realize cost-effective milk P4 tests, so that milk P4 tests can be used as routine tests on dairy farms. As discussed above, milk P4 tests are informative in the reproductive management of dairy cows; especially as using them as routine tests will provide more accurate prediction of estrus and identification of pregnancy, and insight into postpartum cyclicity and ovarian conditions etc.

To develop a new biosensor, each component of the biosensor was optimized to achieve a high-sensitive and easy-to-use milk P4 test. Chapters 2-4 were dedicated to optimizing SPR biosensor components for milk P4 detection, *i.e.* the sensor surface, the bioreceptor and the biosensing assay. Chapter 5 focused on exploring the potential of a newly selected P4 aptamer in replacing *anti*-P4 antibodies for P4 detection.

Chapter 2 investigated the use of a new carboxylated terthiophene (T3C) molecule in functionalizing gold SPR surfaces to immobilize P4 and ovalbumin conjugates (P4-OVAs). Compared with a standard commercial hydro-gel gold surface, a T3C SAM gold surface showed advantages in the fabrication process, cost, SPR signal stimulation and assay sensitives.

Chapter 3 demonstrated a new method of immobilizing P4-OVAs on SPR surfaces. A novel approach of *in situ* synthesis of P4-OVAs on an SPR sensor surface was used to replace the conventional approach in which P4-OVAs were first synthesized in solution before being immobilized on SPR surfaces. This new approach streamlined synthesis and immobilization procedures, reduced time and costs in preparing bioreceptors' immobilized sensor surfaces, and provided an easy way to screen bioconjugates as bioreceptors for optimal assay performances.

Chapter 4 addressed the use of MBs to reduce the milk matrix effect in biosensing. The MBs conjugated with *anti*-P4 antibodies can bind P4 specifically, and thus were used to separate P4 from milk matrix before measurement on an SPR platform. Several different MB and antibody conjugates were synthesized and biosensing assays using these conjugates were optimized for sensitive P4 detection in the buffer and in milk. P4 levels in milk samples collected on a dairy farm were measured by the developed test. To our knowledge, this is the first SPR P4 test using MB conjugates.

Chapter 5 explored the potential of replacing *anti*-P4 antibodies with a newly selected P4 aptamer in P4 detection. Aptamers have several advantages over antibodies in production cost, storage, stability, etc., so P4 aptamers have potential in achieving low-cost and high-sensitive detection of milk P4.

2 Chapter 2: Investigating a Carboxylated Terthiophene Surface for SPR P4 Detection

2.1 Introduction

One of the crucial steps in development of biosensors is immobilization of bioreceptors on sensor surfaces. In terms of SPR detection, where gold surfaces are most commonly used, the surface density and orientation of bioreceptors as well as the distance or proximity of ligand binding sites to SPR gold surfaces play important roles in the sensitivity and reproducibility of assays. The immobilization is usually accomplished by covalent binding of bioreceptors to the chemical groups of coating reagents on gold surfaces [123]. Thus, gold coating reagents are important in the robustness of bioreceptor immobilization as well as the stability and reusability of sensor surfaces. The examples of gold coating reagents are SAMs [112], carboxylated dextran [109], polypeptieds [124], thin films of methacrylic acid copolymer [125], mixtures of poly-L-lysine and titanium oxide [126] and graphene [127]. Among them, a biocompatible dextran hydrogel matrix is one of the best so far, evidenced by its great utility in SPR analyses and commercial success as the Biacore chips. The success of the Biacore chips is mainly attributed to the high binding capacity, wide versatility, good reproducibility and high surface stability of the dextran matrix. However, the procedure to deposit such a carboxylated dextran hydrogel matrix is quite complicated and requires the use of aggressive and toxic reagents such as epibromohydrin, bromoacetic acid and strong alkali [109]. The dextran hydrogel matrix also faces some challenges of non-specific interactions [128] and steric effects [129].

Furthermore, the thickness of the dextran hydrogel [130] (100-200 nm for a CM5 chip) significantly reduces the actual SPR working range on gold surfaces from 300 nm to 100-200 nm, and also decreases SPR effects or sensitivity of assays by holding binding sites away from gold surfaces. Therefore, opportunities exist to investigate other coating reagents which form thinner layers on gold surfaces to increase the SPR effect, and at the same time, retain similar surface biocompatibility and stability, to replace the widely used carboxylated dextran hydrogel matrix on gold surfaces.

Terthiophene (T3) has been investigated over the last two decades mainly for the synthesis of polyterthiophene, a conducting polymer which has special optical and electrical characteristics with wide application in antistatic materials, conductors, photovoltaic cells, electrode materials and organic semiconductors [131]. Also polyterthiophene was used to develop biosensor surfaces, including

electrode coatings for electrochemical biosensors [132-136] and MIPs for SPR biosensors [137]. However, to our knowledge, the use of T3 itself in biosensors is limited, hence it is of our interest to explore the suitability and capability of T3 SAMs in coating gold surfaces for SPR detection. Previously, our group designed a new carboxylated T3 molecule (T3C, Figure 2.1) as a potential coating reagent for gold surfaces. The T3C molecule has multiple sulfurs in the thiophene rings that can adhere to a gold surface, and a pendent chain of a carboxylated oligo ethylene glycol (OEG) to potentially immobilize a bioreceptor which possesses a primary amine group.
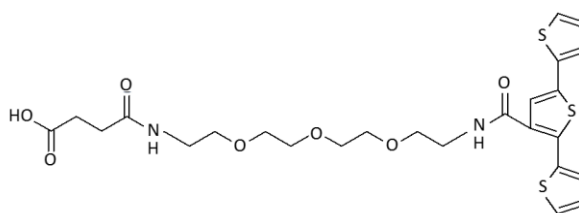
Figure 2.1 Structure of T3C.

In this chapter, gold SPR surfaces were coated by T3C to immobilize P4-OVAs as the bioreceptor in P4 detection assays on an SPR platform. The performance of the T3C SAM gold surface was evaluated in comparison with a commercial dextran hydrogel gold surface, the Biacore CM5 chip. Results show that the T3C SAM surface out-performed the dextran hydrogel surface in antibody binding and P4 detection. Also, the fabrication of the T3C SAM surface was simple and cheap, while the surface was stable and reusable over 250 tests.

2.2   Materials and Methods

2.2.1   Reagents and instrumentation

Phosphate buffered saline (PBS) tablets, ovalbumin (OVA), $NaH_2PO_4.2H_2O$, Na_2HPO_4, *N,N*-dimethylformamide (DMF), *N,N*-Dicyclohexylcarbodiimide (DCC), 1-ethyl-3-(3-dimethylaminopropyl) carbodiimide (EDC), NaOH, glycine, H_2SO_4, H_2O_2, Tween-20 and P4 were purchased from Sigma-Aldrich. *N*-Hydroxysuccinimide (NHS) was supplied by ACROS organics. T3C was provided by Digital Sensing Limited (DSL), New Zealand. 4-Pregnen-3, 20-dione 3-O-Carboxymethyloxime (P4 3-CMO) was supplied by Steraloids, Newport, USA. *Anti*-P4 monoclonal antibody (mAb) raised in mouse was

purchased from AbD Serotec (7720-1430), BioRad. Plain gold chips, CM5 chips, an amine coupling kit, HBS-EP buffer and PD-10 desalting columns were supplied by GE Healthcare Life Science. All the SPR assays were conducted on Biacore Q system from GE Healthcare Life Science. The protein concentrations were determined by Nanodrop 2000 and the steroid conjugation degree was measured by matrix-assisted laser desorption/ionization mass spectrometry with time-of-flights (MALDI-TOF) on UltrafleXtremeTM, Bruker, USA.

2.2.2   Synthesis of P4-OVA

P4 3-CMO (19.4 mg) was dissolved in 0.4 ml of DCC/DMF (206.3 mg/ml) solution with stirring, followed by addition of 0.4 ml of NHS/DMF (115.1 mg/ml) solution. The reaction mixture was stirred at room temperature for 3 hours until white precipitates were formed. Then the mixture was added to a solution of OVA (44.4 mg) in PBS (4 ml, 0.2 M, pH7.4) as illustrated in Scheme 2.1. After stirring at 4°C overnight, the crude P4-OVA conjugates were dialyzed against water over 48 hours, followed by final dialysis against PBS (1.2 L, pH7.4) over 24 hours. The dialyzed product was further purified by passing a PD-10 column. After dialysis and filtration, 7 ml of the P4-OVA conjugates solution was centrifuged at 10,000 rpm for one minute to remove white precipitates and the clean supernatant was collected. The aliquots were stored at -20ºC. The protein concentration of P4-OVA conjugates was determined by Nanodrop 2000 and the steroid conjugation degrees were measured with MALDI-TOF.
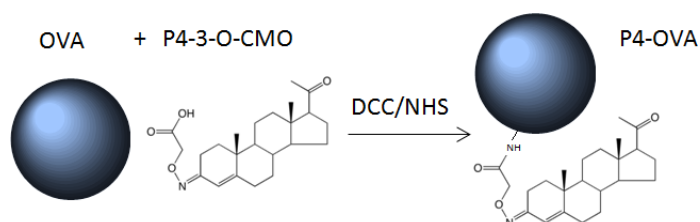
Scheme 2.1 Synthesis of P4-OVA conjugates by amine coupling.

2.2.3   Fabrication of T3C SAM SPR surfaces

Biacore SPR plain gold chips were cleaned with reactive ion etching (RIE) by March CS-1701 (Nordson MARCH, California, USA) using an oxygen plasma (set at 50 W for 30 seconds and 50% O_2) for two minutes before the chips were immediately immersed in T3C (Figure 2.1) solution (10 mM, ethanol)

overnight and thoroughly rinsed with ethanol (100%) and water. Then the chips were dried under nitrogen and assembled into the chip cassettes according to the manufacturer's instructions.

2.2.4   Immobilization of P4-OVA

T3C SAM SPR chips and carboxylated dextran chips (CM5 chip) were activated by 150 µl injection of a mixture (1:1 v/v) of EDC (390 mM) and NHS (100 mM) at 5 µl/min, followed by 150 µl injection of P4-OVA conjugates solution (1:20 v/v, acetate buffer pH 4.0) at 5 µl/min respectively. Then the chips were deactivated by a 100 µl injection of ethanolamine solution (1 M, pH 8.5) at 5 µl/min.

2.2.5   Antibody binding and inhibition assays of P4

A series of mAb solutions were prepared by diluting the stock solution in the PBS buffer containing Tween20 (0.005% v/v) to the desired concentrations. The dilution series of mAb used for P4-OVA that immobilized the T3C SAM SPR surface was 0, 0.2, 0.4, 0.6, 0.8 and 1 µg/ml; and that for the dextran hydrogel surface (CM5 chip) was 0, 0.8, 1.6, 2.4, 3.2 and 4 µg/ml. 60 µl of each mAb solution was injected at 20 µl/min over the two SPR surfaces respectively (Scheme 2.2). Surface regeneration was performed by injection of a 10 µl NaOH solution (10 mM) and glycine (10 mM, pH 2.0) for each. The injection of each mAb solution was repeated in triplicates.

Inhibition assays were conducted by mixing a fixed amount of mAbs (0.8 µg/ml in the assays on T3C SAM SPR surface and 4 µg/ml on CM5 chip respectively) with a series of standard P4 solutions (1:1 v/v). The P4 standards used in the assays on a T3C SAM SPR surface were 0, 0.01, 0.1, 1, 5, 10 and 100 ng/ml; and those on the CM5 chip were 0, 0.1, 1, 5, 10, 20 and 100 ng/ml. After incubation for 30 min, 60 µl of each mixture was injected at 20 µl/min followed by the regeneration of the SPR surfaces as above. The injection of each mixture was repeated in triplicates. The results were analyzed statistically using Sigma Plot version 12.5 and all inhibition assay curves were fitted to 4-parameter logistic regression. The LODs were calculated as the concentrations corresponding to the blank signals less two standard deviations of the blank signals.
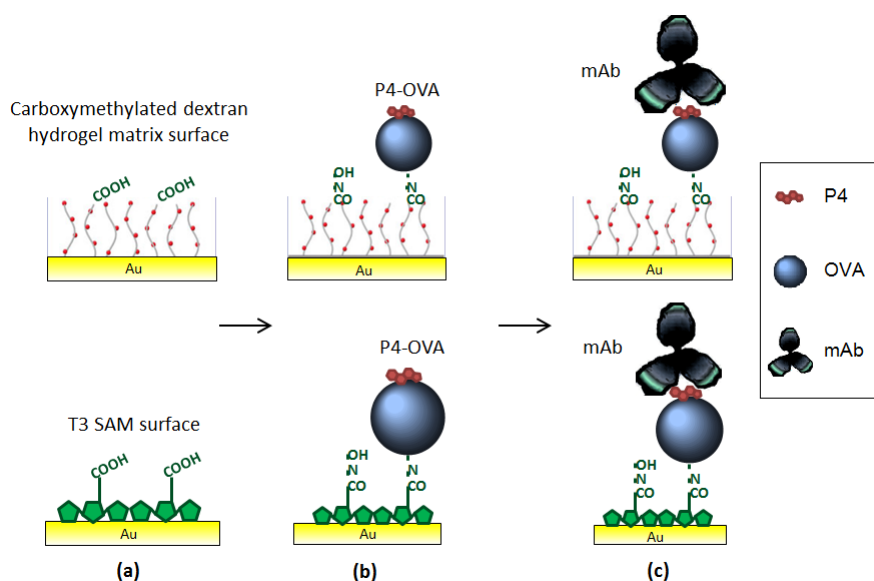
Scheme 2.2 Schemes of surface modification of SPR chips and antibody binding: (a) a T3C SAM surface and a carboxylated dextran surface (CM5 chip), (b) P4-OVA immobilization on the surfaces and (c) mAb binding to the sensor surfaces.

2.3   Results and Discussion

2.3.1   Synthesis of P4-OVA

P4-OVA conjugates were prepared by covalently binding the primary amine group of OVA and the carboxyl group of P4 3-CMO *via* carbodiimide reaction by DCC/NHS. The synthesis procedure also produced a byproduct dicyclohexylurea (DCU) (Scheme 2.3), which was insoluble in both organic solvents and aqueous buffers, and resulted in a white turbid mixture. To remove this byproduct together with excess reagents used for the reaction, dialysis, filtration and centrifugation were performed sequentially, which took about three days. The large amount of DCU formation was a result of excessive reagents used to ensure the conjugation efficiency of P4 and OVA, as P4 3-CMO *N*-hydroxysuccinimidyl esters had low solubility in the aqueous OVA solution. However, the presence of insoluble DCU in the conjugation reaction may impair reaction rates by affecting interaction of P4 3-CMO *N*-hydroxysuccinimidyl esters with OVA and it was difficult to completely remove DCU from the final product even with the use of dialysis, filtration and centrifuge. The impurity of the final P4-OVA conjugates may further affect immobilization to the sensor surface or the sensitivity of the assays. As an alternative, EDC may replace DCC to avoid an insoluble byproduct, but EDC has lower solubility in

DMF and thus may be less efficient in activating P4 3-CMO. Still, the time-consuming purification by dialysis and filtration is not avoidable when P4-OVA is synthesized in solution. Another approach of synthesizing P4-OVA conjugation *in situ* on sensor surfaces was investigated in Chapter 3.
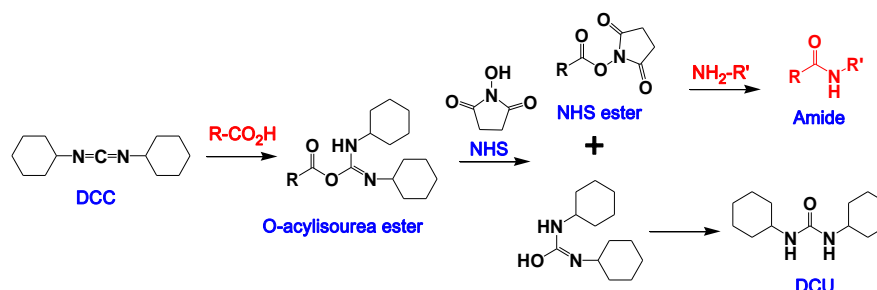
Scheme 2.3 Reaction of carboxylic acid amine coupling mediated by DCC and NHS.

The conjugation degree of P4 moiety in the conjugates was determined by MALDI-TOF as shown in Figure 2.2. The molecular weight (MW) of the unmodified OVA was approximately 44,500 Da according to mass spectroscopic analysis (Figure 2.2a). The MW of two P4-OVA conjugates synthesized separately were 45,739 Da and 45,594 Da (Figure 2.2b, c). As the MW of P4 3-CMO moiety is about 370 Da, on the average, P4-OVA 1 and P4-OVA 2 had approximately 3.3 and 2.9 P4 moieties per OVA respectively. The concentrations of P4-OVA conjugates were measured by NanoDrop using a customized method which measured the absorbance of peptide bonds at 205 nm. The concentration of P4-OVA 1 and 2 was 3.75 mg/ml and 3.82 mg/ml respectively. Thus, the two separate syntheses of P4-OVA resulted in similar yields and degrees of conjugation.
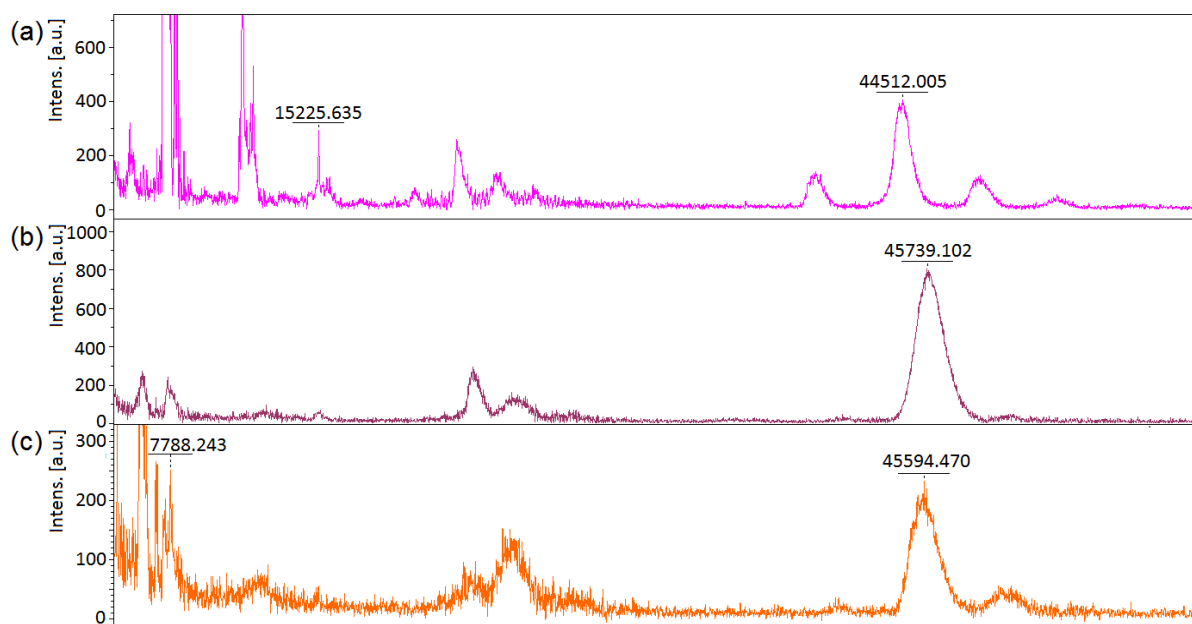
Figure 2.2 The results of MALDI-TOF experiments of OVA and P4-OVA conjugates: (a) an unmodified OVA, (b) P4-OVA 1 and (c) P4-OVA 2.

2.3.2   Fabrication of T3C SAM SPR surface

A T3C SAM layer can be formed on gold surfaces using either immersion or electrochemical coating methods [82, 138]. In this thesis, gold chips were coated by immersion in ethanolic T3C solution. According to the kinetic study of T3 SAM formation on gold surfaces by Matsuura and Shimoyama [139], T3 formed high-density and well-organized SAMs on gold with about 98% of the full-coverage over about 15 hours. At equilibrium, each T3 oriented parallel to gold surfaces, with three sulfur atoms, equally bound to gold surfaces as illustrated in Figure 2.3. Compared to alkanethiol SAMs or thiophene SAMs where each molecule attaches to gold with only one sulfur atom anchor and align itself parallel to other molecules and perpendicular against gold surfaces, the three sulfur anchors of T3 may provide stronger attachment on gold surfaces and high stability of the formed SAM. Higher stability by multiple thiol anchors on gold surfaces was recently demonstrated using bidisulfide-DNA of four sulfur anchors, which was significantly more stable than the corresponding cyclic disulfide-DNA of two sulfur anchors [140]. T3C was assumed to form similar stable SAMs as T3 on gold surfaces.

Further, with the thiophene rings parallel to the surface, the pendant chain of T3C, a carboxylated OEG chain, created a self-spacing mechanism out from the sensor surface (Figure 2.3). When the bioreceptors (in this case P4-OVA) are covalently bound to the OEG chains, they are extended away

from gold surfaces with regular space in between and thus the steric hindrance of ligand binding to the immobilized bioreceptors are reduced, which are favored by the ligand binding. Also, the OEG moiety provides a hydrophilic environment ideal for biomolecular interaction and the carboxylic head group has versatile application in covalently binding the biomolecules *via* carbodiimide reactions with the primary amine groups on proteins and peptides.
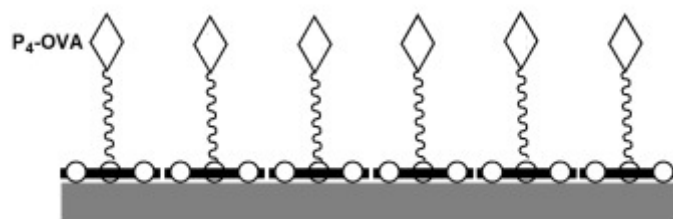
Figure 2.3 T3C SAM formed a gold surfaces at equilibrium and uniform-spaced P4-OVA on the surface.

2.3.3 Immobilization of P4-OVA on the SPR surfaces

The immobilization of P4-OVA conjugates was performed using the Biacore Q instrument on T3C SAM surfaces and dextran hydrogel gold surfaces (CM5 chips). A typical SPR sensorgram (Figure 2.4) depicting the immobilization contained three stages: surface activation by EDC/NHS, P4-OVA attachment, and surface deactivation by ethanolamine. The highest immobilization level of P4-OVA achieved on T3C SAMs surfaces was 2128.7 RU, while that on the dextran hydrogel surface (CM5 chip) was 3500.2 RU. To be noted, since the T3C SAM (only several nanometers thick) is much thinner than the dextran hydrogel (200 nm thick), as the immobilization of same amounts of P4-OVA will result in higher SPR signals on the T3C SAM surface due to the proximity of P4-OVA to the gold surface. Thus, the amount of P4-OVAs immobilized on the dextran hydrogel surface was considerably greater than that on the T3C SAM surface. This was not surprising as there were many more carboxyl groups on the bush-like dextran hydrogel surface than on the flat T3C SAM surface illustrated in Scheme 2.2 [141].
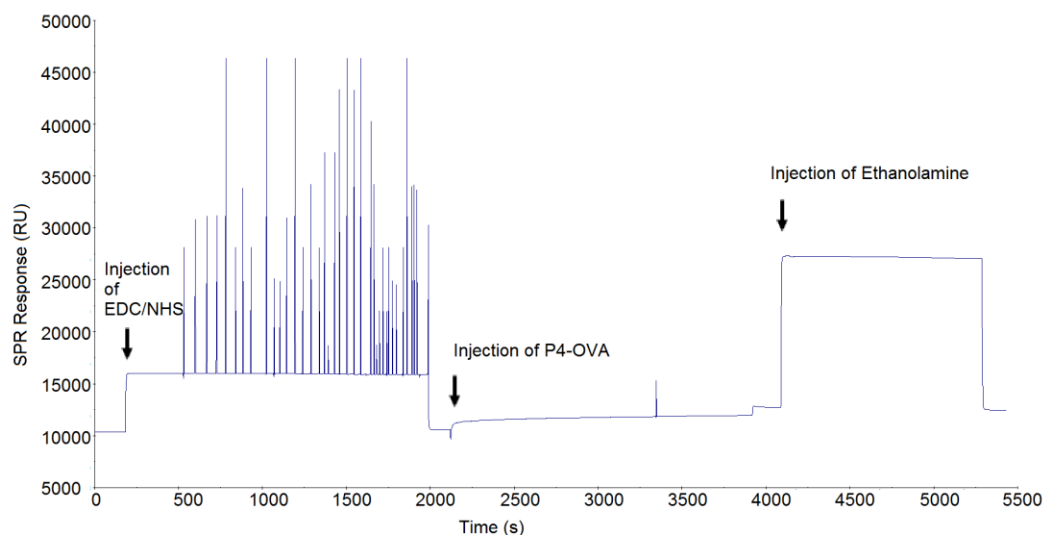
Figure 2.4 The SPR sensorgram during the immobilization of P4-OVA.

Several T3C SAM-coated gold surfaces were prepared by using different methods to clean gold surfaces, different immersion duration in T3C solutions and freshly prepared T3C solutions or old T3C solutions. Then P4-OVA was immobilized using the same method on all the surfaces and the immobilization levels on these T3C SAM gold surfaces are listed in Table 2.1. There was no difference in the immobilization levels of P4-OVA, when either a simple RIE method with oxygen or harsh chemicals were used to clean the gold surface before depositing T3C SAMs. Similar immobilization levels indicated that T3C SAMs of similar density and coverage formed on gold. It was possible that due to the multiple sulfur anchors of T3C the simple RIE method is sufficient for T3C to form SAMs on gold surfaces, while the cleaning prior to alkanethiol SAM formation usually requires harsh cleaning agents, and conditions such as heating the gold surface in Piranha solution [142]. Interestingly, the freshness of the T3C solution seemed to affect T3C SAM formation on gold surfaces according to the results of P4-OVA immobilization. A long immersion time (a week) and re-use of old T3C solution resulted in lower P4-OVA immobilization levels, possibly due to the contamination, dimerization or oxidation of T3C that affected the formation of well-organized T3C SAMs. However, more experiments e.g. atom force microscopy experiments are needed to further investigate this.

Table 2.1 Summary of the preparation methods of T3C SAM surfaces and the immobilization levels of P4-OVA.

Chip No	Cleaning methods of gold surfaces	Duration of immersion in T3C solution	Freshness of T3C solution	Immobilization level of P4-OVA using Biacore
1	RIE	1 week	Fresh+	Average=1472.5 RU, CV=14.1%, n=3
2	RIE	1 night	Fresh+	Average=2087.3 RU, CV=2.8%, n=2
3	Piranha solution*	2 nights	Fresh+	Average=1744.6 RU, CV=6.6%, n=3
4	Piranha solution*	3 nights	restored$	Average=496.0 RU, CV=13.9%, n=3

*Piranha solution is the mixture of H_2SO_4 and H_2O_2 (1:3, w/w). Briefly, the gold substrates were immersed in Piranha solution for 30 min at 55°C in a water bath before being washed with plenty of water and ethanol. Then the substrates were immediately immersed in T3C solutions after being dried under a flow of N_2.

+The T3C solution was prepared right before application.

$The T3C solution was from the previous experiments and had been stored in a sealed bottle protected from light at room temperature for 2.5 months.

2.3.4 Antibody binding assays and inhibition assays for P4 detection

Despite the lower immobilization level of P4-OVA on the T3C SAM surface (2128.7 RU vs 3500.2 RU), the SPR signals of mAb binding were 6.3 x higher on the T3C SAM surface than on the dextran hydrogel surface according to the antibody binding assays on the two surfaces (Figure 2.5).

The chart shows Response (RU) versus Antibody Concentration (µg/ml) with two linear fits:

$$y = 304.14x - 20.92$$
$$R^2 = 1.000$$

$$y = 48.191x + 5.448$$
$$R^2 = 1.000$$
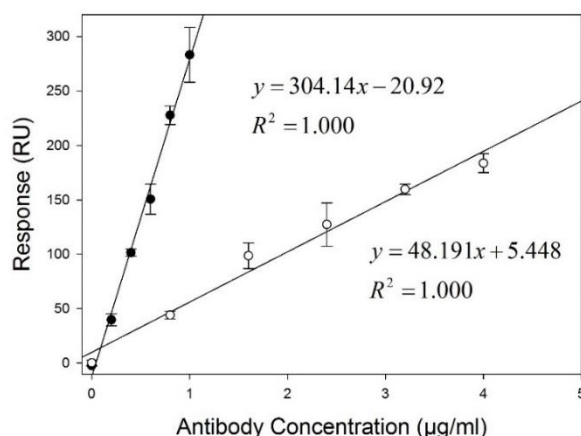
Figure 2.5 mAb binding assays on the T3C SAM surface (●) and on the hydrogel dextran surface (CM5) (○) immobilized with P4-OVA. Each data point was repeated in triplicates.

The sensitive binding of mAbs on the T3C SAM surface reduced the mAb concentration required in P4 inhibition assay (0.8 µg/ml), compared to that on the dextran hydrogel surface (4 µg/ml). P4 inhibition

assays were conducted on the two surfaces respectively (Figure 2.6). The LOD and EC50 on the T3C

SAM surface were 0.82 ng/ml and 1.64 ng/ml of P4, while those on the hydrogel dextran surface were

2.11 ng/ml and 8.28 ng/ml. The T3C SAM surface achieved 3 x higher sensitivity in P4 detection than

the hydrogel dextran surface, even with a low level of P4-OVA immobilization. The improvement in LOD

and EC50 resulted from using mAb of a lower concentration in the inhibition assay, which essentially

improved P4 detection sensitivity. The results of other inhibition assays conducted on the two surfaces

are available in Table A1 and Figure A1 in the Appendices.
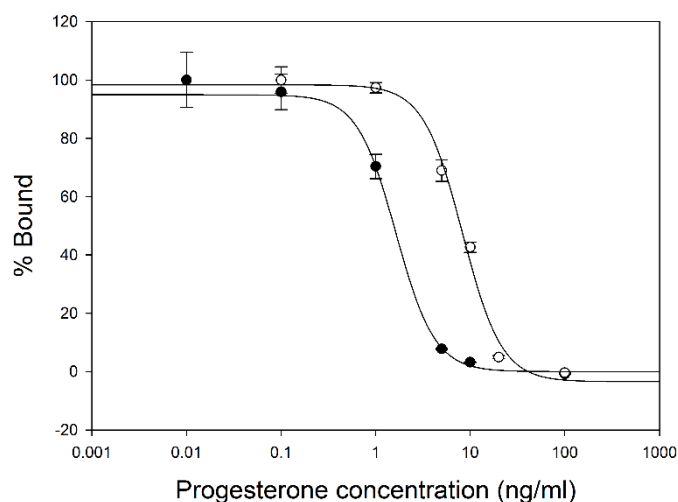
Figure 2.6 P4 inhibition assays on the T3C SAM surface (●) and the hydrogel dextran surface (○) immobilized with P4-OVA. Each data point was repeated in triplicates.

The sensitive SPR detection on the T3C SAM surface was thought to result from (1) T3C SAMs led to

a well-organized P4 configuration on gold surfaces, where the steric hindrance of antibody binding was

reduced; (2) the long dextran layer of CM5 chips resulted in heterogeneity of P4-OVA orientation on

sensor surfaces and affected the affinity of antibody binding [141]; and (3) the thinner T3C SAM layer

brought antibody binding sites closer to the gold surface, which improved SPR stimulation. The close

proximity of binding sites can also have a detrimental effect on antibody binding by increasing steric

hindrance. The commercial CM1 chip, which has a gold surface coated with a flat carboxylated SAM

without the dextran layer, showed poor ligand binding performance even with an adequate

immobilization level of bioreceptors [141]. Even though T3C SAM surfaces had similar topography to

the CM1 chip surfaces, the parallel-positioned thiophene rings and the perpendicular-positioned,

regular-spaced pendant chains provided a better P4-OVA configuration on the sensor surface for antibody binding.

Interestingly, in the inhibition assays on both the T3C SAM surface and the hydrogel dextran surface, the binding of the mixture of the blank (P4 = 0 ng/ml, data not shown) and mAbs often resulted in a slightly lower signal than the mixture of mAbs and the P4 standards of low concentrations (*i.e.* 0.01 and 0.1 ng/ml). This was similar to what is described as the 'hook effect' observed in other immunoassay studies [106, 143]. It was possible that: (1) as antibodies bind to P4 in a divalent fashion, in the mixture of P4 and mAbs, one antibody molecule may bind to P4-OVA on the sensor surface even when it has already bound to one P4 molecule, which can result in greater mass loading onto the surface than the mixture of mAbs and the blank (P4 = 0 ng/ml); or (2) when antibodies are bound to one antigen molecule, it may go through some conformational change that increases the affinity of its binding to a second antigen molecule [143]. Thus, the chance was that the binding of mAb to one P4 molecule led to a higher binding affinity of mAb to P4-OVA surfaces, which resulted in a higher binding signal.

2.3.5   Stability of the P4-OVA immobilized the T3C surface

The absolute SPR responses of the baselines of a T3C SAM surface over more than 250 binding/regeneration cycles were plotted in Figure 2.7. The chip was undocked after around 130 cycles, which resulted in a baseline shift from approximately 12,500 RU to 13,000 RU. The baselines were stable with no obvious decrease on antibody binding capacity, indicating the high stability of the T3C SAM surface. The stability of this SAM surface may attribute to both the stability of T3C SAM on gold and the use of P4-OVA as the bioreceptor on the T3C SAM surface. Compared to directly attaching P4 on SAM surfaces, P4-OVA immobilized on SAM surfaces provided protection of chemical bonds on gold from chemical oxidizers and other contaminants [69, 144].
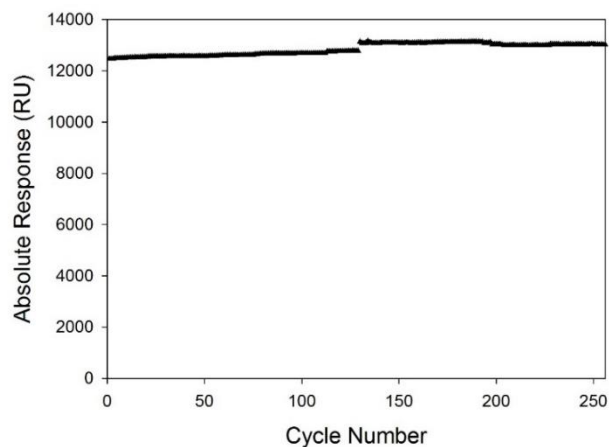
Figure 2.7 The baseline responses of the T3C SAM surface immobilized with P4-OVA over multiple antibody binding/regeneration cycles.

2.4   Conclusions

In comparison to the commercial dextran hydrogel gold surfaces (CM5 chips), T3C SAM gold surfaces showed premier capability in antibody binding and P4 detection using SPR. This is likely to have resulted from its stability *via* multiple thiol-anchors and high coverage of gold surfaces, its ability to uniformly orient and space P4-OVA on sensor surfaces, and the proximity of binding sites to enhance SPR effects. In addition, the method of preparing T3C SAM surfaces was simple; the immobilization of bioreceptors *via* amine coupling was versatile among biomolecules; and T3C SAM surfaces were capable of multiple reuses. In addition, the thin T3C SAM provided the potential of using large particles (e.g. magnetic beads) in SPR assays despite the restrained distance (300 nm) from gold surfaces that evanescent wave travels for effective SPR stimulation of Biacore systems.

3 Chapter 3: Functionalizing Sensor Surfaces for P4 Detection by Surface *in situ* Synthesizing P4-OVAs

3.1 Introduction

Small molecule and protein conjugates have wide applications in the research of biomolecular interactions as well as the development of novel materials, drugs and biosensors [145]. For small detection of small molecules in biosensors, the use of small molecule and protein conjugates as bioreceptors on sensor surfaces rather than direct attachment of small molecules is of particular interest, as it increases surface densities of small molecules by attachment to protein three-dimensional structures, stabilizes chemical bonds between antigen and sensor surfaces with protein protection, and decreases non-specific binding *via* the hydrophilic protein layer [142].

Small molecule and protein conjugates are usually synthesized in solution before being immobilized onto sensor surfaces, as described in Chapter 2. Small molecules are conjugated to protein *via* covalent bonds [113], yet many small molecules, such as steroids, have limited solubility in an aqueous buffer, which results in low efficiency of conjugation in aqueous protein solutions [115]. Thus, excess reagents are often used to increase conjugation rates and unreacted reagents need to be removed afterwards together with by-products. For this purpose, gel filtration and dialysis are often used, but both are time-consuming and may cause loss of intermedia and final products [114], especially when the synthesis of small molecule and protein conjugates involves multiple intermediate reactions.

In contrast, solid-phase conjugation first fixes proteins on a solid support before small molecules are conjugated to the immobilized proteins, then the bioconjugates are cleaved from solid support for further application [116]. The solid-phase conjugation allows fast reactions and efficient washing, avoids product loss during intermediate steps and improves the solvation of intermediate products [117]. Although solid-phase conjugations greatly simplify the procedures in preparing small molecule and protein conjugates compared with in solution conjugations, other challenges remain, such as effective elution of final products and immobilization of conjugates on sensor surfaces. It showed that the insertion of a long molecular linker between small molecules and proteins could significantly increase antibody binding and further improve SPR assay sensitivities, but some long linkers might cause steric hindrance that prevented the immobilization of the conjugates on sensor surfaces [107, 146]. Therefore,

it is a challenge to improve the methods of synthesizing and immobilizing small molecule and protein conjugates with a long molecular linker for sensitive immunoassays.

In this chapter, a new approach to functionalizing sensor surfaces with small molecule and protein conjugates was demonstrated using P4-OVAs as models. Five P4-OVA conjugates with molecular linkers of different lengths and compositions were *in situ* synthesized on five SPR sensor surfaces respectively, and these surfaces were directly used for detecting P4 by inhibition immunoassays on an SPR platform. These different conjugates led to different LODs (0.15-0.33 ng/ml of P4). The *in situ* conjugation approach takes advantage of solid phase conjugation and streamlines the processes of synthesis and immobilization of conjugates. It is much faster than the conventional approach and provides a facile and efficient way to functionalize sensor surfaces with small molecule and protein conjugates.

3.2   Materials and Methods

3.2.1   Reagents and instrumentation

P4 3-CMO was supplied by Steraloids (Newport, USA). Bis(sulfosuccinimidyl)suberate, BS3 crosslinker was purchased from Protochem (Hurricane, USA). Amino-PEG4-acid, $H_2N-C_2H_4-(OCH_2CH_2)_4CO_2H$ (BP-20423) or $H_2N-PEG4-CO_2H$ was purchased from Broadpham (San Diego, USA). *Anti*-P4 monoclonal antibody (7720-1430) raised in mouse was purchased from AbD Serotec, BioRad. CM5 chips, an amine coupling kit, a sodium acetate buffer (pH 4.0) and HBS-EP buffer were supplied by GE Healthcare Life Science (Uppsala, Sweden). All the SPR assays were conducted on a Biacore Q system from GE Healthcare Life Science. All the other chemicals were from Sigma.

3.2.2   *In situ* conjugation of P4-OVA (Conjugate-1, 2, 3, 4 and 5) on the CM5 chips

The surface of the CM5 chip was activated by injection of 100 μl of the mixture (1:1, v/v) of EDC (390 mM) and NHS (100 mM) at a flow rate of 10 μl/min followed by injection of 150 μl OVA solution (2 mg/ml, sodium acetate buffer pH 4.0), then the surface was deactivated by injection of 100 μl ethanolamine solution (1 M, pH 8.5) at a flow rate of 5 μl/min.

To attach P4, P4 3-CMO (4 mg/0.6 ml ethanol) was converted to its *N*-hydroxysuccinimidyl ester by adding EDC (37.5mg/0.2 ml, ethanol) and NHS (22.5 mg/0.2 ml ethanol) and incubated at room

temperature for 3 hours under constant stirring. Using the external Surface Prep Unit of Biacore Q, 100 µl reactive P4 3-CMO *N*-hydroxysuccinimidyl ester was injected at 5 µl/min over the OVA surface to form the Conjugate-1 (Scheme 3.1 (1)). The sensor surface was washed with ethanol (100%) and then water.

The other conjugates were *in situ* synthesized in a similar manner to Conjugate-1 with the additional steps of linker extension between the steps of the OVA immobilization and the P4 3-CMO *N*-hydroxysuccinimidyl ester attachment.

Briefly, after OVA immobilization, 150 µl BS3 crosslinker solution (25 mg/ml, PBS pH 7.4) was injected onto each OVA surface for initial linker insertion. Then various linker elongations were performed as the following: for Conjugate-2 (Scheme 3.1 (2)), 150 µl 1,6-hexamethylenediamine (25 mg/ml, PBS pH 9.0) was injected at 5 µl/min followed by surface deactivation with 100 µl ethanolamine solution; for Conjugate-3 (Scheme 3.1 (3)), 150 µl 6-aminocaproic acid (25 mg/ml, PBS pH 9.0) was injected at 5 µl/min before surface activation with 100 µl EDC/NHS again, and then 150 µl 1,6-hexamethylenediamine and 100 µl ethanolamine were injected as for Conjugate-2; for Conjugate-4 (Scheme 3.1 (4)), the same 6-aminocaproic acid injection and EDC/NHS activation were performed twice as for Conjugate-3 before the injection of 1,6-hexamethylenediamine and ethanolamine as for Conjugate-2; for Conjugate-5 (Scheme 3.1 (5)), 150 µl H_2N-PEG4-$CH_2CH_2CO_2H$ (25 mg/ml, PBS pH 9.0) was injected on the BS3 surface at 5 µl/min before surface activation with 100 µl EDC/NHS again, and then 150 µl 1,3-diaminopropane (25 mg/ml, PBS pH 9.0) was injected followed by surface deactivation at 5 µl/min with 100 µl ethanolamine solution. After the linker extensions, P4 attachment on the OVA-linker-NH_2 surfaces were performed as for Conjugate-1 to form P4-OVA conjugates on the surfaces.

3.2.3   Antibody binding and P4 inhibition assays

To perform the antibody binding assays, a series of mAb solutions were prepared by diluting the stock solution (1 mg/ml) in HBS-EP buffer to the desired concentrations. 60 µl of each mAb solution was injected at 20 µl/min over the P4-OVA immobilized surface using HBS-EP as the running buffer. The surfaces were regenerated by a pulse of 5 µl NaOH (50 mM) and 5 µl glycine (pH 2) each at 20 µl/min. The injection of each mAb solution was repeated in triplicates.

Inhibition assays were conducted by mixing a fixed concentration of mAbs (1:1, v/v) with a series of standard P4 solutions prepared by diluting the stock solution (10 mg/ml, DMF) in HBS buffer. After incubation for 30 min, 60 µl of each mixture was injected at 20 µl/min followed by the regeneration of the SPR surface as above. Injection of each mixture was repeated in triplicate. According to the antibody binding assays, the concentrations of mAbs used in the inhibition assays were 4.8 µg/ml on the surface coated with Conjugate-1, 1.25 µg/ml for Conjugate-4 and 1.5 µg/ml for Conjugate-5 to ensure adequate SPR signals. The P4 standards used in the assays on the surface coated with the Conjugate-1 were 0.001, 0.01, 0.1, 1, 2, 5 and 10 ng/ml; and those used on surface coated with Conjugates-4 and 5 were 0.001, 0.01, 0.1, 0.5, 1, 5 and 10 ng/ml. The results were analyzed using Sigma Plot version 12.5 and all inhibition assay curves were fitted to 4-parameter logistic regression. The LODs were calculated as concentrations corresponding to the blank signals, less two standard deviations of the blank signals.
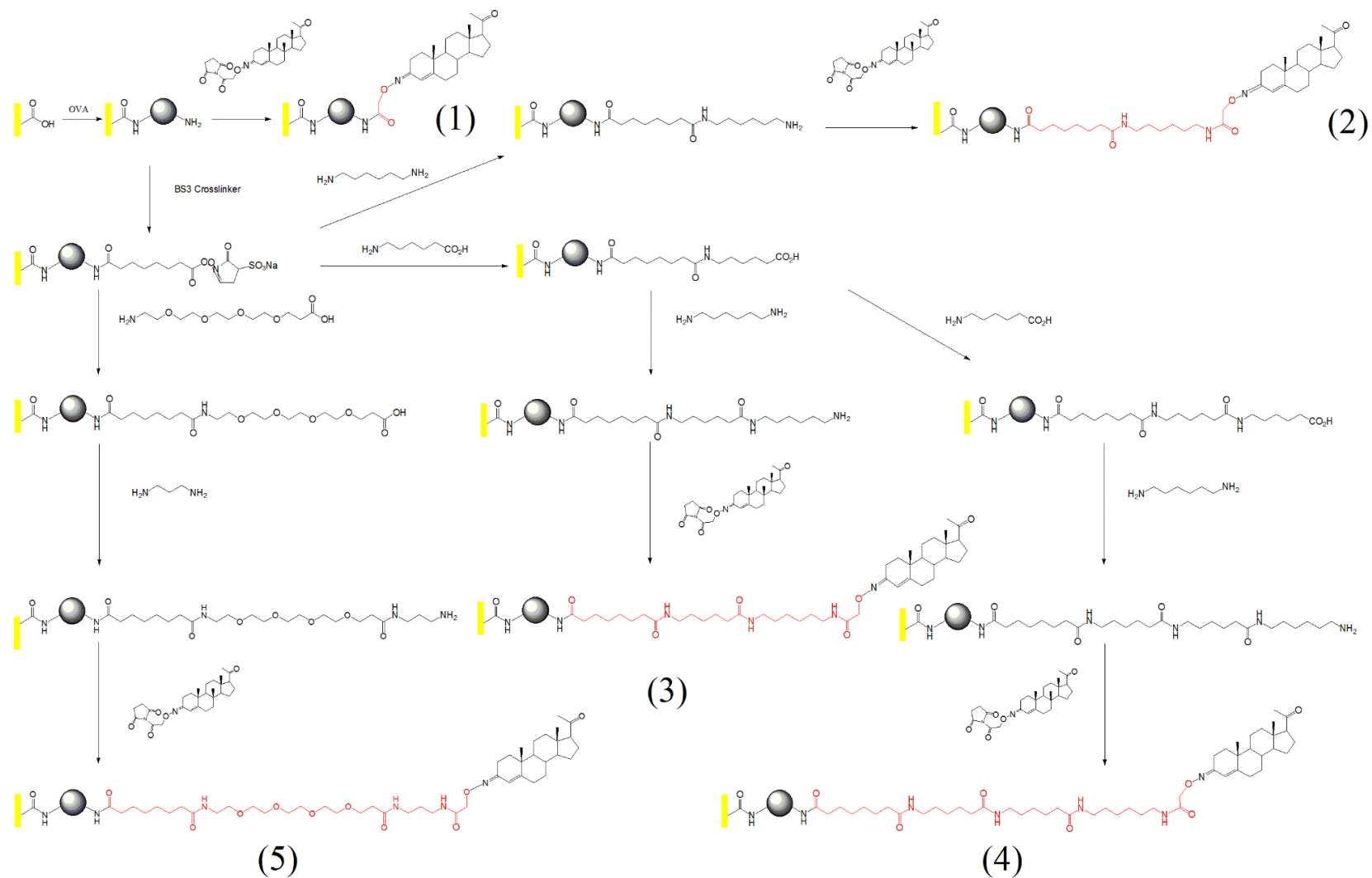
Scheme 3.1 *In situ* synthesis of five P4-OVA conjugates with various molecular linkers on the SPR surfaces respectively.

3.3 Results and Discussions

3.3.1 *In situ* synthesis of the P4-OVA conjugates on the SPR sensor surfaces

The *in situ* syntheses of the P4-OVA conjugates on a CM5 chip were achieved using an SPR instrument (BiaCore Q), without wet-lab chemical syntheses or washing/separation/purification. The initial immobilization of OVA using EDC and NHS resulted in similar relative SPR responses among all the five surfaces (average = 15795.4 RU, CV = 1.6%), so that similar amounts of OVA were immobilized for *in situ* synthesis of P4-OVA conjugates.

Then, a series of homo-bifunctional linkers (BS3, 1,6-hexamethylenediamine and 1,3-diaminopropane) and hetero-bifunctional linkers (6-aminocaproic acid and H_2N-PEG4-CO_2H) were sequentially injected over the OVA surfaces as illustrated in Scheme 3.1. These short linkers covalently bound to the surfaces *via* amine coupling to build up the longer linkers. After each linker reaction, the unreacted *N*-hydroxysuccinimidyl esters on the surfaces were deactivated by ethanolamine before the next linker reactions to ensure that consecutive linker extension occurred only on the previously attached linkers. Finally, P4 3-CMO *N*-hydroxysuccinimidyl esters were injected over the OVA-linker surfaces to react with the amine ends of the long linkers to form various P4-linker-OVA conjugates. Five P4-linker-OVA conjugates with linkers of different lengths and compositions were *in situ* synthesized on five surfaces separately as illustrated in Figure 3.1. The linker length of each conjugate was noted as the number of atoms on the straight chain between the nitrogen-atom of the amine group of OVA and the nitrogen-atom of P4 3-CMO moiety. Thus, P4-OVA Conjugate-1 in Scheme 3.1 had a 3 atoms linker between P4 and OVA, while Conjugates-2, 3, 4 and 5 had a 19 atoms linker, a 26 atoms linker, a 33 atoms linker and a 32 atoms linker with poly(ethylene glycol) (PEG) moiety respectively. These P4-OVA immobilized surfaces were directly used to perform SPR assays.
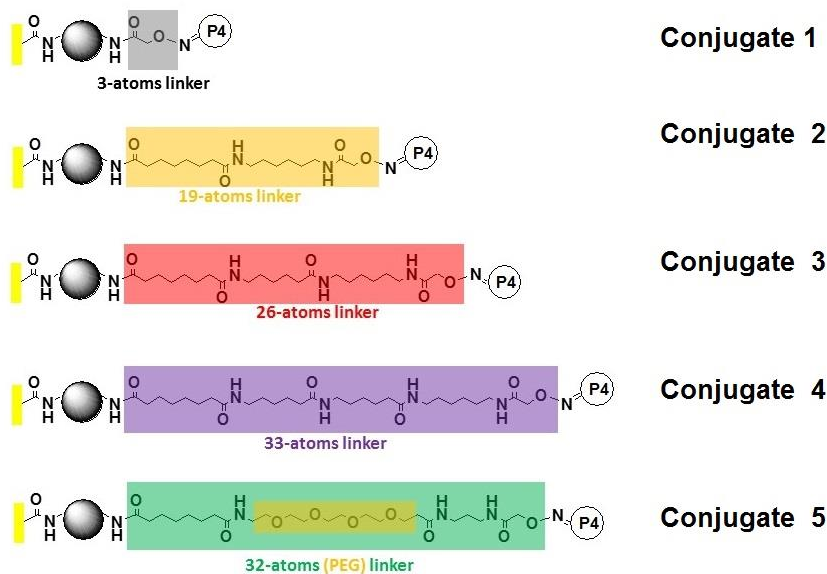
Figure 3.1 Five P4-OVA conjugates with various linkers *in situ* synthesized on five sensor surfaces.

The *in situ* synthesis approach is more efficient than the conventional approach, which involves synthesis of small molecule and protein conjugates in solution followed by surface immobilization (as the method used in Chapter 2). During the in-solution conjugation, P4 3-CMO *N*-hydroxysuccinimidyl ester had low solubility in aqueous buffers and precipitated when it was mixed with aqueous OVA solutions, which affected the conjugation efficiency. Thus, excessive P4 3-CMO *N*-hydroxysuccinimidyl ester and long conjugation reaction time was required, producing many by-products as well. Both unreacted reactants and by-products needed to be removed by dialysis and/or gel filtration which were time-consuming. In contrast, in the *in situ* synthesis approach, P4 3-CMO *N*-hydroxysuccinimidyl esters were dissolved in organic solvents and flowed through the OVA-linker immobilized surfaces, which allowed the formation of amide bonds in organic solvents using less P4 3-CMO *N*-hydroxysuccinimidyl ester. Also, the reaction of P4 3-CMO *N*-hydroxysuccinimidyl ester and amine groups on the surfaces took only 20 minutes, much shorter than the reaction time in the in solution conjugation (overnight), since the *in situ* synthesis approach, which is similar to solid-phase conjugation, tends to be more efficient [116]. Meanwhile, the flow through system of BiaCore Q removed the unreacted reactants and by-products immediately, and as a result, no extensive purification or washing steps were required. Thus, the *in situ* synthesis approach saved time and materials during the synthesis of conjugates,

especially compared to the in solution synthesis of P4-linker-OVAs which involves multiple steps of chemical synthesis, purification and washing of intermedia and final products [107, 115]. The entire process of *in situ* synthesis of P4-OVA with a 3 atoms linker on a sensor surface took only half a day, while the in-solution conjugation needed 2.5 days. In addition, the in-solution conjugation sometimes resulted in a low conjugation yield and impaired purity due to the limited methods of purification of intermediate or final products, while the *in situ* synthesis approach efficiently removed the unreacted reactants and by-products, and potentially resulted in higher purity of final products [113, 117]. Further, the immobilization of pre-synthesized conjugates on sensor surfaces may be problematic due to the steric hindrance caused by long molecular linkers [107]. This did not occur in the *in situ* synthesis, as proteins, short linkers and small molecules were immobilized onto sensor surfaces consecutively.

Thus, the *in situ* synthesis approach provides an efficient way to functionalize sensor surfaces with small molecule and protein conjugates. Eliminating extensive purification/washing steps such as extraction, gel filtration and dialysis, this approach may be automated. Also, given its simplicity and short turnaround time, this approach makes it possible to quickly screen different conjugates for optimal assay performance during the development of biosensors.

3.3.2   Control of the surface density of P4 on the sensor surface

The amounts of P4 immobilized on sensor surfaces were affected by the injection time of P4 3-CMO *N*-hydroxysuccinimidyl esters over sensor surfaces. Four sensing surfaces were first immobilized with similar amounts of OVA before reactive P4 3-CMO *N*-hydroxysuccinimidyl ester was injected for various periods of time (5, 10, 20 and 30 min) over the OVA surfaces (Table 3.1). Given that the same P4-OVA conjugate, P4-OVA with a 3 atoms linker (Figure 3.1 Conjugate-1) was synthesized on these four surfaces, the capacity of antibody binding was only affected by the surface density of P4. According to the antibody binding assays on these surfaces (Figure 3.2), increasing the injection time of P4 3-CMO *N*-hydroxysuccinimidyl ester from 5 minutes to 10 minutes increased mAb binding to the surfaces, while no significant difference was observed for longer injections. It indicated that P4 density on the surfaces increased with the injection time of P4 3-CMO *N*-hydroxysuccinimidyl ester over the surface, but it might have reached saturation after 10 minuntes. Meanwhile, it showed that it was possible to control the

surface density of P4 by changing the amount of P4 3-CMO *N*-hydroxysuccinimidyl ester flowing over

the surface (*e.g.* the injection duration and ester concentration).

Table 3.1 OVA immobilization levels of the four surfaces where different amounts of P4 3-CMO *N*-hydroxysuccinimidyl ester was injected.

Flow cell	OVA immobilization level (Response Unit, RU)	Injection of P4 3-CMO *N*-hydroxysuccinimidyl ester over the OVA surfaces
1	12066.0	5 min, 5 µl/min
2	14224.2	10 min, 5 µl/min
3	10911.6	20 min, 5 µl/min
4	11939.4	30 min, 5 µl/min
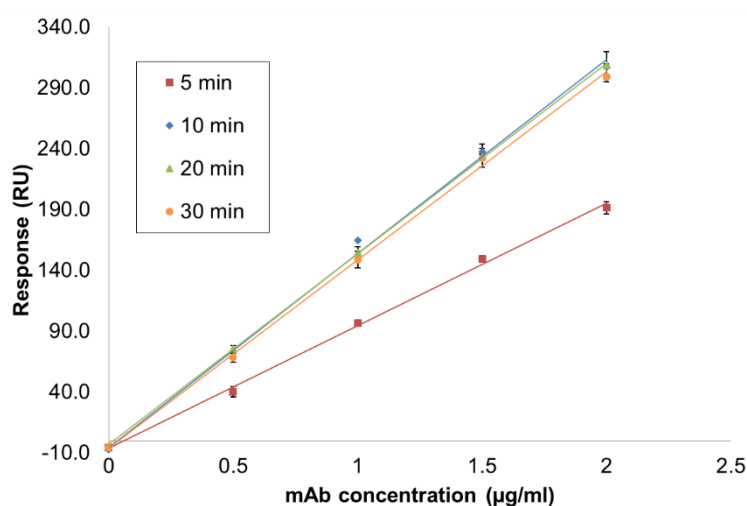
Figure 3.2 Antibody binding assays on the four P4-OVA surfaces prepared by injection of P4 3-CMO *N*-hydroxysuccinimidyl esters over OVA surfaces for different time peroids (5, 10, 20 and 30 min). Each data point was repeated in triplicates.

3.3.3 Effect of linker lengths on the assays performances

To investigate the effect of linker lengths on the assay performance, antibody binding assays and P4

inhibition assays (Figure 3.3) were performed on the surfaces immobilized with four different P4-OVAs

which had linkers of different lengths (Conjugates-1, 2, 3, and 4 in Figure 3.1). The performances of

these assays on the four surfaces were significantly improved with the increase of linker lengths, as

summarized in Table 3.2. The surface immobilized with Conjugate-4, which had the longest 33 atoms

linker, had 3.7 folds more antibody binding than Conjugate-1, which had the shortest 3 atoms linker.

The inhibition assay on the surface immobilized with Conjugate-4 was more sensitive with a 2.8 folds lower EC_{50} and a 2.2 folds lower LOD than Conjugate-1. It was assumed that long linkers increased the distance between P4 and OVA in the conjugates and thus reduced the steric hindrance of binding between antibody and P4 so that the assay performances were improved. Similar improvements were also observed in enzyme linked immunoassays [147, 148],electrochemical sensors [149] and SPR sensors [107].
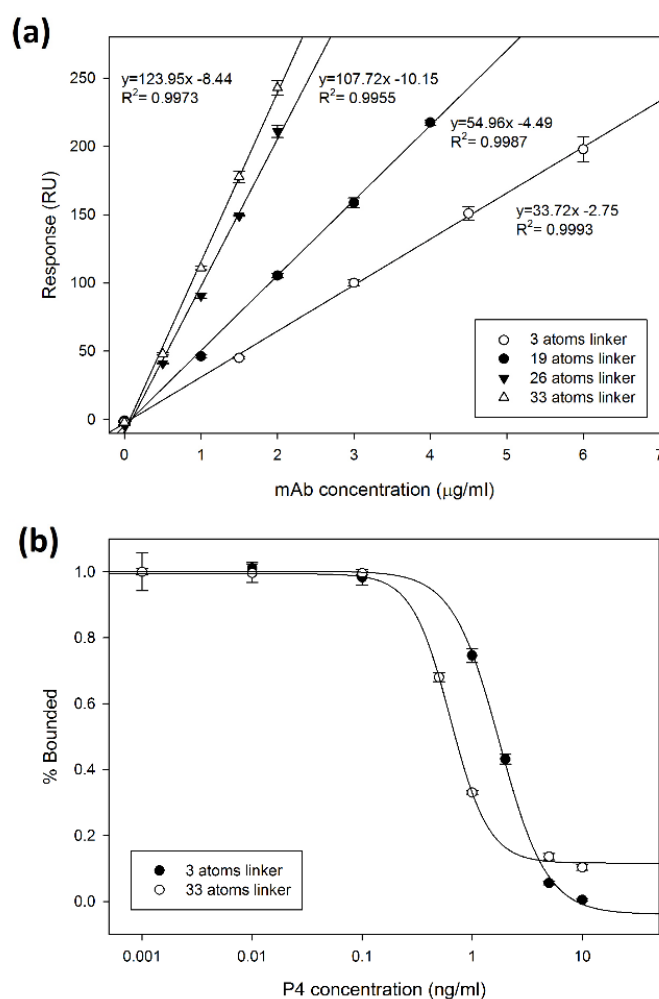
Figure 3.3 Antibody binding assays (a) and P4 inhibition assays (b) on the surfaces where P4-OVA conjugates had different linker lengths (Conjugates-1, 2, 3, and 4 in Figure 3.1) were *in situ* synthesized. Each data point was repeated in triplicates.

However, it was also noted that there was limited improvement of assay performance by linker lengths, since increasing the linker lengths from 26 atoms to 33 atoms did not considerably increase antibody

binding. It was possible that steric hindrance due to the proximity of P4 to OVA surfaces was reduced to a minimum by a linker length of 26 atoms. Meanwhile, two effects of the longer linkers are to be considered: first, the efficiency of linker synthesis may decrease with the increase in the number of steps to form longer linkers and it may result in a lower yield of conjugates on sensor surfaces; second, the distance of binding sites from gold surfaces increases with longer linkers and may result in reducing SPR effects. Therefore, the optimal linker length for SPR assays may result from the balance between the reduction in steric hindrance of binding, and the efficiency of conjugate synthesis and SPR signal stimulation. In addition, other researchers suggested that linkers of conjugates not be too long to avoid potential loss in antibody binding through decreasing hydrophilicity of conjugates [148]. Finally, increase in hydrophobicity may increase non-specific binding in lipid-rich media such as milk samples.

Table 3.2 Summary of the results of antibody binding and P4 inhibition assays on surfaces where P4-OVAs with different linkers (Conjugates-1, 2, 3, 4, and 5 in Figure 3.1) were *in situ* synthesized.

Conjugate	Linker	Linker lengths (atoms)	PEG moiety in the linker	Enhancement of antibody binding compared to Conjugate-1 (fold)	LOD of P4 inhibition assays (ng/ml)	EC50 of P4 inhibition assays (ng/ml)
1	$-COCH_2O-$	3	No	1	0.33	1.78
2	$-CO(CH_2)_6CO-$ $NH(CH_2)_6NH-$ $COCH_2O-$	19	No	1.6	-	-
3	$-CO-$ $(CH_2)_6CO-$ $NH(CH_2)_5CO-$ $NH(CH_2)_6NH-$ $COCH_2O-$	26	No	3.2	-	-
4	$-CO(CH_2)_6CO-$ $NH(CH_2)_5CO-$ $NH(CH_2)_5CO-$ $NH(CH_2)_6NH-$ $COCH_2O-$	33	No	3.7	0.15	0.63
5	$-CO(CH_2)_6CO-$ $NH(CH_2)_2(O-$ $CH_2-CH_2)_4CO-$ $NH(CH_2)_3NH-$ $COCH_2O-$	32	Yes	3.2	0.18	0.86

3.3.4   Effects of PEG moiety in the linker of P4-OVA conjugates on assay performances

The inclusion of PEG moiety in the linkers was reported to improve the synthesis efficiency of conjugates [142], increase the flexibility of the linker to facilitate the movement of bound small molecules in media [150], stabilize conjugates in a chemical and biophysical environment [151], reduce the non-specific adsorption of proteins [152, 153], and improve assay performances [68]. P4-OVA with 32 atoms PEG linker was *in situ* synthesized (Conjugate-5 in Figure 3.1) on a sensor surface to investigate the effect of PEG moiety on assay performance by comparing with P4-OVA with a non-PEG linker of similar length, and P4-OVA with 33 atoms linker (Conjugate-4 in Figure 3.1). As shown in Figure 3.4, Conjugate-5 showed similar, or slightly lower sensitivity, than Conjugate-4 in both antibody binding assay and P4 inhibition assay.
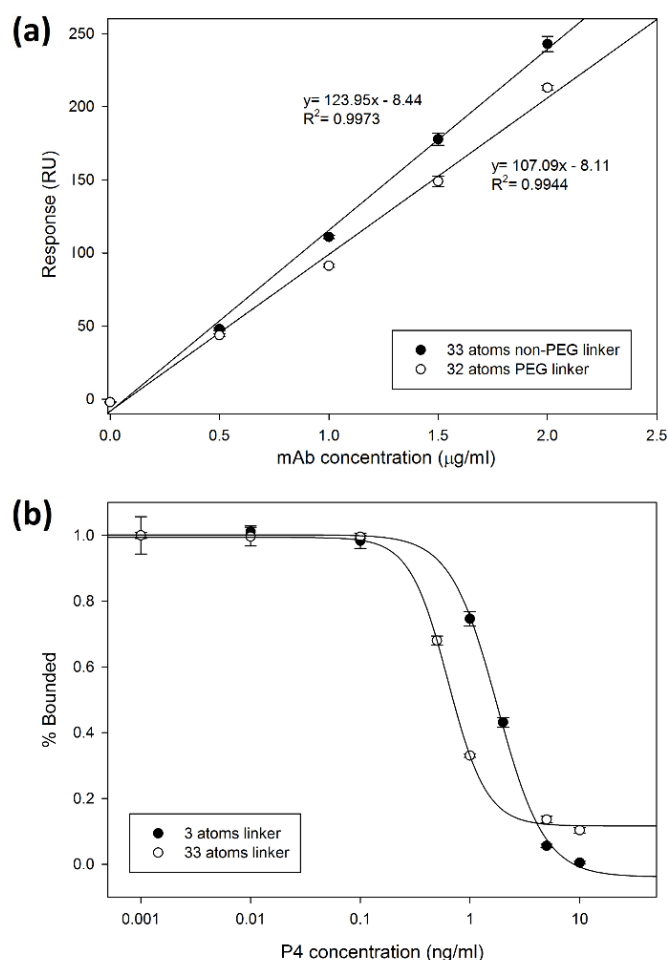
Figure 3.4 Antibody binding assays and P4 inhibition assays on the surfaces where P4-OVA of a 33 atoms non-PEG linker (Figure 3.1 Conjugate-4) and a 32 atoms PEG linker (Figure 3.1 Conjugate-5) were *in situ* synthesized. Each data point was repeated in triplicates.

In our experiments, PEG moiety in the linker of the conjugate did not result in more sensitive assays, thus conflicting with the findings of other studies. The difference between the in-solution conjugation and *in situ* synthesis may account for the discrepancy. First, different molecules were pegylated in the two methods. In the in-solution conjugation, P4 3-CMO *N*-hydroxysuccinimidyl esters were pegylated before conjugation with proteins, which resulted in a higher degree of conjugation, as the pegylation increased the solubility of P4 esters in aqueous OVA solutions and improved the reaction rates [142, 154]. However, in the *in situ* synthesis approach, the linkers extended from sensor surfaces were pegylated and the surfaces became more hydrophilic, which was less favored by hydrophobic P4 3-CMO *N*-hydroxysuccinimidyl ester dissolved in solvent and might lower the reaction rates. In contrast, the non-PEG aliphatic linkers led to a more hydrophobic surface, which was preferred by hydrophobic P4 3-CMO *N*-hydroxysuccinimidyl ester. Second, the flexible PEG linkers were found to increase the mobility of P4 on sensor surfaces for antibodies to access and further improved the binding [142, 150].

However, in the *in situ* synthesis approach, the flexibility of the PEG linkers might make it possible for the amine groups at the end of the PEG linkers to fold towards sensor surfaces and become less accessible to P4 3-CMO *N*-hydroxysuccinimidyl ester during conjugation reactions, which might [144, 153] decrease the conjugation efficiency. The folding of the long PEG linker was evidenced by the failure in *in situ* synthesizing P4-OVA conjugate with a 26 atoms PEG linker using a long PEG diamine (trioxa-1,13-tridecanediamine). It was assumed that the long PEG diamine was foldable and both amine groups at the two ends could fold back towards the carboxylated surface to form covalent bonds with the surface carboxyl groups. The preference of linkers with certain rigidity was also proposed by other biosensor studies [155]. The above effects may decrease the efficiency of P4 attachment and resulted in lower P4 surface density that affected assay performances.

Meanwhile, non-specific bindings of the surfaces immobilized with P4-OVA with a 32 atoms PEG linker (Conjugate-5 in Figure 3.1) and a 33 atoms non-PEG linker (Conjugate-4 in Figure 3.1) were evaluated with an *anti*-estradiol monoclonal antibody and an *anti*-mouse IgG polyclonal antibody. As shown in Figure 3.5, both the *anti*-estradiol (*anti*-E2) monoclonal antibody and the *anti*-mouse IgG polyclonal antibody of higher concentrations (10 µg/ml) showed lower binding to both surfaces compared to the *anti*-P4 monoclonal antibody of a lower concentration (2 µg/ml). The non-specific binding of *anti*-E2 mAb were calculated as 4% and 2.8% on the surfaces immobilized with P4-OVA with a 33 atoms linker

and 32 atoms PEG linker respectively. Those of *anti*-mouse polyclonal antibodies were calculated as 13.4% and 9.6% on the surfaces immobilized with P4-OVA with a 33 atoms linker and 32 atoms PEG linker respectively. The polyclonal *anti*-mouse antibody had relatively higher, non-specific binding than the monoclonal *anti*-estradiol antibody, possibly due to its lower specificity. The binding of the monoclonal *anti*-estradiol antibody to the surfaces may result from its cross-reactivity to P4 due to the structure similarity of the two hormones but the binding was negligible compared to the *anti*-P4 monoclonal antibody.
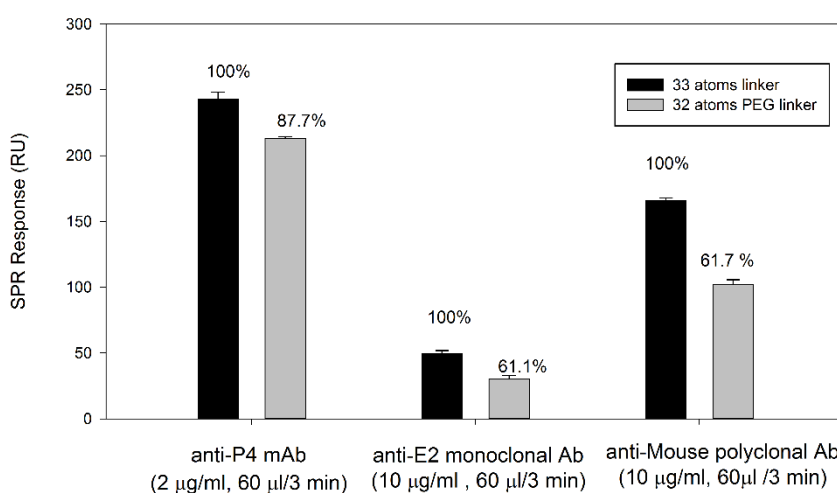
Figure 3.5 Non-specific bindings of anti-E2 monoclonal antibodies and anti-Mouse polyclonal antibodies on the surfaces coated with P4-OVA of a 32 atoms PEG linker (Conjugate-5 in Figure 3.1) and a 33 atoms non-PEG linker (Conjugate-4 in Figure 3.1). Each data point was repeated in triplicates.

Therefore, the PEG linker did reduce non-specific binding on the sensor surface, although no improvement on the sensitivity of P4 detection was observed. It may be because the current assay conditions actually involved little non-specific binding, as only the *anti*-P4 monoclonal antibodies and the P4 standards in the buffer were presented, but no other molecules or biomolecules that caused non-specific binding and interfered in the assays. However, relatively lower non-specific binding of the PEG modified surfaces may benefit those assays involving sample matrix and other contaminants.

3.3.5 Comparison with the surface immobilized with P4-OVA synthesized in solution

To further understand the difference between the *in situ* synthesis and in-solution conjugation of P4-OVA, two surfaces functionalized with Conjugate-1 were prepared by the *in situ* synthesis approach and the in-solution conjugated P4-OVA respectively. The detection of antibody binding was 1.7 fold more sensitive on the surface immobilized with the in-solution synthesized P4-OVA than on the *in situ* conjugated P4-OVA surface (Figure 3.6). It was noticed that much less protein was immobilized on the in solution conjugated P4-OVA surface than on the *in situ* conjugated P4-OVA surface (5709.1 RU of P4-OVA vs 15942.2 RU of OVA). A possibly lower P4 surface density was obtained on the *in situ* synthesized P4-OVA surface, where P4 molecules could only attach to OVA's amine groups that directed outwards from the chip surface and were exposed to the flow of P4 3-CMO *N*-hydroxysuccinimidyl ester. That limited the amine groups of OVA that P4 could be covalently bound to. However, during the in solution conjugation, P4 can bind to any primary amine group on the OVA surface. Nevertheless, given the much shorter period of reaction time (20 min vs overnight) in the *in situ* synthesis, the *in situ* conjugation approach is still regarded as highly efficient.
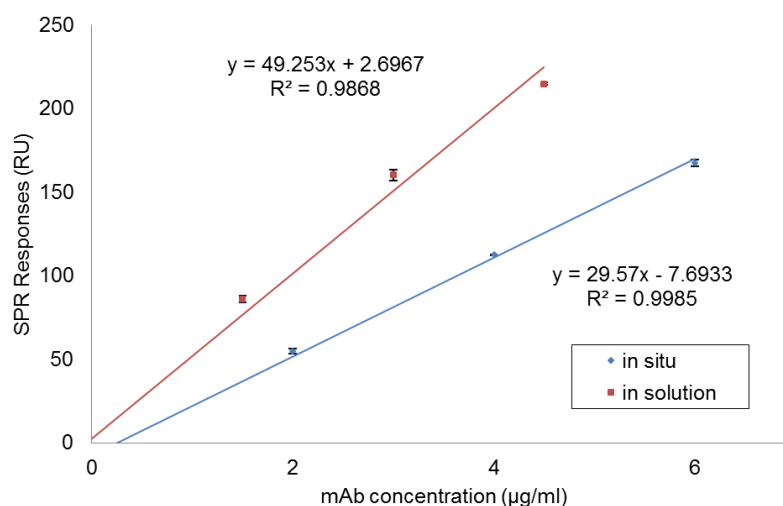
Figure 3.6 Antibody binding assays on surfaces immobilized with P4-OVA with a 3 atoms linker (Figure 3.1 Conjugate-1) synthesized in solution and *in situ*. Each data point was repeated in triplicates.

3.3.6   Indications on the repeatability of the *in situ* synthesis method

Four separate *in situ* synthesis experiments were performed and during each experiment several P4-OVA conjugates were synthesized. Over these experiments, the conditions and procedures of activating P4 3-CMO and attaching P4 3-CMO *N*-hydroxysuccinimidyl ester were optimized (summarized in Table A2 in Appendices) to facilitate P4 attachment inside the Biacore system. Initially, P4 3-CMO was activated by DCC/NHS in DMF. However, Biacore is not compatible with DMF and insoluble DCU formed during the P4 3-CMO activation process contaminated the chip surfaces and blocked the Biacore system. EDC and ethanol appeared to be compatible with Biacore systems and SPR chips, and were finally selected for the optimized *in situ* synthesis method as described in Section 3.2.2. More details in the experiment procedures, the conjugates synthesized during each synthesis, and observations during the experiments were summarized in Table A2 in the Appendices.

Figure A3 in the Appendices showed mAb binding assays on surfaces immobilized with the same P4-linker-OVA conjugates which were prepared in different synthesis experiments. Variations of antibody binding were observed as indicated by the slopes of antibody binding curves. The possible reasons for variations were: (1) the use of different P4 attachment methods; (2) the difference in OVA immobilization levels; (3) the variation in linker extension efficiency; and (4) the variation among antibody batches and preparation. Firstly, among different P4 activation and attachment methods, more concentrated reactive P4 3-CMO *N*-hydroxysuccinimidyl ester was prepared in Synthesis 1 and 2 using DCC/NHS in DMF, which might increase the yields of *in situ* synthesis. Also, during Synthesis 1, the reaction time of attaching P4 3-CMO *N*-hydroxysuccinimidyl ester to the surfaces was longer, potentially increasing the yields. Yet, using DCC and DMF contaminated chip surfaces as well as the Biacore system, as described in Table A2 in Appendices. This is likely due to insoluble DCU formed during P4 3-CMO activation. The white substances observed on the surfaces in Synthesis 1 and 2 were likely the insoluble DCU that adsorbed to the surfaces. These potentially affected repeatability of synthesis and assays. Also, DMF is not compatible with Biacore systems which may damage the Biacore fluidic system. Later, P4 3-CMO *N*-hydroxysuccinimidyl ester solution was prepared by EDC/NHS in ethanol and was completely soluble without DCU. Ethanol was more compatible with Biacore fluidic systems so that P4 attachment was performed within Biacore in a controlled manner.

However, P4 3-CMO *N*-hydroxysuccinimidyl ester was prepared at a lower concentration due to lower solubility of P4 in ethanol, which may have affected the yields. Thus Synthesis 3 and 4 appeared to have lower binding than Synthesis 1 and 2 in general. Also, ethanol and DMF may have different effects on P4 attachment due to the difference in hydrophilicity/hydrophobicity depending on the linkers that P4 3-CMO *N*-hydroxysuccinimidyl ester bound to. Secondly, there was a difference in immobilization levels of OVA as summarized in Table A2, which may affect the total yields. Thirdly, the efficiency of linker extension might vary, especially BS3 crosslinkers that may not be stable over long storage. They are easy to hydrolyze and lose their functions. These four synthesis experiments were spread out over a one year period, during which time some BS3 crosslinkers may have hydrolyzed. Finally, the experiments were conducted using mAb of different batches and separate preparation, which could cause variations in antibody binding assay performances.

However, the effects of linker lengths on antibody bindings were consistent as shown in Figure A2 in the Appendices, where each synthesis experiment was plotted separately to compare antibody binding on the surfaces immobilized with different OVA-conjugates. The results showed positive relationships between linker lengths and antibody binding, except P4-26 atoms PEG-OVA. The reason for this was explained in Figure 3.3.4. The inhibition assays performed on these surfaces are summarized in Table A3 and Figure A4 in the Appendices.

In the future, it is worth studying the repeatability of *in situ* synthesis systematically, as it was not possible to compute the yields of each reaction step and final products. Such study can be done by repeating synthesizing P4-OVA conjugates of different linkers several times by using the optimized synthesis process described in Section 3.2.2, and conducting antibody binding assays on them using the same batch of mAb. This will shed light on the reliability of this method and provide information on the effect of linker lengths and types on synthesis efficiency and repeatability.

3.4   Conclusions

In this chapter, a novel approach to functionalize sensor surfaces by *in situ* synthesis of small molecule and protein conjugates on sensor surfaces was developed. The steps of the *in situ* synthesis include immobilization of protein on sensor surfaces, and extension of linker molecules and attachment of small molecules. This approach largely reduces the use of wet lab chemistry and saves time and materials in

conjugate synthesis and immobilization. For the development of biosensors, it offered an opportunity to quickly screen the linker effects on assay performance. The *in situ* synthesized P4-OVA conjugates with a long PEG linker showed good assay performance and low non-specific binding, and this method was used in Chapter 4 for detecting milk P4.

4 Chapter 4: Developing antibody and MB conjugates based SPR assays for detecting milk P4

4.1 Introduction

P4 tests are useful for the productive management of cows to verify the onset of estrus, diagnose pregnancy, monitor postpartum ovarian status and evaluate responses to hormone treatments [14]. Although P4 is present in various cow's bio-fluids such as blood, milk and urine, using cow's milk to measure P4 levels is ideal for dairy farms due to easy access to milk. P4 concentrations in cow's milk can be as low as less than 1 ng/ml at or near estrus, and as high as more than 20 ng/ml during pregnancy and in the middle of estrous cycles [14, 28, 29]. It requires milk P4 tests of high sensitivity to detect P4 of low concentrations at or near estrus. Meanwhile, milk is a complex food matrix composed of various proteins, fat, lactose, minerals, and other hormones, *etc.* [156] Thus, it is important that milk P4 tests are of high specificity to limit the interference by milk matrix. In addition, it is essential for routine tests on dairy farms to be cost-effective, easy to operate and fast.

P4 immunoassays developed on SPR platforms are fast, sensitive and specific [33, 67-69, 102, 157]. Compared to ELISAs, SPR immunoassays eliminate the use of enzymes in signal transduction so that they reduce reagent costs and increase repeatability of results. Further, portable SPR sensors have been developed [158-162], which make it possible to perform SPR assays on site. Yet, the major obstacle in detecting milk P4 on SPR platforms is milk matrix, which usually causes non-specific binding to SPR sensor surfaces and affects the interaction between P4 and its antibody. That leads to decreased sensitivities, or even failure of P4 tests [33-35]. One of the easy ways to reduce the milk matrix effect is to dilute milk with buffers, which lowers the concentrations of milk components, and thus reduces non-specific binding and interference of milk components in assays. However, P4 in milk will be diluted at the same time, so assays of higher sensitivity are required to measure P4 in diluted milk. P4 can also be separated from milk before tests to reduce matrix effects. There are methods developed for chromatographic and spectrometric analysis, which extract and purify P4 from samples before analysis on instruments, but they are time-consuming, complicated and expensive, so they are not practical for dairy farms. Using magnetic beads (MBs) to isolate target analytes from samples is simple; and it also provides opportunities to concentrate on target analytes, which may increase detection sensitivity of assays. MBs have been used in the tests of nutrients, chemical residues, antibiotics, toxins,

hormones and bacteria present in milk or milk products [44-51]. Very recently an enzyme-linked immunoassay was developed to detect milk P4 using MBs and antibody conjugates; and it achieved a detection limit of 0.08-0.09 ng/ml P4 in milk [52]. However, there is no report on SPR P4 assays using MBs yet.

In this chapter, several mAb and MB conjugates were synthesized to separate P4 from cow's milk before SPR measurement, to reduce the milk matrix effect. The SPR assays using mAb and MB conjugates were first developed in the buffer; and by using one of the conjugates the SPR assay achieved an LOD of 0.020 ± 0.006 ng/ml of P4 in the buffer. High detection sensitivity of the assay allowed its application to measure P4 in diluted milk, and P4 inhibition assay conducted in diluted raw milk (1:100 v/v) showed an LOD of 0.036 ± 0.010 ng/ml of P4 (equivalent to 3.6 ± 1.0 ng/ml in undiluted milk). Thus, using mAb and MB conjugates in the SPR assays not only reduced the milk matrix effect, but also improved the sensitivity of P4 detection compared to the SPR assays using mAbs only. Finally, P4 concentrations in cow's milk collected during the estrous cycles of two cows were measured. The P4 concentrations determined by the SPR assays using mAb and MB conjugates showed good correlation (P values < 0.05) with the P4 concentrations measured by commercial milk P4 ELISA kits, and exhibited expected trends that followed cows' estrous cycles, although there was a difference between the concentrations measured by the two methods. Further optimization of the assay conditions and procedures may improve the accuracy and precision of the developed SPR assay. It was noticed that the SPR responses obtained from the milk samples also showed good correlation with the P4 concentrations measured by ELISAs (P values < 0.01) and coincided with the estrous cycles. Thus, it is possible to use SPR responses to predict the onset of estrus without calculating P4 concentrations from standard curves.

4.2   Materials and Methods

4.2.1   Reagents and instrumentation

P4 3-CMO was supplied by Steraloids (Newport, USA). BS3 and succinimidyl-4-[N-maleimidomethyl]cyclohexane-1-carboxylate (sulfo-SMCC) were purchased from Proteochem (Hurricane, USA). Amino-PEG4-acid (catalog no. BP-20423) was purchased from Broadpham (San Diego, USA). mAb raised in mouse (catalog no. 7720-1430) was purchased from AbD Serotec, BioRad.

Anti-mouse IgG antibody raised in rabbits (catalog no. M7023) was purchased from Sigma-Aldrich. SPR gold chips, an amine coupling kit, a sodium acetate buffer (pH4.0), and surfactant P20 and HBS-EP buffer were supplied by GE Healthcare Life Science. All the SPR assays were conducted on the Biacore Q system from GE Healthcare Life Science. MBs (diameter = 100nm) coated with dextran and functionalized with PEG-COOH groups (PEG-COOH-MBs) (catalog no. 84-56-102), PEG-NH$_2$ groups (PEG-NH$_2$-MBs) (catalog no. 84-55-102) and streptavidin (catalog no. 84-19-102) were purchased from Micromod Partikeltechnologie GmbH (Germany). TCEP, EZ-Link™Maleimide-PEG solid phase biotinylation kit (catalog no. 21930) and Zeba™ Spin Desalting Columns (catalog no. 89882) are from Thermo Fisher. NHS was supplied by ACROS organics. Raw milk samples and T3C was supplied by DSL. All the other chemicals were purchased from Sigma-Aldrich.

4.2.2 Synthesis of sAb and MB conjugates (sAb-MBs)

Anti-mouse IgG antibodies raised in rabbits were used as secondary antibodies (sAbs) to mAbs and were covalently bound to MBs by amine coupling using EDC/NHS. 100 µl of the mixture (1:1 v/v) of EDC (50 mg/ml, 0.5 M MES buffer) and NHS (50mg/ml, 0.5M MES buffer) was added to 400 µl diluted PEG-COOH-MBs (1:1 v/v, H$_2$O) and incubated at room temperature for 2 hours on a vertical rotator. The MBs were separated from the solution on a magnet for 10 min and the supernatant was removed before 800 µl sAbs (1 mg/ml) was added to the MBs. After incubation at room temperature overnight under constant rotation, the supernatant was removed and the remaining active sites on the MBs surfaces were deactivated by 800 µl ethanolamine (0.2 M) for 4 hours. The sAb and MB conjugates (sAb-MBs) were washed with 1 ml of PBS with 0.005% Tween 20 (PBST) three times before being suspended in 1 ml PBST to a final concentration of 1:5 (v/v) from the original MB stock.

4.2.3 Conjugation of mAbs to sAb-MBs (mAb-sAb-MBs, Scheme 4.1a)

500µl sAb-MBs was mixed with 500 µl mAbs (10 µg/ml) and incubated for one hour under constant rotation for sAb-MB to bind to mAbs. After the supernatant was removed, the beads were washed three times before being suspended in 500 µl BS3 solution (0.025 mM, phosphate buffer pH 8.0) and incubated at room temperature for 10 min to crosslink mAbs with sAb-MBs. Then 25 µl ethanolamine (1 M) was added to the mixture for one hour to terminate the reaction before the cross-linked mAb and

sAb- MBs (mAb-sAb-MBs) were washed six times with 1 ml PBST and suspended in 500 µl PBST to a final concentration of 1:5 (v/v) from the original MB stock.

4.2.4   Synthesis of mAb and MB conjugates *via* sulfo-SMCC (mAb-SMCC-MBs, Scheme 4.1b)

400 µl of 1:4 diluted PEG-NH$_2$-MBs in PBS with 2 mM EDTA (PBS-EDTA) were mixed with 100 µl sulfo-SMCC (0.1 mM, PBS-EDTA) and incubated at room temperature for one hour under constant rotation before the supernatant of MBs was removed and the sulfo-SMCC activated MBs were washed twice by PBS-EDTA and suspended in 460 µl PBS-EDTA. Meanwhile, 20 µl mAbs (1 mg/ml) was reduced by adding 20 µl TCEP (0.4 mM, PBS-EDTA) and incubated at room temperature for 30 min before TCEP was removed by gel filtration using Zeba™ Spin Desalting Columns. The reduced mAbs and sulfo-SMCC activated MBs were mixed and incubated at room temperature for 2 hours under constant rotation before being washed three times with PBS. The beads were re-suspended in 1000 µl Cysteine (0.05 mM, PBS-EDTA) to deactivate the unreacted sulfo-SMCC for one hour and the conjugates were washed another three times before being suspended in 500 µl HBS-EP buffer to a final concentration of 1:5 (v/v) from the original MB stock.
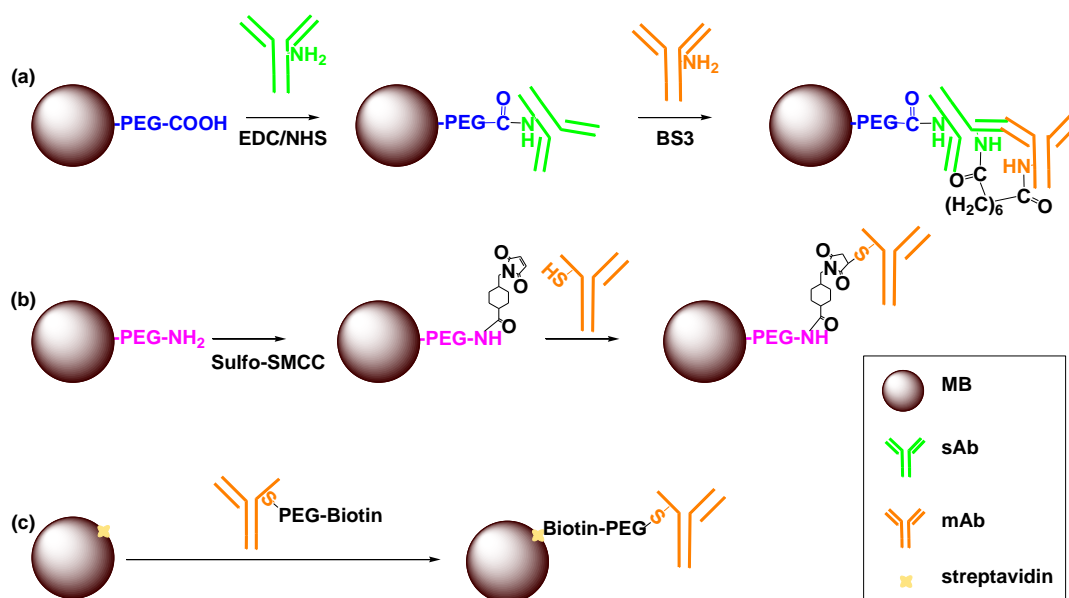
Scheme 4.1 Synthesis of three different mAb and MB conjugates: (a) mAb-sAb-MBs, (b) mAb-SMCC-MBs and (c) b-mAb-str-MBs.

4.2.5 Synthesis of biotinylated mAb and streptavidin coated MB conjugates (b-mAb-str-MBs, Scheme 4.1c)

mAb was biotinylated using the EZ-Link™Maleimide-PEG solid phase biotinylation kit according to the manufacturer's instructions. Briefly, 500 µl mAbs (0.2 mg/ml) was added to the HisPur Ni-NTA spin column for binding before the sulfhydryl groups of mAbs were reduced on the column by TCEP at the final concentration of 0.2 mM. Then, maleimide-PEG2-biotin was added to the column containing the reduced mAbs at a final concentration of 0.5 mg/ml before the biotinylated mAbs were eluted from the column by 200 µl imidazole (4 M). 100 µl of diluted streptavidin coated MBs (1:5 v/v, PBS) were mixed with 900 µl diluted biotinylated mAbs (1:1000 v/v, PBS) and incubated at room temperature for 30 min on constant rotation before the supernatant was removed and the beads were washed three times with PBS and suspended in 100 µl PBST to a final concentration of 1:5 (v/v) from the original MB stock.

4.2.6 Preparation of the SPR sensor surfaces

The SAMs of T3C were deposited on the gold chips in the same manner as described in Chapter 2. Briefly, Biacore gold chips were immersed in T3C solution (10 mM, ethanol) overnight and washed with ethanol and water. Then the chips were dried under nitrogen and assembled into the chip cassettes according to the manufacturer's instruction. Then the T3C SAM surfaces were functionalized with P4 and OVA conjugates using the *in situ* synthesis approach described in Chapter 3. Briefly, the T3C SAM surfaces were first activated by injection of 100 µl of the mixture (1:1 v/v) of EDC (390 mM) and NHS (100 mM) followed by injection of 150 µl OVA solution (2 mg/ml, acetate buffer pH 4.0), then the surface was deactivated by injection of 100 µl ethanolamine solution (1 M, pH 8.5) at the flow rate of 5 µl/min. After OVA immobilization, a 26 atoms linker (Scheme 4.2a) with a primary amine group at the end of the aliphatic chain was formed by sequential injection of 150 µl BS3 crosslinker solution (25 mg/ml, PBS pH 7.4), 150 µl aminocaproic acid (25 mg/ml, PBS pH 9.0), 100 µl ethanolamine solution (1 M, pH 8.5), 100 µl EDC/NHS (1:1 v/v) and 150 µl 1,6-hexanediamine (25 mg/ml, PBS pH9.0) on the OVA immobilized surfaces at 5 µl/min. A 32 atoms PEG linker (Scheme 4.2b) was formed on the OVA immobilized surface in a similar manner, except that aminocaproic acid was replaced by amino-PEG4-acid.

To attach P4 to the linkers on the surfaces, P4 3-CMO (4 mg/0.6 ml ethanol) was converted to its N-hydroxysuccinimidyl ester by incubation in EDC (37.5 mg/0.2 ml ethanol) and NHS (22.5 mg/0.2 ml

ethanol) at room temperature for 3 hours under constant stirring. 100 µl of this reactivated P4 succinimidyl ester was injected at 5 µl/min over the OVA-linker surfaces. The sensor surfaces were rinsed with ethanol and water thoroughly and air dried to be used for the assays directly.
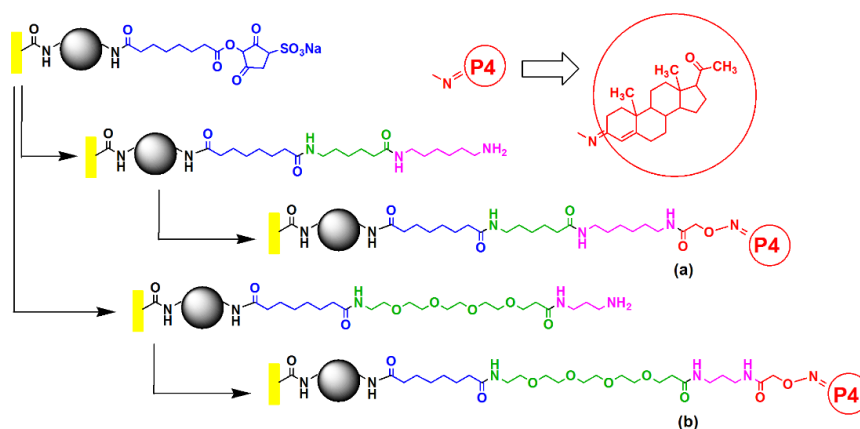
Scheme 4.2 *In situ* synthesis of two different P4-OVA conjugates with different linkers between P4 and OVA on the T3C SAM surfaces: (a) P4–OVA with 26 atoms linker and (b) P4-OVA with 32 atoms PEG linker.

4.2.7   P4 inhibition assays using mAbs

A series of standard P4 solutions were prepared by diluting P4 stock solution (10 mg/ml, DMF) in a HBS-EP buffer to the desired concentration. Then, the inhibition assays were conducted by mixing mAbs (0.6 µg/ml) with each P4 standard solution (1:1 v/v) respectively. After incubation for 30 min, 60 µl of each mixture was injected at 20 µl/min followed by regeneration of the SPR surface with NaOH (10 mM). Injection of each mixture was repeated in triplicates. The results were analyzed statistically using Sigma Plot version 12.5 and all inhibition assay curves were fitted to 4-parameter logistic regression. The LODs were calculated as the concentrations corresponding to the blank signals less two standard deviations of the blank signals, and the detection range was calculated as 10% to 90% of total inhibition.

4.2.8   P4 inhibition assays using mAb and sAb-MBs

The inhibition assays were conducted by mixing an antibody solution composed of 20 µl mAbs (20 µg/ml) and 20 µl sAb-MBs with 180 µl of each P4 standard (0, 0.01, 0.01, 1, 10, 100, 1000 ng/ml) (1:1 v/v) respectively. After incubation for 30 min, the beads were separated using a magnet applied to the side

of the tube for 6 min and the supernatant was removed before the beads were re-suspended in 400 µl HBS-EP buffer with 1% PEG400, and 60 µl of each bead re-suspension was injected at 20 µl/min followed by regeneration of the SPR surface with NaOH (10 mM). Each data point was repeated in triplicates. The results were analyzed as described above.

4.2.9 Non-specific binding of milk on sAb-MBs

Homogenized and pasteurized milk (3.3% fat) was obtained from local supermarkets and diluted to 1:10, 1:100 and 1:1000 (v/v) in HBS-EP; and the raw milk of an anestrous cow was diluted to 1:100 (v/v) in HBS-EP. 20 µl of each diluted or undiluted milk was mixed with 20 µl mAbs (20 µg/ml) and 20 µl sAb-MBs and incubated at room temperature for 30 min before the beads were separated on a magnet for 6 min and the supernatant was removed before the beads were re-suspended in 400 µl HBS-EP buffer with 1% PEG40. 60 µl of the bead re-suspension was injected at 20 µl/min.

4.2.10 P4 inhibition assays using mAb and MB conjugates (Scheme 4.3)

The inhibition assays were performed on a T3C SAM surface immobilized with OVA-26 atoms linker-P4 conjugates (Scheme 4.2a). To perform P4 inhibition assays with mAb-sAb-MBs, 15 µl of mAb-sAb-MBs were mixed with 285 µl P4 standards (0, 0.01, 0.01, 1, 10, 100, 1000 ng/ml) and incubated at room temperature for 30 min before they were separated on a magnet for 6 min and the supernatant was removed. Then the beads were washed with HBS-EP once and suspended in 300 µl HBS-EP buffer with 1% PEG400. 30 µl of the bead suspension was injected at 10 µl/min followed by regeneration of the SPR surface and repeated in triplicates. The inhibition assays of b-mAb-str-MBs and mAb-MBs were conducted in the same manner, except that 30 µl beads were mixed with 570 µl P4 standards initially.
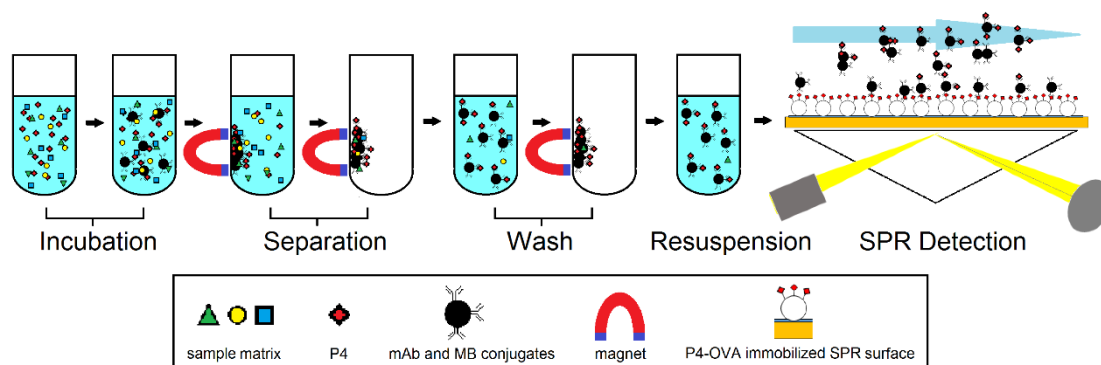
Scheme 4.3 Procedures of P4 inhibition assays using mAb and MB conjugates. mAb and MB conjugates were incubated with P4 solution before separation on a magnet and washing by a buffer; then the conjugates were re-suspended in the buffer and injected over P4-OVA immobilized SPR surfaces.

4.2.11 Binding assays of mAb and MB conjugates

A series of mAb and MB conjugate dilutions were prepared by diluting the mAb and MB conjugate stock solution in an HBS-EP buffer. 30 µl of each dilution was injected at 20 µl/min over the SPR surfaces immobilized with P4 and OVA conjugates followed by surface regeneration by NaOH solution. Injection of each mAb-MBs solution was repeated in duplicates.

4.2.12 P4 inhibition assays with raw milk spiked with P4 standards

To prepare raw milk P4 standards, a series of standard P4 solutions prepared in DMF (0, 100, 200, 500, 1000, 2000 and 5000 ng/ml) were spiked into raw milk. The raw milk was from an anestrous cow with a very low P4 level verified by Ridgeway's milk P4 ELISA kit. The milk was incubated in a water bath of 40°C for 5 min before mixing well by vortexing. 1 µl of each P4 standard solution was spiked into 100 µl raw milk and each mixture was incubated in a water bath of 40°C for 5 min and well mixed by vortexing. These raw milk standards containing 0, 1, 2, 5, 10, 20 and 50 ng/ml of P4 respectively were stored at 4°C as stock solution. Before each inhibition assay, raw milk standards were incubated in a water bath of 40°C for 5 min and well mixed by vortexing to distribute the cream evenly before 3 µl was taken from each standard stock and diluted in 300 µl HBS-EP buffer containing 0.01% P20 (1:100 v/v).

P4 inhibition assays with raw milk P4 standards were performed using mAb-SMCC-MBs on the T3C SAM SPR surface immobilized with P4-32 atoms PEG linker-OVA (Scheme 4.2b) in a similar manner to the inhibition assays described above, except for a few modifications in order to further reduce the

effect of milk matrix. 300 µl of diluted raw milk P4 standards (1:100 v/v, HBS-EP) was mixed with 30 µl mAb-SMCC-MBs and incubated at room temperature for 40 min under constant shaking. After the mAb-SMCC-MBs were separated on a magnet for 6 min and the supernatant was removed, the mAb-SMCC-MBs were washed 4 times in HBS-EP buffer containing 0.01% P20 and suspended in 150 µl HBS-EP buffer containing 1% PEG400 and 0.01% P20. 30 µl of each bead suspension was injected at 10 µl/min followed by the regeneration of the SPR surface and was repeated in duplicates. This inhibition assay was conducted in the same manner with P4 standards (0, 0.001, 0.005, 0.01, 0.05, 0.1, 0.5 ng/ml) prepared in a HBS-EP buffer to investigate the milk matrix effect for detection sensitivity. The results were analyzed as described above.

4.2.13 Raw milk samples and milk P4 tests

Raw milk samples were collected by the Livestock Improvement Corporation New Zealand (LIC) between 3rd October and 27th November 2013 and stored at -80°C. The P4 concentrations measured by Ridgeway's Milk P4 kit were provided by LIC or DSL. Raw milk samples were equilibrated to 4°C, heated at 40°C for 5 min, and mixed by vortexing for 30 seconds before being diluted 1:100 (v/v) in HBS-EP buffer. Then the P4 concentrations in the diluted raw milk samples were measured on an SPR together with the diluted raw milk P4 standards using the P4 inhibition assays described above. The concentrations of the diluted raw milk samples were calculated based on the equation shown below and derived from the diluted raw milk P4 standards, where *x* represents P4 concentration, *y* represents SPR responses and *max, min, EC50* and *Hillslope* are the parameters derived from the diluted raw milk P4 standards. Then the original P4 concentrations in undiluted raw milk were calculated by multiplying that in the diluted raw milk samples by 100.

$$y = min + \frac{max - min}{1 + (\frac{x}{EC50})^{-Hillslope}} \qquad \text{or} \qquad x = EC50 \times \sqrt[-Hillslope]{\left(\frac{max - min}{y - min} - 1\right)}$$

4.3   Results and Discussions

4.3.1   Synthesis of sAb-MB conjugates and P4 inhibition assays using mAbs and sAb-MBs

Diluted raw milk (1:100 v/v) had high binding to SPR surfaces (> 500 RU for injections of 3 min) and resulted in slowly decreasing and unstable SPR responses, which was not possible for analysis. mAb and MB conjugates can be used to separate P4 from other milk constituents before SPR measurement to reduce the milk matrix effect. Initially, mAbs were directly conjugated to PEG-COOH-MBs *via* amine coupling by EDC/NHS. However, the conjugates were not able to bind to the T3C SAM SPR surface immobilized with pre-synthesized P4-OVA, prepared as described in Chapter 2. It was suspected that random orientation of mAbs on the MB surfaces and/or short distance of mAbs from the MB surfaces, using this conjugation method, caused steric hindrance of binding and led to low binding affinity of the conjugates to the P4-OVA SPR surface [163]. It is critical for mAb and MB conjugates to have high binding affinity to the P4-OVA surface for SPR detection, since (1) the concentrations of MB conjugates were limited (in the nanomolar range); and (2) the detection was conducted in real time while mAb and MB conjugates flew through the sensor surface in a short period of time, which was different from the binding events in solution for hours. Therefore, despite the high binding affinity of mAbs to this P4-OVA surface, the binding of mAb and MB conjugates is affected by the conjugation of mAbs to MBs. To improve the binding, one of the strategies is to reduce steric hindrance of binding by extending mAbs away from the MB surfaces. It was attempted to bind mAbs to MBs *via* sAbs. sAb-MBs were synthesized first and incubated in mAb solution to bind mAb. After MBs were removed from mAb solution and re-suspended in the buffer, the mAb-bound sAb-MBs showed binding to the P4-OVA surface. In this format of mAb and MB conjugates, sAbs served as a linker between mAbs and MBs to extend mAb away from the MB surface and the steric hindrance of binding was reduced.

Further, the P4 inhibition assay using mAbs and sAb-MBs showed an LOD of 0.043 ng/ml P4 in the buffer, which was more sensitive than that of using mAbs alone (0.82 ng/ml, see Section 2.3.4 in Chapter 2). Also, this assay achieved a wider range of P4 detection towards both lower and higher concentrations of P4 (Figure 4.1). However, it was observed that sAb-MBs might have some non-specific binding to this P4-OVA surface, as about 20% of binding remained even when 1 µg/ml P4 was used to inhibit binding.
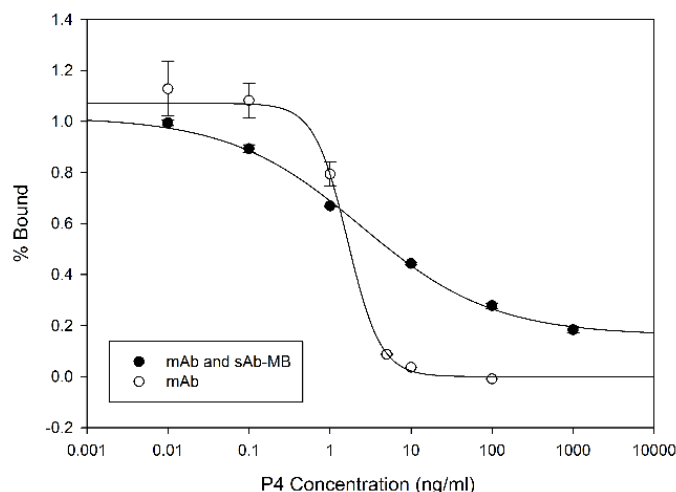
Figure 4.1 P4 inhibition assay using mAbs and sAb-MBs compared to that of using mAbs alone. Each data point was repeated in triplicates.

MBs can effectively amplify SPR signals due to their high refractive index and high molecular weight [164, 165], so they can improve SPR detection sensitivity and enable the detection of P4 of lower concentrations. The LOD of the P4 inhibition assay using mAbs and sAb-MBs was as sensitive as those using sAbs to enhance SPR signals [68, 69]. Although some P4 SPR assays enhanced by GNPs achieved higher detection sensitivity [69], the regeneration of SPR surfaces is often very difficult when GNPs are used, which affects the reuse of SPR surfaces. However, these MB conjugates did not cause such a problem. The regeneration of the P4-OVA surfaces after MB conjugate binding was performed by injection of NaOH (up to 50 mM) with P20 (up to 0.05% v/v) for less than 1 min. The baselines were reasonably stable over multiple binding and regeneration cycles; and the P4-OVA surfaces were used for hundreds of binding and regeneration cycles over several months. The baselines of a P4-OVA surface used for assays with MBs over multiple binding and regeneration cycles are provided in Figure A5 in the Appendices. Also, the large surface area of MB allowed multiple antibodies to attach to one MB. The numbers of mAb molecules on MB surfaces likely have distribution from one mAb to multiple mAbs per MB. MBs with more mAb molecules bound to it need P4 of higher concentrations to block all the binding sites, which resulted in complete inhibition of MB conjugates at higher concentrations of P4 and enabled the detection of P4 of higher concentrations. Thus, the detection range of the P4 SPR assay using mAbs and sAb-MBs was wider than using mAbs alone.

4.3.2 Non-specific binding of milk in P4 inhibition assays using mAbs and sAb-MBs

Although mAbs specifically bind P4, milk components such as proteins, fats and carbohydrates may bind to MBs, mAbs and sAbs non-specifically, which may affect the interaction between P4, mAbs and sAb-MBs in assays, and may also cause the carry-over of milk components to SPR measurement and affect the measurement. To assess non-specific binding of milk, mAbs and sAb-MBs were incubated with diluted or undiluted milk before being separated using a magnet and re-suspended in HBS-EP buffer. Then the beads were examined visually (Figure 4.2) and their bindings to the P4-OVA SPR surface were compared to mAbs and sAb-MBs incubated in the buffer (Figure 4.3).

Visually, MBs incubated in undiluted milk, and 1:10 diluted raw milk, formed aggregates upon separation by using a magnet and did not disperse well in HBS-EP buffer. Also, the color of these MBs changed from dark brown to light brown, and the bead re-suspension appeared more turbid and 'milky' compared to the other MBs (Figure 4.2). The aggregation possibly occurred during separation using a magnet when the beads gathered due to the magnetic field. It was likely that the milk components which non-specifically bound MBs or antibodies caused the aggregation *via* protein-interaction, electrostatic attraction, hydrophobic interaction, *etc.* In contrast, MBs incubated in 1:100, 1:1000 diluted milk and 1:10 diluted homogenized and pasteurized milk did not appear visually different from the control (MBs incubated in HBS-EP buffer), therefore the bindings of these MBs to the P4-OVA surface were measured.

	HBS-EP buffer (control)	Homogenized and pasteurized milk				Raw milk			
		Diluted (v/v)			un-diluted	un-diluted	Diluted (v/v)		
		1:10	1:100	1:1000			1:10	1:100	1:1000
Mixture of mAb, sAb-MB and milk or buffer									
Separation of mAb and sAb-MB from milk or buffer									
Resuspension of mAb and sAb-MB in buffer									
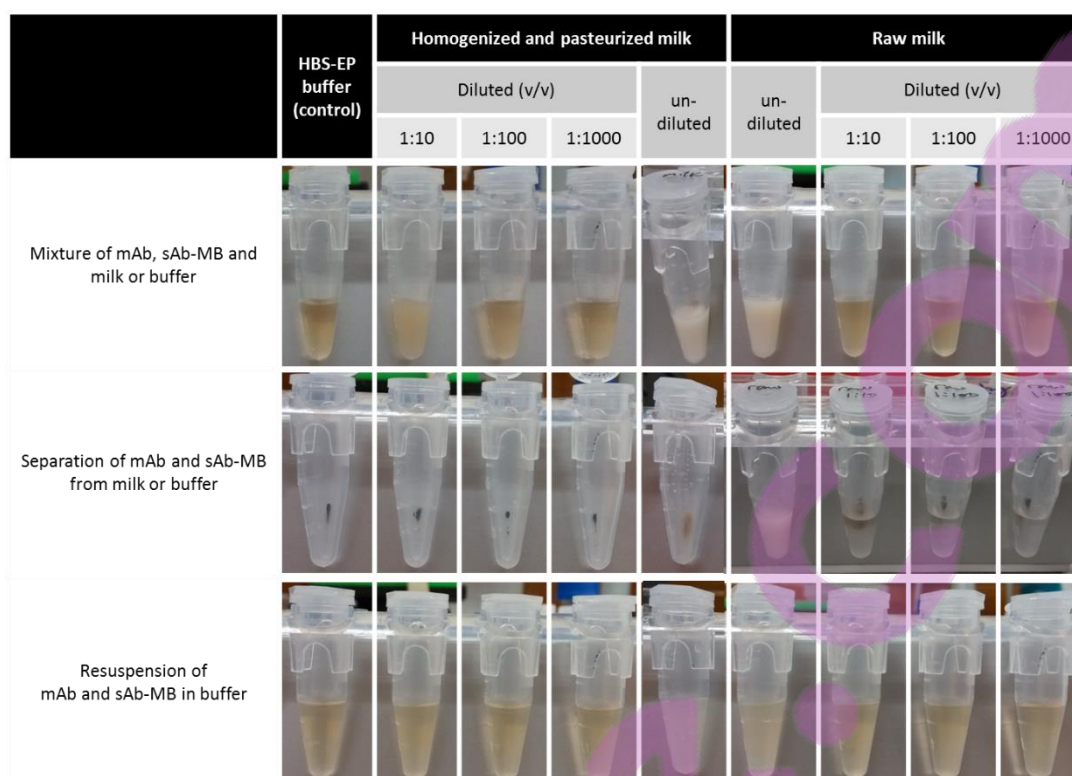
Figure 4.2 Non-specific binding of milk to mAbs and sAb-MBs.

Compared to the control, MBs incubated with 1:100 diluted milk showed no obvious difference in the binding to the P4-OVA SPR surface (Figure 4.3), but the bindings of MBs incubated with 1:10 diluted homogenized and pasteurized milk resulted in much higher SPR signals. Thus, 1:100 dilution of milk is preferred. The increase in the SPR signals was possibly caused by the milk components carried over *via* non-specific binding to MBs and antibodies, or *via* adhesion to the bead surfaces and the tube walls due to surface tension. Such carry-over of milk may be reduced by washing MBs in the buffer (multiple cycles of separation and re-suspension of MBs in the buffer).
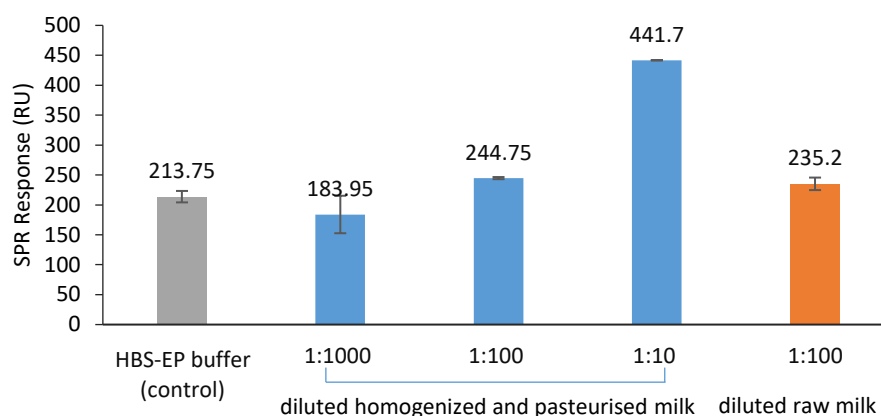
Figure 4.3 The bindings of mAbs and sAb-MBs to the P4-OVA SPR surface after incubation in diluted milk and the buffer. Each data point with error bar was repeated in duplicates.

However, after MBs were washed in the buffer, the binding of MBs to the P4-OVA SPR surface dropped significantly, ~50% decrease after three washes (experiment data available in Table A4 in the Appendices). Similarly, when MBs coated with Protein A were used to replace sAb-MBs in the assays, they initially bound to the SPR surface well, but the bindings decreased significantly after one wash in the buffer. It was likely that washing MBs in the buffer affected the binding equilibrium of mAbs and sAbs or Protein A (Figure 4.4a). After incubation in mAb, the binding of mAb and sAbs, or Protein A, reached equilibrium. Yet, the separation of MBs from mAb solution, and the resuspension of them in the buffer, removed free mAbs and caused the binding complex to dissociate and release free mAbs to reach a new equilibrium. Washing MBs in the buffer kept removing free mAbs and led to more dissociation of mAb from MBs. The dissociation constants (KD) of the binding between sAbs or Protein A and mAb are in the nanomolar range (10^{-7} to 10^{-9} M) [166-168] and the total concentration of sAbs or Protein A in the assays was in the low nanomolar range (10^{-8} to 10^{-9} M). Therefore, after free mAbs were removed and new equilibriums reached, the ratio of free Protein A, or sAb to KD, (represented by [A]/KD in Figure 4.4c) was close to or less than 1, and the ratio of bounded mAbs and free mAbs (represented by [AB]/ [B] in Figure 4.4c) as well. That means a significant portion of mAbs would dissociate from sAb or Protein A on the MB surfaces, which causes the decrease of MB bindings to the P4-OVA SPR surface. To solve this problem, mAbs need to be bound to MBs irreversibly *via* covalent bonds or using bindings of higher affinity such biotin and streptavidin interaction [169].

(a) $AB \leftrightarrow A + B$ (b) $K_D = \frac{[A][B]}{[AB]}$ (c) $\frac{[AB]}{[B]} = \frac{[A]}{K_D}$
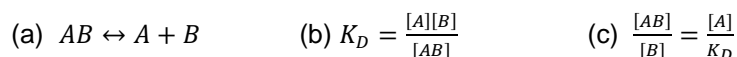
Figure 4.4 Binding between mAbs and sAbs or Protein A reaction, where 'A' represents free sAb or Protein A, 'B' represents free mAbs and 'AB' represents bounded mAbs: (a) binding reaction; (b) definition of K_D, where [A], [B] and [AB] are the concentrations of A, B and AB; (c) the ratio between the concentrations of the bounded mAbs [AB] and free mAbs [B] at equilibrium.

4.3.3 Synthesis of mAb and MB conjugates and their binding on the SPR surface

While it is necessary to bind mAbs and MBs covalently, it is also important to maintain the binding of mAb and MB conjugates to P4 on the SPR surface. Both the SPR surface and the mAb and MB conjugates were optimized. A T3C SAM SPR surface was immobilized with a P4-26 atoms linker-OVA using the *in situ* synthesis approach developed in Chapter 3 (Scheme 4.2a) to replace the T3C SAM surface immobilized with pre-synthesized P4-OVA. On the new SPR surface, P4 was extended further away from the surface and thus was more accessible to MBs for binding. Meanwhile, it was aimed to synthesize mAb and MB conjugates where mAbs were away from the MB surfaces and/or arranged with better orientation on the MB surfaces. Three different mAb and MB conjugates, mAb-sAb-MBs, b-mAb-str-MBs, and mAb-SMCC-MBs were synthesized as illustrated in Scheme 4.1. In these conjugates, mAbs were bound to MBs stably *via* either covalent bonds, or streptavidin and biotin interaction to ensure no dissociation of mAbs from MBs during the assays.

All three mAb and MB conjugates could bind to the new T3C SAM surface immobilized with P4-26 atoms linker-OVAs. Yet, these conjugates had different structural features. On one side, the distances between mAbs and MB surfaces were different. Among the three conjugates, mAbs were extended farthest away (~13 nm) from MB surfaces in mAb-sAb-MBs by PEG600-COOH coating on MB surfaces (~5 nm) [170] and sAbs (~8.5 nm) [171]. In b-mAb-str-MBs, mAbs were closer to MB surfaces (~8nm), linked by streptavidin (~5 nm) [172] and PEG2-biotin (~2.9 nm). In mAb-SMCC-MBs, mAbs were closest (~6nm), linked by PEG600-NH$_2$ coating on MB surfaces (~5 nm) and sulfo-SMCC crosslinkers (~0.8 nm). On the other side, the orientation of mAbs on MB were different. mAbs in both mAb-SMCC-MBs and b-mAb-str-MBs were linked to MBs *via* sulfhydryl groups reduced from disulphide bonds of mAbs, while mAbs in mAb-sAb-MBs were linked *via* primary amine groups of mAbs. There are only four disulphide bonds per antibody molecule, while the primary amine groups are more abundant. The linkages *via* sulfhydryl groups reduced from limited disulphide bonds resulted in a more uniformed

orientation of mAbs on MB surfaces than those *via* primary amine groups of mAbs. Uniformed orientation was found to improve the binding of antibody and particle conjugates by increasing surface density of antibodies and retaining antigen binding capacity better [163].

Therefore, the linkages *via* sulfhydryl groups of mAbs are preferable. This was also supported by our previous findings that the mAb and MB conjugates synthesized by covalently binding mAbs to MBs *via* primary amine groups failed to bind to the P4-OVA SPR surface. The linkages *via* amine groups probably resulted in poorly-oriented mAbs on MB surfaces, which had high steric hindrance from neighboring mAbs or a low surface density of mAb, or such linkages might lead to loss of antigen binding capacity. Thus, both the distance between mAbs and MBs, and the orientation of mAbs on the MB surfaces are important in the binding affinity between mAb and MB conjugates and P4.

According to the binding assays of these mAb and MB conjugates, 1:20 (v/v) diluted mAb-sAb-MBs, 1:10 (v/v) diluted b-mAb-str-MBs and 1:10 (v/v) diluted mAb-SMCC-MBs from stock suspensions of respective conjugates all had around 150 RU responses on the P4-26 atoms linker-OVA SPR surface, which was adequate for P4 inhibition assays. The binding affinities of these mAb and MB conjugates could not be compared based on these binding assays, as (1) the weight of these conjugates varied and SPR responses are related to the weight of bounded molecules or particles; and (2) the different conjugation procedures resulted in different bead concentrations of stock suspensions, although they were all theoretically calculated as a 1:5 (v/v) dilution from original MB stocks (6×10^{12} beads/ml). For example, there were 12 magnetic separations of MBs from supernatant during the synthesis of mAb-sAb-MBs, while there were only 4 separations and 10 separations for b-mAb-str-MBs and mAb-SMCC-MBs respectively. Although MBs were always left on a magnet long enough until the supernatants turned clear, not all the MBs would be separated from the supernatants and the loss of a small amount was unavoidable when the supernatants were removed. The more separation and removal of supernatants, the more loss of MBs and the lower concentrations of MBs. Besides, it was observed that during the synthesis of mAb-sAb-MBs some carboxylated MBs adhered to the tube walls after activation using EDC/NHS and could not be re-suspended into buffers, which led to the loss of beads.

4.3.4   Comparison of P4 inhibition assays using mAb and MB conjugates

The P4 inhibition assays using these three mAb and MB conjugates (Figure 4.5) showed different detection sensitivity and detection ranges of P4 as summarized in Table 4.1. The assay using mAb-SMCC-MBs showed the highest detection sensitivity. Both assays using mAb-SMCC-MBs and using mAb-sAb-MBs were more sensitive than the assay using mAb on this P4-26 atoms linker-OVA surface (Table 4.1). Also, the detection ranges were wider in the assays using mAb-SMCC-MBs and using mAb-sAb-MBs than those using mAbs (Figure 4.5). These were very similar to what were found previously with the P4 inhibition assay using mAbs and sAb-MBs (discussed in Section 4.3.1 in this chapter). Unexpectedly, the assay using b-mAb-str-MBs showed much lower detection sensitivity than the other two mAb and MB conjugates, possibly due to a relatively low binding affinity of b-mAb-sAb-MBs to the P4 SPR surface. It was suspected that mAbs in b-mAb-str-MBs were less flexible and less accessible to P4 on the SPR surface. mAbs in b-mAb-str-MBs were attached to streptavidin-MBs, where streptavidin was directly bound to MB surfaces without PEG600 as linkers between streptavidin and MB surfaces. In contrast, mAb-SMCC-MBs and mAb-sAb-MBs both had a PEG600 coating and the functional groups at the end of PEG600 (-COOH or $-NH_2$) were used to attach antibodies. PEG600 is a group of polyether compounds with an average molecular weight of around 600 Daltons and a length of ~5 nm. PEG600 is flexible and hydrophilic, which provides the flexibility to the bounded molecules on MB surfaces and increased their accessibility in aqueous buffers. Thus, lack of PEG600 may affect the binding of mAb and MB conjugates to the P4 SPR surface.
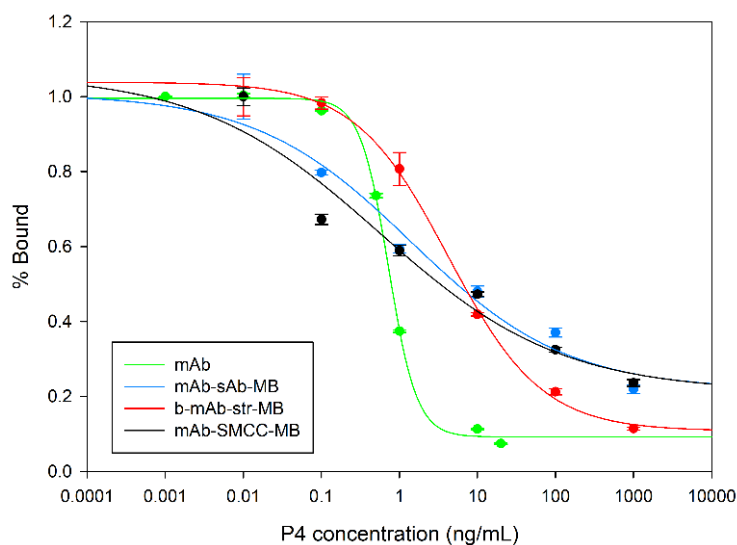
Figure 4.5 P4 inhibition assays using mAb and MB conjugates and mAb. Each data point was repeated in triplicates.

mAb-sAb-MBs and mAb-SMCC-MBs were similar in P4 detection sensitivity and detection ranges, but the polyclonal sAbs in mAb-sAb-MBs may cause more non-specific binding of milk matrix to MB conjugates, and the synthesis of mAb-sAb-MBs was more complicated and expensive than that of mAb-SMCC-MBs. Thus, mAb-SMCC-MBs were used for further experiments.

Table 4.1 Summary of LODs, EC50s and dynamic ranges of P4 inhibition assays using mAb and MB conjugates or mAb.

mAb and MB conjugates or mAb used in the inhibition assays	LOD (ng/ml)	EC 50 (ng/ml)	Detection range* (ng/ml)
mAb-sAb-MB	0.038	1.41	0.0091-217.87
b-mAb-str-MB	0.13	4.23	0.21-87.36
mAb-SMCC-MB	0.017	0.56	0.0015-196.68
mAb	0.12	0.72	0.29-1.81

* The detection range was defined as 10% to 90% of total inhibition.

4.3.5   Effects of different P4-OVA conjugates on the binding of mAb-SMCC-MBs

To further improve the detection sensitivity, it was attempted to improve P4-OVA conjugates immobilized on the SPR surface. In Chapter 3, the P4-OVA conjugate with a 32 atoms PEG linker was found to improve the binding of mAb to the sensor surfaces with relatively low non-specific binding due to the PEG moiety in the linker [107, 147-149]. Therefore, a new SPR surface was prepared by *in situ* synthesizing P4-32 atoms PEG linker-OVA (Scheme 4.2b). According to the binding assays of mAb-SMCC-MBs (Figure 4.6), mAb-SMCC-MBs bound 1.62 x more efficiently on the P4-32 atoms PEG linker-OVA surface than on the P4-26 atoms linker-OVA surface (Scheme 4.2a) used previously. The longer linker length extended P4 further away from the SPR surface and the PEG linker improved the flexibility of P4 movement, which increased P4 accessibility to mAb-SMCC-MBs and improved the binding. Further, relatively low non-specific bindings of P4-32 atoms PEG linker-OVA surfaces found in Chapter 3 are helpful to reduce the milk matrix effect. Thus, the P4-32 atoms PEG linker-OVA surface was used in the assays to test milk samples.
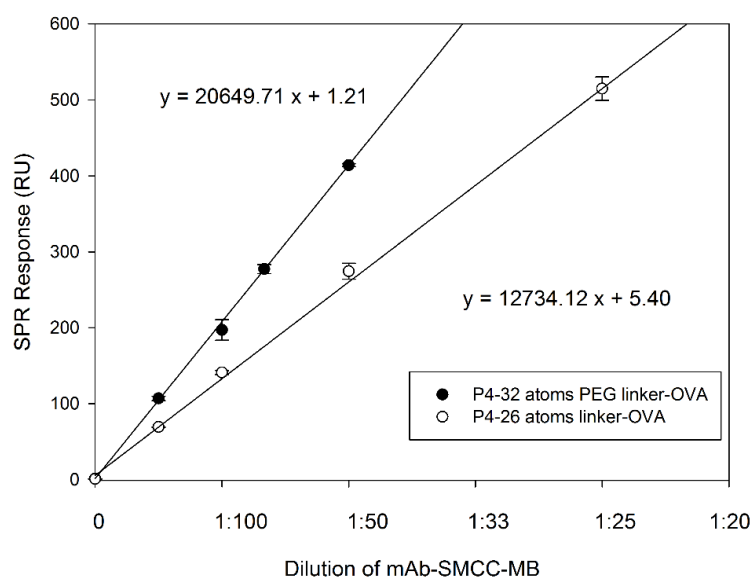
Figure 4.6 Binding assays of mAb-SMCC-MBs on the P4-26 atoms linker-OVA SPR surface and P4-32 atoms PEG linker-OVA SPR surface. Each data point was repeated in triplicates.

4.3.6   Performance of P4 inhibition assays using raw milk P4 standards

P4 inhibition assays were conducted using 1:100 (v/v) diluted raw milk P4 standards, as undiluted raw milk and 1:10 (v/v) diluted raw milk were found previously to cause the aggregation of MBs. Two examples of the inhibition assays conducted using diluted milk P4 standards, and P4 standards in the buffer, are shown in Figure 4.7 and Figure A6 in the Appendices. The LOD and EC50 of P4 inhibition assays using diluted raw milk P4 standards (1:100 v/v) were 0.036 ± 0.010 ng/ml (n=6, equivalent to 3.6 $\pm$ 1.0 ng/ml in undiluted raw milk) and 0.058 ± 0.017 ng/ml (n=6, equivalent to 5.8 $\pm$ 1.7 ng/ml in undiluted raw milk) respectively, while the LOD and EC50 of the assays using P4 standards in the buffer were 0.020 $\pm$ 0.006 ng/ml and 0.056 $\pm$ 0.022 ng/ml (n=4) respectively.

To be mentioned, the inhibition assays were conducted using P4 standards between 0-0.50 ng/ml and achieved about 20% or 25% inhibition (~100 RU) by 0.50 ng/ml P4 in diluted raw milk or in the buffer. Further inhibition could be achieved using P4 standards of higher concentrations as shown in Figure 4.5, where the binding of mAb-SMCC-MBs was reduced by ~75% using 100 ng/ml P4. Although the inhibition assays shown in Figure 4.5 were performed on the surface immobilized with a different P4-OVA conjugate – P4-26 atoms linker-OVA – it is expected that more inhibition of mAb-SMCC-MB binding on this P4-32 atoms PEG linker-OVA immobilized surface would be achieved using P4 standards of higher concentrations similarly. However, since cow's milk usually contains less than 50 ng/ml P4 (equivalent to 0.5 ng/ml when diluted 100 times), P4 standards of higher concentrations were not relevant to milk P4 detection and therefore were not used.
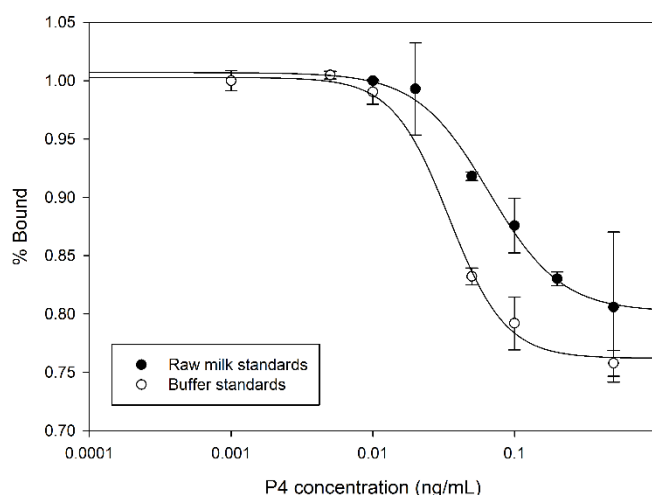
Figure 4.7 P4 inhibition assays using P4 standards prepared in the buffer and in diluted raw milk. Each data point was repeated in duplicates.

T-tests were performed to compare standard curves obtained by using P4 standards prepared in the buffer and in milk. A significant difference ($P<0.01$) was found between the two LODs but not the two EC50s (details available in Table A5 and Table A6 in the Appendices). In addition, the two standard curves were different in three aspects. First, the raw milk standard curve was shallower than the buffer one, which indicated that raw milk P4 standards were less effective in inhibiting the binding of mAb-SMCC-MBs. Second, mAb-SMCC-MBs incubated in raw milk P4 standards had (~ 20 RU) higher SPR responses than those incubated in the buffer standards of the same P4 concentrations. Third, standard deviations (SDs) of the SPR responses of mAb-SMCC-MBs incubated in raw milk standards were bigger than those incubated in P4 standards in the buffer. These differences were likely due to the milk matrix effect. Milk components may interfere in the binding of mAb-SMCC-MBs and P4 in milk, which led to less inhibition by milk P4 standards. Also, milk components may non-specifically bind to mAb-SMCC-MBs and not be removed by the wash steps and carried over to SPR measurement, which further led to higher SPR responses and bigger SDs. SDs affected detection sensitivity which may contribute to the difference in LODs.

The non-specific binding of milk components to MB surfaces was investigated using unmodified PEG-NH2-MBs of the same dilution following the same assay procedures of inhibition assays as described in Section 4.2.12. It was observed that non-specific binding of unmodified PEG-NH2-MBs on P4-OVA

surfaces was low (20-30 RU) and their binding responses increased slightly after incubation in HBS-EP for 30 mins (40-60 RU). Several types of milk and milk components were prepared to investigate non-specific binding of milk on unmodified beads. Milk fat was prepared by separating the top lipid layer of raw milk, which was heated at 50°C for 5 min and centrifuged at 18000 xg for 10 min. Protein-reduced raw milk was prepared by removing the bottom layer containing denatured proteins from raw milk, which was heated at 98°C for 10 min and centrifuged at 18000 xg for 10 min. Reconstituted non-fat milk was prepared using phosphate buffered saline with 5% non-fat milk (pH 7.3) from Sigma (P4739). Milk fat and protein-reduced raw milk as well as raw milk were diluted by 1:100 v/v and reconstituted 5% non-fat milk was diluted by 1:20 v/v using HBS-EP buffer with 0.01% P20. When unmodified PEG-NH2-MBs were incubated in the different diluted milks and washed as in the inhibition assays, the bindings of these unmodified MBs to P4-OVA surfaces increased up to 3 folds higher. Diluted raw milk led to the highest binding of unmodified MBs, followed by milk fat, protein-reduced raw milk and reconstituted non-fat milk. It indicated that milk fat played an important role in non-specific binding to MB surfaces. Compared to raw milks, the reconstituted non-fat milk from Sigma seemed to have less non-specific binding, likely due to fewer contaminates such as bacteria fragments, soil and dust and a more homogenized texture. These contaminates may also contribute to non-specific binding on MBs surfaces. Increasing surfactant concentrations in the buffers was found to reduce some non-specific binding, but varying salt concentrations in the buffers did not improve the results and sometimes led to aggregation of MBs. The effect of surfactants in the buffers also supported that fat may be a major source of non-specific binding on MB surfaces.

Some modifications of the assay procedures were attempted to further reduce the matrix effect on the assay: (1) raw milk was preheated to denature milk proteins and centrifuged to remove proteins and fat before incubation with mAb-SMCC-MBs; (2) mAb-SMCC-MBs were blocked by 1% BSA before incubation with raw milk; (3) 0.1% BSA was added to incubation buffer; (4) different wash procedures were compared, such as adding salt (0-1M NaCl) and detergent (0.01 – 0.5% Tween 20, Triton X-100 or P20) in the washing buffer, including a surface wash step by injecting buffer over the SPR surface after the injection of mAb-SMCC-MBs, and using more vigorous washing by vortexing mAb-SMCC-MBs, *etc.*; and (5) injection buffers and running buffers of various compositions (PBS and HBS) and detergents (0-1% PEG and 0-0.01% P20) were tested. Detergents, salt and BSA are commonly used

in immunoassays to reduce non-specific binding. Detergents disrupt ionic and hydrophobic bonds, salt neutralizes the surface charge and interrupts electrostatic attraction, and BSA occupies non-specific binding sites on surfaces. However, none of the above modifications of assay procedures could further reduce the milk matrix effect and improve assay results, while some of them caused other problems. For example, it was difficult to remove milk protein and fat after heating and centrifuging milk samples, which caused variations in sample preparation and further assay results; some of the washing buffers led to aggregation of MBs; some detergents such as Tween 20 of high concentrations (> 0.05%) and Triton X-100 in the washing buffer, running buffer or injection buffer affected the binding of mAb-SMCC-MBs to milk P4 or P4 on the SPR surface; mAb-SMCC-MBs blocked by 1% BSA resulted in lower detection sensitivity of P4 inhibition assay and big SDs.

The difficulty in reducing the milk matrix effect lies in the complications and limited understanding of the milk matrix effect on immunoassays, *i.e.* which milk component affects assays and what kind of interference it is. Only limited publications are found on how milk components affect immunoassays. Parker *et al.* suggested the denaturation of whey proteins, particularly α-lactalbumin affected electrochemical immunoassays [173]. Brandon *et al.* found milk sugar such as galactose and lactose increased dissociation of antibody and antigen binding [174]. Vogt *et al.* found non-fat milk or casein formed a monomolecular film of casein on plastic surface of ELISA microtiter plates [175]. Thus, various milk components such as proteins, sugar and fat are possible to interfere in immunoassays, thus it was difficult to identify the sources of interference and use specific methods to reduce their effects.

Further, the problem with the milk matrix is complicated by heterogeneity of raw milk from different cows, *i.e.* variations in protein and fat contents, somatic cell counts and pH values. Some raw milk samples were so different from each other that they could be easily distinguished by color and viscosity of the samples. The heterogeneity of raw milk is related to the genetic background [176], physiological condition [177], collection time [178] and dietary composition [179] of cows. In addition, unpasteurized raw milk potentially contains bacteria [180] of various amounts and species. All these variations among individual samples may result in different types and levels of effects on immunoassays, which led to inconsistency in the effectiveness of milk pretreatment methods and wash steps. In addition, P4 inhibition assays using MBs on SPR involve two types of surfaces, MB surfaces and the SPR surfaces, so non-specific binding of milk matrix needs to be reduced on both. In particular, not all the common

methods to reduce non-specific binding are suitable for SPR surfaces, due to the flow-through configuration of SPR instruments. For example, protein blockers are not cost-effective on SPR surfaces as they will be removed by regeneration steps and then blocking will need to be repeated before every injection. All of the above made it difficult to reduce the milk matrix effect on immunoassays and SPR measurements.

4.3.7   Measurement of P4 in raw milk samples

Raw milk samples were collected from two cows on different days during their estrous cycles. The P4 concentrations of these samples were measured by P4 inhibition assays using mAb-SMCC-MBs on SPR and by Ridgeway's milk P4 ELISA assays. The concentrations measured by the two methods were listed in Table 4.2 as well as the recovery rates, which were calculated by dividing the P4 concentration measured by SPR assays by that measured by ELISA assays. The recovery rates varied between 19% and 371%, indicating that the concentrations measured by SPR assays did not accurately represent those measured by ELISA. However, the concentrations measured by the two methods showed good correlation (P values < 0.05). Also, when the P4 concentrations were plotted against the sample collection days (Figure 4.8), the P4 concentrations measured by both methods showed similar trends of P4 level changes, which followed the estrous cycles of the cows.

Table 4.2 Summary of milk P4 concentrations of two cows on different days during their estrous cycles measured by SPR assays and ELISA.

Cow no.	Day	P4 concentration by SPR (ng/ml)	P4 concentration by ELISA (ng/ml)	% recovery *	Pearson correlation efficient	P value
310	15	54.9	22.7	241%	0.967	<0.01
	17	3.3	4.9	66%		
	18	0.5	2.2	21%		
	21	0.5	2.6	18%		
	24	3.3	4.3	78%		
	25	11.6	11.8	99%		
	28	37.6	24.6	153%		
	32	67.6	39.2	173%		
59	1	11.5	10.8	107%	0.842	0.0354
	6	-**	0.3	-		
	10	14.0	7.0	200%		
	18	63.4	17.1	371%		
	21	13.1	10.8	121%		
	24	1.3	0.5	265%		
	27	1.0	0.6	173%		

* % recovery = (P4 concentration measured by SPR assays) / (P4 concentration measured by ELISA) x 100%

** The SPR response of the sample was higher than the upper limitation of the equation. The concentration was expected to be close to 0.

Some issues during milk P4 measurement by the developed SPR assays were noticed. First, the measurement of raw milk samples had relatively big SDs, which was likely due to the milk matrix effect as discussed in Section 4.3.6. Big SDs led to low accuracy of P4 measurement. Second, the dynamic range of the raw milk P4 standard curve was about 1 - 20 ng/ml P4 in undiluted milk (Figure 4.7), but the standard curve tended to reach platforms at P4 < 2 ng/ml and > 10 ng/ml, which made the measurement of P4 in these concentration ranges less reliable. Third, SPR responses of some samples were outside the SPR response ranges of raw milk P4 standards. This was likely due to the difference in non-specific binding on MBs and SPR surfaces caused by the heterogeneity of raw milks of individual

cows, as discussed in Section 4.3.6. Fourth, the measurement of P4 concentrations of the same milk samples varied between assays, which may be partly caused by non-homogenization of raw milk.
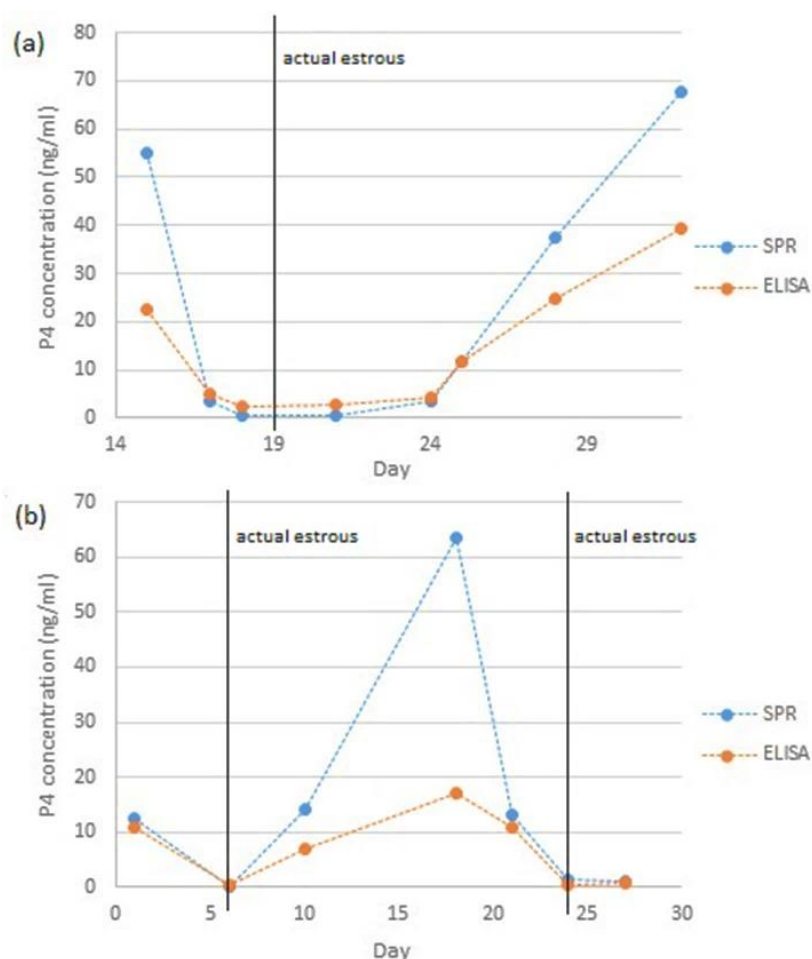
Figure 4.8 The P4 concentrations measured by SPR assays and by ELISA plotted against the days during estrous cycles of two cows: (a) cow no. 310 and (b) cow no. 59.

Raw milk is not homogenized, in which fat globules of small sizes dispersed in the aqueous phase of milk and those of large sizes form a layer of cream on the top [156]. Since P4 in milk is largely (~80%) associated with milk fat [181, 182], it is important that milk fat is distributed evenly before sampling. Thus, before sampling these raw milk samples, each sample was heated at 40°C to melt the cream layer and then was vortexed to form relatively homogenized emulsion. However, temperature changes and the homogenization process [183] potentially affect milk fat globules [184]. When raw milk samples as well as raw milk P4 standards were used several times, they went through multiple cycles of heating, vortexing and cooling over days, which affect milk fat globules and even deteriorate milk. Also, these

79

raw milk samples were collected three years ago and long term storage of milk was found to affect milk fat globules [185]. The changes of physic-chemical characters of milk, especially milk fat, may affect the partitioning of P4 in milk [186, 187], the quality of milk and further milk P4 measurement. Thus, besides the heterogeneity of raw milk from different cows (discussed in Section 4.3.6), non-homogenization and a long storage history of raw milk samples may be partly accounted for the limited accuracy and consistency of milk P4 measurement using the developed SPR assay.

To improve the developed SPR assay on milk P4 measurement, efforts can be made on: (1) investigating more relevant blocking reagents (*e.g.* casein solution) and more effective wash methods to further reduce the milk matrix effect; (2) developing better homogenization (*e.g.* sonication) methods to improve consistency in sampling and limit temperature changes of milk samples; (3) exploring more accurate and reliable milk P4 standards (*e.g.* commercial available milk P4 standards); (4) optimizing detection range of the assay (*e.g.* adjusting the concentrations of mAb-SMCC-MBs); and (5) determining a practical cut-off of P4 concentrations that can be measured by the assays and further diluting samples (>1:100) over this value to improve the measurement at the high concentration range.

It is worth mentioning that raw milk P4 standards are critical to the accuracy of measurement. In the current method, the raw milk P4 standards were prepared by spiking small amounts of concentrated P4 standards in raw milk of an anestrous cow. In this raw milk sample, no P4 was detected by ELISA. In nature cow's milk, ~80% P4 was found in the lipid fraction, 19% in the casein fraction, and 1% in the aqueous phase of milk [182]. However, it was unknown whether spiking P4 in raw milk resulted in similar partition of P4, and different partition of P4 may lead to different P4 measurement results. The other concern is that whether P4 in nature cow's milk is associated with any biomolecule, and whether P4 in raw milk standards does the same, since free P4 and bound P4 may interact differently with mAbs and further lead to different assay results.

Interestingly, the SPR responses obtained during the SPR assays from milk samples correlated to the P4 concentrations of these samples measured by ELISA. Figure 4.9a and 4.9c plotted the SPR responses, and the P4 concentrations measured by ELISA of each sample along the sample collection days during the estrous cycles for the two cows respectively. It is to be noted that the axes of P4 concentrations were in a reverse order. Clearly, the changes of SPR responses matched the

changes of P4 concentrations and coincided with the estrous cycles. In Figure 4.9b and 4.9d, the SPR responses were plotted against the P4 concentrations measured by ELISA and they showed good negative correlation (P values < 0.01). Therefore, it may be possible to predict the onset of estrus of cows using SPR responses directly, without the need of calculating P4 concentrations from raw milk P4 standard curves. That would simplify experiment and analysis procedures, save time and workloads and solve the issues related to raw milk P4 standards.
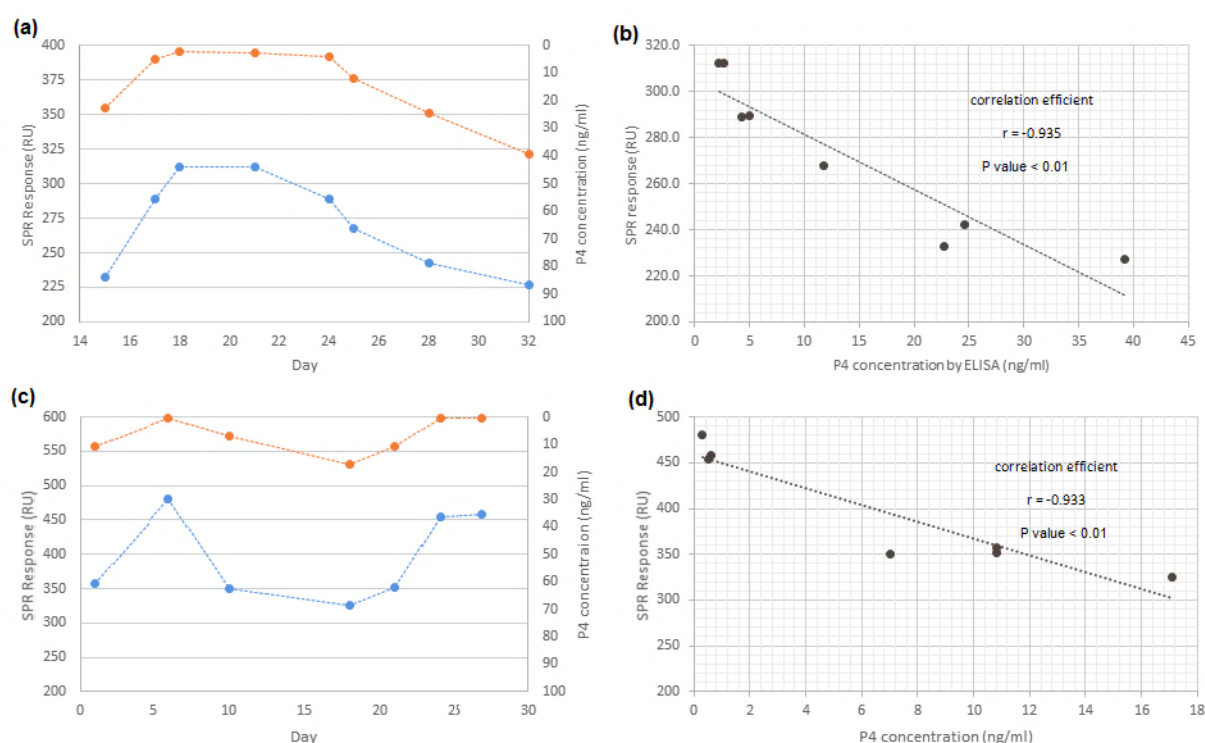
Figure 4.9 Comparison of the SPR responses obtained during the SPR assays on milk samples and P4 concentrations of the samples measured by ELISA: (a) and (c), the SPR responses (blue) and the P4 concentrations (orange) of each milk sample plotted along the sample collection days during the estrous cycles of cow no. 310 and no. 59 respectively; (b) and (d), the SPR responses plotted against the P4 concentrations measured by ELISA of milk samples of cow no. 310 and cow no. 59 respectively.

4.4   Conclusions

In this chapter, a sensitive SPR inhibition assay using mAb and MB conjugates was developed for P4 detection and achieved an LOD of 0.020 ± 0.006 ng/ml P4 in the buffer. The detection sensitivity of this assay was higher than the assay using mAb alone, due to SPR signal enhancement by MBs. The high sensitivity of the developed assay allowed testing P4 from diluted milk samples while diluting milk with

a buffer reduces the matrix effect. mAb and MB conjugates were used to separate P4 from raw milk before SPR measurement, and thus the milk matrix effect was further reduced. The inhibition assay using diluted P4 standards prepared in raw milk showed a similar detection sensitivity (0.036 ± 0.010 ng/ml P4) to that of using P4 standards in the buffer. P4 concentrations of raw milk samples were measured directly by the developed SPR assay. Although there were differences between the P4 concentrations determined by this SPR assay, and those measured by a commercial ELISA kit, they showed good correlation with each other (P values < 0.05) and exhibited the expected patterns of P4 level changes during the estrous cycles. In addition, the SPR responses obtained during the assays from milk samples correlated well with the P4 concentrations measured by ELISA (P values < 0.01) and may be used to predict estrous cycles of cows directly, without the need of calculating P4 concentrations from a standard curve. Future improvements on this SPR inhibition assay using mAb and MB conjugates for milk P4 measurement would focus on further lowering milk matrix effects, increasing the milk P4 detection range and developing better milk handling methods to achieve more accurate and consistent measurements. Nevertheless, to our knowledge, the P4 test developed here was one of the first SPR P4 tests using MB-antibody conjugates. Also, it may have other applications such as monitoring P4 levels in river or waste water, whose matrix effects are less complicated than that of milk.

5 Chapter 5: Investigating a P4 Aptamers for the Replacement of *anti*-P4 Antibodies

5.1 Introduction

Aptamers, whose name derives from the Latin word *aptus,* which means 'to fit', are commonly thought of as nucleic acid molecules (both RNAs and DNAs) that specifically bind to their target molecules [86], though they may also refer to functional peptides [188, 189]. Since the *in vitro* approaches to select and isolate aptamers were developed in 1990 [92], aptamers have been selected for almost all kinds of targets including metal ions, small molecules, proteins, viruses, cells, *etc.* and applied in the research, purification, biosensors, diagnostics and therapeutics [190]. With rapid progresses in aptamer research, several aptamer databases are made available online [191].

Aptamers are expected to be good substitutions for antibodies. Antibodies, especially monoclonal antibodies, have been widely and successfully used in the research and application field for over 60 years, but they have a few limitations such as expensive and laborious selection and production processes, immunogenicity in *in vivo* application in non-host species, instability due to change of temperature and pH, a short shelf life, batch variation, and limitation on target molecules. In comparison, aptamers are relatively easy to develop, cheap to produce, consistent between batches and stable during storage. A more detailed comparison is available in Chapter 1 of this thesis, and in the reviews by Jayasena, Stolenburg *et al* [92] and Mairal *et al* [193]. Therefore, it is of interest to investigate the potential of P4 aptamers in replacing mAbs as recognition molecules of P4 in the biosensors to develop P4 aptasensors.

Currently, there are seven publications that focus on P4 aptamers including eight different single strand DNA (ssDNA) aptamer sequences (Table 5.1). The first publication on P4 aptamers reported five DNA aptamers (P4-G03, P4-G04, P4-G06, P4-G11 and P4-G13 in Table 5.1) with the K_D in the nanomolar range determined by fluorescence assays and EIS, and an EIS aptasensor was developed using a P4-G13 aptamer and achieved an LOD of 0.9 ng/ml P4 in the buffer [97]. Using the same aptamer P4-G13, two colorimetric aptasensors were developed based on GNP aggregation analysis and achieved LODs of 0.8 ng/ml and 0.27 ng/ml P4 respectively [100, 101]. The binding sequences of P4-G13 were investigated using truncated sequences of P4-G13 and a 21 nucleotides truncated sequence of P4-G13 (P4-G13T2 in Table 5.1) was found to bind P4 more effectively. Using this P4-G13T2, a fluorescent

aptasensor achieved an LOD of 0.11 ng/ml P4 in the buffer [194]. Also, the interaction of P4 to P4-G13 was investigated using eight structurally-similar molecules of P4 and it was found that the A-ring of P4, the hydrogen substituents of the C1 and C2 atoms, together with the C19 methyl, in particular, was important for the binding [195]. Very recently, a luminescent aptasensor was developed using the P4-G03 aptamer together with an estradiol aptamer to detect P4 and 17β-estradiol simultaneously, and it achieved LODs of around 0.3 ng/ml for both hormones in the buffer [105]. This indicated good selectivity of these two aptamers between P4 and estradiol. In addition, aptamers composed with chemically modified nucleic acids were also selected for P4 binding. Three X-aptamers (P4-X3, P4-X4 and P4-X5 in Table 5.1), which use modified uridines and monothiophosphate backbone in oligonucleotides [196], were selected for P4 and showed K_D in the picomolar range measured by SPRi assays [102]. A sandwich assay using two of them achieved an LOD of 1.575 ng/ml P4 in the buffer, and to our knowledge this is the only sandwich assay for P4 detection so far.

Table 5.1 P4 aptamer sequences and related sequences reported in publications and developed by Neoventures Biotechnology for this project.

No.	Name	Description	Sequence	Length	K_D reported in the publications	References
1	P4-G13	P4 aptamer	5' GCA TCA CAC ACC GAT ACT CAC CCG CCT GAT TAA CAT TAG CCC ACC GCC CAC CCC CGC TGC 3'	60	35.23±8.30 nM (fluorescence assays) [97] 16.81±3.12 nM (EIS) [97] 1.1±0.7 nM (MST) [194]	[97, 100, 101, 194, 195]
2	Complementary-G13	A short complementary ssDNA to P4-G13, whose hybridization complex with P4-G13 was reported to increase the binding affinity of P4-G13 to P4	5' TGG GCG GTG G 3'	10	Not relevant	[97]
3	P4-G06	P4 aptamer	5' CAC GCA CAC AAC AGC CAA TAA TGT ATA ACG CTG TCC ACT GTG TGG TGT CCC CCG CGT CG 3'	59	28.66±12.20 nM (fluorescence assays) [97]	[97]
4	P4-G11	P4 aptamer	5' CAA CGA TCG TAC CAC AGT ACC CAC CCA CCA GCC CCA ACA TCA TGC CCA TGC GTC GGT GTG 3'	60	15.14±3.75 nM (fluorescence assays) [97] 12.58±1.39 nM (EIS) [97]	[97]
5	P4-G03	P4 aptamer	5' CAC ACA CGC AGC AAG GTC GTC GAT ACA AAA CGT ATC GAC CCG TCA CAG ACT GCC CCG GGT 3'	60	9.63±3.12 nM (fluorescence assays) [97]	[97, 105]
6	P4-G04	P4 aptamer	5' GGC ACG GCA AAG GGG TAC AGC CTA CCG AAC CGT GGC TGT AAG GGT GGT TGT GGT GTG 3'	57	133.30±40.51 nM (fluorescence assays) [97]	[97]
7	P4-G13T2	P4 aptamer, a truncated form of P4-G13	5' GAT TAA CAT TAG CCC ACC GCC CAC C 3'	25	2.1 nM (fluorescence-based displacement assays) [194]	[194]
8	P4-X3	P4 aptamer	5' TTT TTT TCT AGA GAT GTY TGT CTC AAC GTG CCC TGC GWC GTG ATC TTT TT 3' *	50	21.74±0.087 pM (SPRi) [102]	

No.	Name	Description	Sequence	Length	K_D reported in the publications	References
9	P4-X4	P4 aptamer	5' TTT TTT TCT AGA GAA GTY TGT CTT TCG CAY CAA GAG WTA CGG ATC TTT TT 3' *	50	28.10 ±0.107 pM (SPRi) [102]	[102]
10	P4-X5	P4 aptamer	5' TTT TTT TCT AGC TTC CGT GAA AYC AAC GTG CCC TGG WWC GTC TAG TTT TT 3' *	50	25.58 ±0.081 pM (SPRi) [102]	[102]
11	P4-CA	P4 aptamer	5' ATG CAG GTA AGG TCG ATG TGT TAA TTA AAA GTG TAT GCC G 3'	40	Not tested	Neoventures Biotechnology
12	Antisense-CA	A short antisense probe to P4-CA, whose binding to P4-CA was designed to be inhibited by the binding of P4 to P4-CA	5' ACA CTT TTC ACA TCG 3'	15	Not relevant	Neoventures Biotechnology

* The sequences include chemically modified nucleic acids. W represents dU with indole (tryptophan) attached to position 5 and Y represents dU with phenol (tyrosine) attached to position 5.

For this project, a P4 aptamer, P4-CA in Table 5.1 was selected and prepared by Neoventures Biotechnology Inc. (Canada), together with an antisense probe, Antisense-CA in Table 5.1. Antisense-CA was partially complementary to the P4-CA aptamer and was designed to compete with P4 in binding to P4-CA in inhibition assays. After selection, the binding of P4-CA to P4 was verified using GNP analysis and the effect of P4 on binding of P4-CA and Antisense-CA was investigated using SPRi by Neoventures (see the details in *Section 5.3.1* of this chapter). It is recommended to verify aptamer and target bindings using more than one method, since different methods often lead to different binding affinities and specificities of aptamers [197]. In addition, most methods only work with some aptamers but not all [198]. Therefore, in this chapter, several biosensing methods, or called aptasensors, were designed to verify the binding of P4, P4-CA and Antisense-CA using three different types of signals: SPR, fluorescence and colorimetric signals (Scheme 5.1-5.3), based on the experiment skills and the devices and materials available (Experimental procedures are provided in *Section 5.2 Materials and Methods* of this chapter).
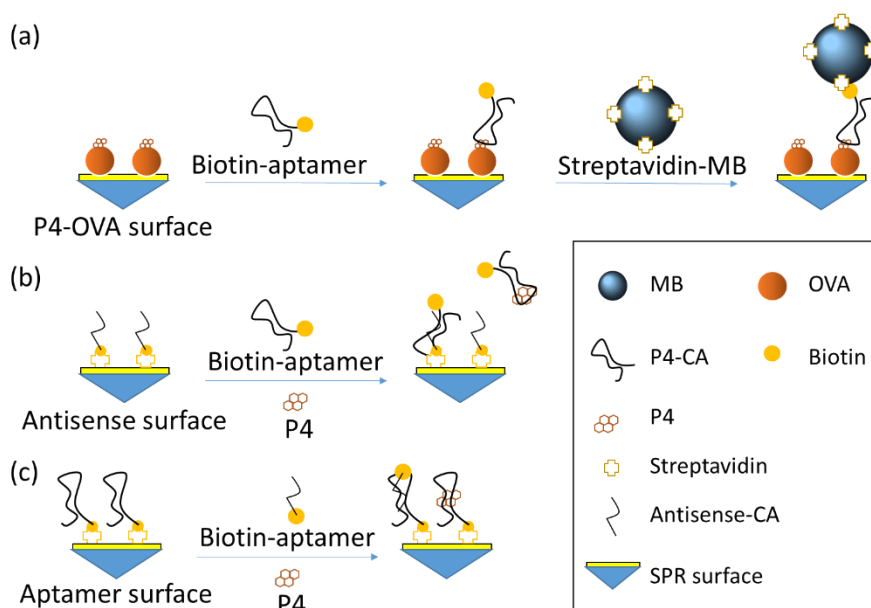
Scheme 5.1 SPR aptasensors: (a) direct assays to detect the binding of P4-CA on a P4-OVA immobilized surface with signal amplification by MBs; (b) and (c) indirect assays to detect the effect of P4 on the binding of P4-CA and Antisense-CA on SPR surfaces.
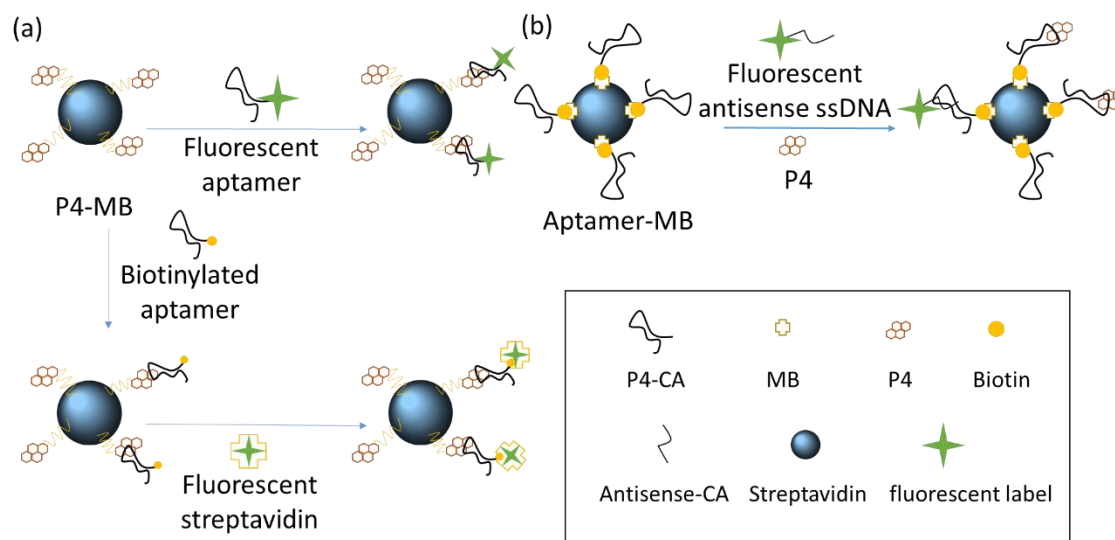
Scheme 5.2 Fluorescent aptasensors: (a) direct assays to detect the binding of fluorescent labeled P4-CA to P4 and MB conjugates; (b) indirect assays to detect the effect of P4 on the binding of P4-CA and Antisense-CA on MB surfaces.
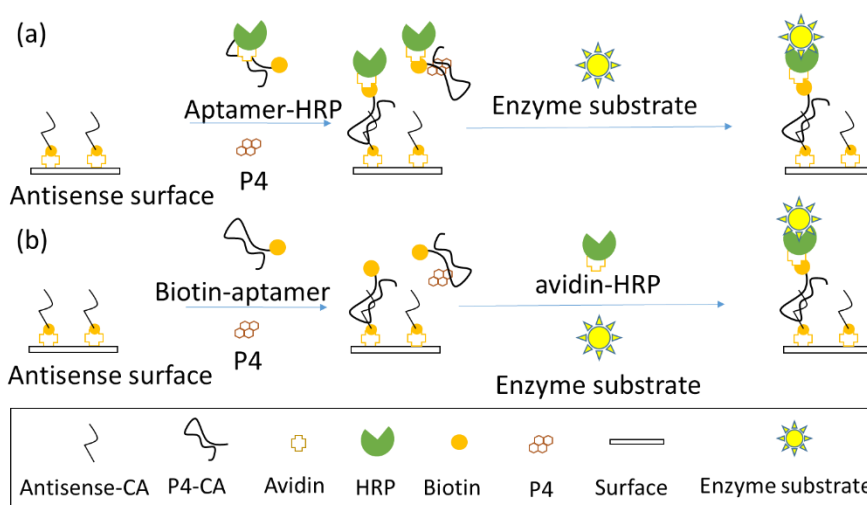
Scheme 5.3 Colorimetric aptasensors based on enzymatic reactions of horseradish peroxidase (HRP): (a) and (b) Indirect assays to detect the effect of P4 on the binding of P4-CA and Antisense-CA on sensor surfaces.

These aptasensors and assays vary in the modifications (immobilization and labeling) and the interaction of P4, P4-CA and Antisense-CA, as well as the transduction of signals so that they have different advantages and disadvantages as summarized in Table 5.2. Given the differences in these

aptasensors and assays, it was expected that the binding of P4-CA and P4 could be detected with all or some of them and the binding affinity of P4-CA to P4 could be compared with *anti-P4* antibodies to investigate the potential of P4-CA in replacing *anti-P4* antibodies in P4 detection.

Table 5.2 Comparison of the SPR, fluorescence and colorimetric P4-CA aptasensors.

Aptasensors	Advantages	Disadvantages
SPR	• Real-time detection • Quick detection (only a few minutes) • Simple procedures (no wash steps needed) • Sensor surfaces previously verified by the assays using P4 mAb • Efficient signal amplification by MBs	• Short interaction time limited by the injection volumes • Large amounts of materials required if aptamers of high concentrations are injected at high flow rates for a long time, which can be very expensive • Steric hindrance due to immobilization of P4 on relatively large SPR surfaces during direct assays • Inefficient SPR stimulation due to low molecular weights of P4 aptamers compared to *anti*-P4 antibodies • Electrostatic repulsion due to the negative charges of SPR surfaces (especially CM5 chips) and P4 aptamers
Fluorescent	• Relatively low steric hindrance due to relatively small surfaces of MBs compared to SPR surfaces • Long interaction time of P4 aptamer and P4 • Use of high concentrations of P4-CA and P4 in the assays without a huge cost due to a small reaction volume required	• Signal amplification limited by the number of fluorophores per aptamer (1-3 fluorophores per aptamer) • New sensor surfaces to be verified by *anti*-P4 mAbs binding before being used for aptamer test • More complicated and longer procedures (wash steps required)
Colorimetric	• Long interaction time of P4 aptamer and P4 • Use of high concentrations of P4-CA and P4 in the assays without a huge cost due to a small reaction volume required • Efficient signal amplification by enzymatic reactions	• New type of sensor surfaces, unfamiliar with physicochemical properties of such surfaces e.g. non-specific binding • More complicated and longer procedures (wash steps and enzymatic reaction required) • Variations due to performances of enzyme reactions

Direct binding of P4 and the aptamer P4-CA was detected using both the SPR and fluorescent aptasensors, but the binding signals of 1 μM P4-CA were much lower than those of 1 μg/ml (~6.6 nM) *anti*-P4 antibodies on the same sensor surfaces of both SPR and fluorescent aptasensors. Meanwhile,

P4 showed inhibition on the binding of P4-CA and Antisense-CA on the SPR, fluorescent and colorimetric aptasensors. However, the maximum inhibition effect of P4 was only about 18%, when 1 nM P4-CA was pre-incubated with 50 µg/ml P4 for one hour before being added to the Antisense-CA surface of the colorimetric aptasensor. Given the lower direct binding of P4-CA and the P4 surfaces, and the limited inhibition effects of P4 on the binding of P4-CA and Antisense-CA, it was suspected that the binding affinity of P4-CA and P4 was low, especially compared to *anti*-P4 mAb. It is possible to modify the design of these aptasensors to increase the binding of P4 and P4-CA or the inhibition effect of P4. However, since the information on P4-CA's binding affinity, binding sequences, etc. was not available, it was difficult to diagnose problems that might have caused the low binding between P4-CA and P4, or the limited inhibition effect of P4 on P4-CA and Antisense-CA. In the future, it would be helpful to develop methods to determine the binding affinity of P4-CA and study its binding sequences, from which it is possible to optimize P4-CA sequences for higher binding affinity, redesign its antisense probes, and improve these aptasensors for better performances in P4 detection.

5.2   Materials and Methods

5.2.1   Materials and instrumentations

The fluorescent labeled P4-CA and Antisense-CA were synthesized by Macrogen (Korea) with 5' modification of CY3 (Figure 5.1a). The biotinylated P4-CA and Antisense-CA were synthesized by IDT (USA) with biotin modification (Figure 5.1b) at 5' and 3' ends respectively. All the aptamers were dissolved in milli-Q water to 100 µM and stored at -20°C in the dark.
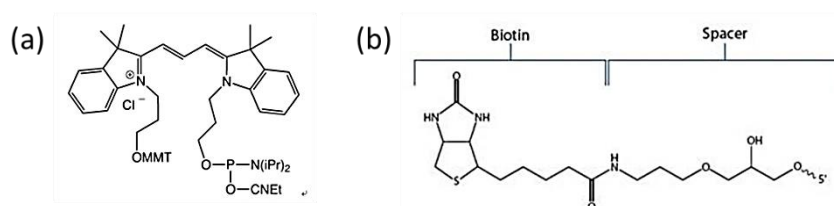
Figure 5.1 Modifiers of P4-CA and Antisense-CA: (a) CY3 and (b) biotin.

P4 3-CMO was supplied by Steraloids (Newport, USA). Anti-P4 monoclonal antibodies (7720-1430) were purchased from AbD Serotec, BioRad. The Cy3-labeled secondary antibody (F-sAb) (A10521)

was supplied by life technologies. Streptavidin (S4762), P4, biotin-PEG-amine (689882), bovine serum albumin (BSA), streptavidin-cy3 conjugates (F-streptavidin, S6402), avidin-horseradish peroxidase conjugate (avidin-HRP, 11371), avidin (A9275), 3,3',5,5'-Tetramethylbenzidine (TMB, 863306), hydrogen peroxide solution (216763) and PEG 400 were purchased from Sigma-Aldrich. NHS was supplied by ACROS organics. SPR CM5 chips, an amine coupling kit, a sodium acetate buffer (pH4.5), surfactant P20 and HBS-EP buffer were supplied by GE Healthcare Life Science. PEG-COOH-MBs (84-56-102), PEG-NH$_2$-MBs (84-55-102) and MBs (diameter = 100nm) coated with streptavidin (84-19-102) were purchased from Micromod Partikeltechnologie GmbH (Germany). TCEP (77720), Pierce™ NeutrAvidin™ Coated Plates (15129) and Zeba™ Spin Desalting Columns 7K MWCO (89882) were purchased from Thermo Fisher. 96 well high binding microplates (65506) were purchased from Greiner Bio One (Austria). T3C was supplied by DSL. Sulfo-SMCC crosslinker was purchased from Proteochem (Hurricane, USA). All other chemicals were purchased from Sigma-Aldrich.

The following buffers were used. PBS buffer (pH 7.4) contained 0.01 M phosphate buffer, 2.7 mM KCl and 137 mM NaCl. 10mM HEPES buffer (pH 7.4) contained 10 mM HEPES, 120 mM NaCl, and 5 mM KCl. HBS-EP buffer (pH 7.4) from GE healthcare contains 10 mM HEPES, 150 mM NaCl, 3 mM EDTA with 0.005% v/v P20.

All the SPR aptasensors were conducted on the Biacore Q system from GE Healthcare Life Science. The fluorescence intensity was measured by a FLUOstar Omega microplate reader from BMG LABTECH (Germany). The optical density (OD) values of colorimetric assays were measured by Epoch 2 from BioTek (USA).

5.2.2 SPR aptasensors

5.2.2.1 P4-CA binding on the P4-OVA surface (Scheme 5.1a)

0-1 µM biotinylated P4-CA was prepared by diluting biotinylated P4-CA stock solution (100 µM) in a 10 mM HEPES buffer. A gold SPR chip was coated with T3C self-assembled monolayer and immobilized with a pre-synthesized P4-OVA with a long PEG linker using the methods described in Chapter 2. 50 µl biotinylated P4-CA of each concentration were injected for 10 min on the P4-OVA surface before 30 µl diluted streptavidin-MBs (1:100 v/, 10 mM HEPES buffer containing 1% PEG400) was injected for 3 min. The surface was regenerated by multiple pulses of HCl (up to 10 mM), glycine (pH 2.0), NaOH (up to

100 mM), SDS (up to 0.1%) and P20 (up to 0.01% v/v) until SPR responses returned to previous baseline responses or could not be reduced further.

In addition, biotinylated P4-CA (0-500 nM) was mixed (1:1 v/v) with diluted streptavidin-MBs (1:5 v/v, 10mM HEPES buffer) respectively and incubated at room temperature for one hour under constant shaking to form P4-CA and MB conjugates, before the beads were washed three times and re-suspended in the buffer to a final dilution of 1:100 v/v. 30µl of 1:100 diluted P4-CA and MB conjugates were injected over the P4-OVA surface for 3 min before the surface was regenerated as described above. Each data point was repeated in duplicates.

5.2.2.2 Immobilization P4-CA or Antisense-CA on the SPR surfaces

To prepare the streptavidin surface, the flow cells of the CM5 chip were activated by injection of 100 µl of the mixture (1:1 v/v) of EDC (390 mM) and NHS (100 mM) for 10 min followed by injection of 150 µl streptavidin solution (0.2 mg/ml, sodium acetate buffer pH 4.5) for 30 min, then the surface was deactivated by injection of 100 µl ethanolamine solution (1 M, pH 8.5) for 20 min. To prepare the P4-CA surface and the Antisense-CA surface, 150 µl biotinylated P4-CA (2 µM, HBS-EP buffer) and biotinylated Antisense-CA (2 µM, HBS-EP buffer) were injected over two streptavidin surfaces for 30 min respectively before the surfaces were deactivated by injection of 100 µl biotin-PEG-amine (1 mg/ml) for 20 min.

5.2.2.3 P4-CA and Antisense-CA binding on SPR

A serial dilution of fluorescent-labeled Antisense-CA was prepared from stock solution in a 10mM HEPES buffer with 0.002% P20 and 50 µl of each dilution was injected over the P4-CA surface for 5 min. The surface was regenerated by HCl and NaOH.

Similarly, a series dilution of fluorescent-labeled P4-CA was prepared in a 10mM HEPES buffer with 0.002% P20 and 50 µl of each dilution was injected over the Antisense-CA surface. The effect of the flow rate was investigated by injecting P4-CA (100 nM) for 3 mins at different flow rates (5, 20, 50 µl/min) over the Antisense-CA surface. The effect of magnesium ion (Mg^{2+}) was investigated by injecting P4-CA (20 nM) for 2 min in 10mM HEPES buffer with 0.002% P20 containing various concentrations of magnesium chloride ($MgCl_2$) (0 - 15 mM) as both the injection buffers and the running buffers.

5.2.2.4 *The effect of P4 on the binding of P4-CA and Antisense-CA on SPR (Scheme 5.1b, c)*

On the P4-CA surface, the effect of P4 on the binding of Antisense-CA was tested in two formats; the pre-mix format and sequential injection format. In the pre-mix format, 40 nM fluorescent Antisense-CA (10mM HEPES buffer with 0.002% P20) was mixed with P4 (0, 100 ng/ml, 100 µg/ml) (1:1 v/v) respectively before 50 µl of the mixture was injected for 5 min over the P4-CA surface. In the sequential format, 50 µl of P4 (0, 50 ng/ml) was injected for 5 min before 50 µl of 20 nM Antisense-CA was injected for 5 min respectively. Each data point was repeated in duplicates.

Similarly, on the Antisense-CA surface, the effect of P4 on the binding of P4-CA was tested. In the pre-mix format, 20 nM fluorescent-labeled P4-CA (10 mM HEPES buffer with 10 mM $MgCl_2$) was mixed with P4 (0, 100 ng/ml, 100 µg/ml) (1:1 v/v) respectively and incubated at room temperature for one hour before 50 µl of each mixture was injected for 5 min. In the sequential format, 50 µl of 10 nM P4-CA was injected for 5 min before 50 µl of P4 (0, 50 ng/ml, 50 µg/ml) was injected for 5 min. Then the injection sequence of P4 and P4-CA was reversed. Each data point was repeated in duplicates.

5.2.3 **Fluorescent aptasensors**

5.2.3.1 *Synthesis of P4 and MB conjugates*

To conjugate P4 with PEG-NH_2-MBs, 1 mg (2.58 µmol) P4 3-CMO was activated by 9 mg (46.9 µmol) EDC and 5.5 mg (47.8 µmol) NHS in 1ml DMF for three hours under constant stirring. 500 µl diluted and activated P4 3-CMO (1:1000 v/v, PBS, 2.58 µM) was mixed with 500 µl diluted PEG-NH_2-MBs (1:5 v/v, PBS, 2 nM) and incubated at room temperature for 2 hours under agitation. Then the synthesized conjugates (P4-NH_2-MBs, Figure 5.2a) were washed with PBS six times and re-suspended in 500 µl PBS with 0.005% P20 to a final concentration of 1:5 v/v (2 nM) from the original PEG-NH_2-MB stock.

5.2.3.2 *Synthesis of P4-OVA and MB conjugates*

Two different P4-OVA and MB conjugates were synthesized using PEG-COOH-MBs or PEG-NH_2-MBs.

To conjugate P4-OVA with PEG-COOH-MBs, 200 µl PEG-COOH-MBs were separated on a magnet to remove the supernatant before they were activated by 4 mg EDC and 8 mg NHS in 500 µl 0.1 M MES buffer at room temperature for one hour under agitation. Then the activated beads were washed twice

with PBS and re-suspended in 500 µl PBS before being mixed with 500 µl P4-OVA solution (400 µg/ml, PBS). The mixture was incubated at room temperature for three hours under agitation before the beads were washed once and deactivation using 1ml Glycine (1 M, PBS) for an hour. Finally, the synthesized conjugates (P4-OVA-COOH-MBs, Figure 5.2b) were washed three times and re-suspended in 1ml PBS with 0.05% P20 to a final concentration of 1:5 (v/v) from the original PEG-COOH-MB stock.

To conjugate P4-OVA with PEG-NH$_2$-MBs, 100 µl PEG-NH$_2$-MBs were re-suspended in 500 µl sulfo-SMCC (20 µM, PBS with 2 mM EDTA) and incubated at room temperature for one hour under agitation. Then the activated beads were washed twice before being re-suspended in 500 µl PBS and mixed with 500 µl P4-OVA solution (20 µg/ml, PBS with 2 mM EDTA). The mixture was incubated at room temperature for two hours under agitation before the beads were washed and the surface was deactivated using 1ml cysteine solution (2.5 mM, PBS with 2 mM EDTA) for one hour. Finally, the synthesized conjugates (P4-OVA-NH$_2$-MBs, Figure 5.2c) were washed three times and suspended in 500 µl PBS with 0.05% P20 to a final concentration of 1:5 (v/v) from the original PEG-NH$_2$-MB stock.
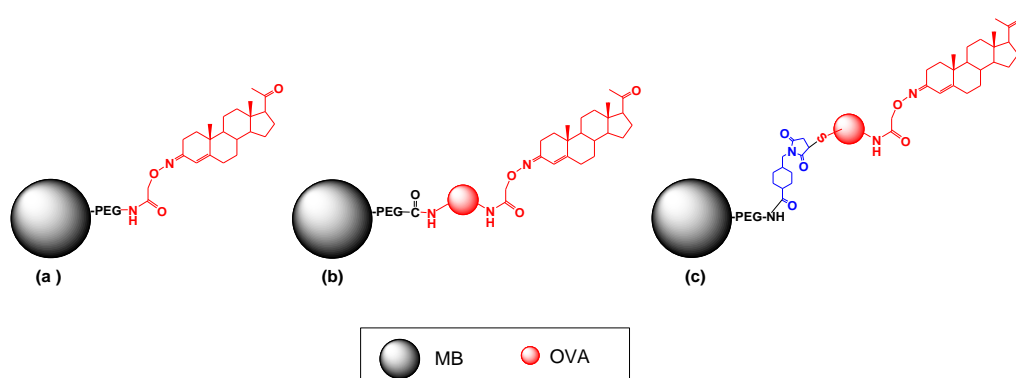
Figure 5.2 Conjugates of P4 or P4-OVA and MBs: (a) P4-NH$_2$-MBs, (b) P4-OVA-COOH-MBs and (c) P4-OVA-NH$_2$-MBs.

5.2.3.3 Evaluate P4-OVA/P4 and MB conjugates

Three conjugates, P4-OVA-COOH-MBs, P4-OVA-NH$_2$-MBs and P4-NH$_2$-MBs, were evaluated on their binding performance using mAbs and F-sAbs (Scheme 5.4). 100 µl of each conjugate was separated on a magnet to remove the supernatant and blocked by 200 µl 1% BSA (HBS-EP with 0.05% P20) for one hour before being washed and re-suspended in 200 µl 0.1% BSA (HBS-EP with 0.05% P20). Then

the conjugates were mixed (1:1 v/v) with 1 µg/ml mAbs (HBS-EP with 0.1% BSA and 0.05% P20) and incubated at room temperature for one hour under constant shaking before being washed three times and re-suspended in 200 µl 0.1% BSA (HBS-EP with 0.05% P20). Then the beads were mixed (1:1 v/v) with 1:1000 diluted F-sAb (HBS-EP with 0.1% BSA and 0.05% P20) and incubated at room temperature for one hour under constant shaking before being washed three times and re-suspended in 200 µl HBS-EP buffer. 100 µl of each bead re-suspension was added to the wells of black-walled microplates and the fluorescence was measured by FLUOstar using the excitation filter 'Ex544' and the emission filter '590-10' with a gain value of 2800. The mAb and MB conjugates (mAb-SMCC-MBs synthesized in Chapter 4) were used as positive controls and the unmodified PEG-NH$_2$-MBs as negative controls. Each data point was repeated in duplicates.
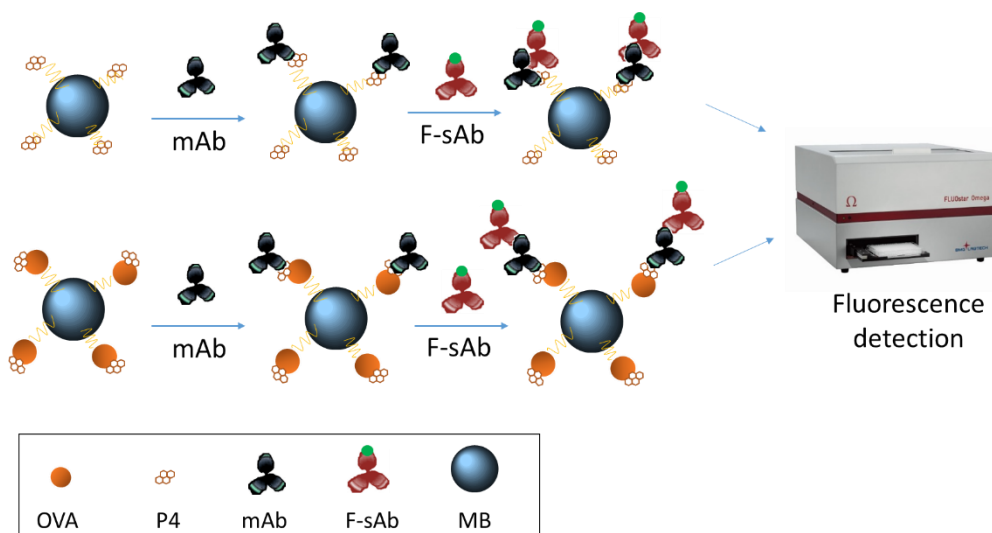
Scheme 5.4 Evaluation of P4 or P4-OVA and MB conjugates using mAbs and F-sAbs.

5.2.3.4 P4-CA binding to P4-NH$_2$-MBs (Scheme 5.2a)

The binding of P4-CA to P4-NH$_2$-MBs was detected in two formats as shown in Scheme 5.2a. 100 µl P4-NH$_2$-MBs were re-suspended in 100 µl 10mM HEPES buffer before being mixed with 1 µM fluorescent-labeled P4-CA (1:1 v/v, 10 mM HEPES buffer) and incubated at room temperature for one hour under constant shaking. After the beads were washed three times and re-suspended in 200 µl PBS, the fluorescence intensity of the bead re-suspension was measured as described above. The

unmodified PEG-NH$_2$-MBs mixed with fluorescent-labeled P4-CA and the P4-NH$_2$-MBs mixed with the buffer were used as negative controls. Each data point was repeated in duplicates.

In addition, 100 µl P4-NH$_2$-MBs were re-suspended in 100 µl 10mM HEPES buffer before being mixed with 1 µM biotinylated P4-CA (1:1 v/v, 10mM HEPES buffer) and incubated at room temperature for one hour under constant shaking. After the beads were washed three times, they were re-suspended in 200 µl 10 mM HEPES buffer and mixed with 200 µl diluted F-streptavidin (1:500 v/v, 10 mM HEPES buffer with 0.05% P20) and incubated at room temperature for another hour. Finally, the beads were washed three times and re-suspended in 200 µl 10 mM HEPES buffer. The fluorescence of the bead re-suspension was measured as described above. The unmodified PEG-NH$_2$-MBs incubated with fluorescent-labeled P4-CA, and F-streptavidin and the P4-NH$_2$-MBs incubated with the buffer and F-streptavidin were used as negative controls. Each data point was repeated in duplicates.

5.2.3.5 P4-CA and Antisense-CA binding on streptavidin-MBs

40 µl fluorescent-labeled Antisense-CA (200 nM) and 40 µl biotinylated P4-CA (200 nM) were mixed at room temperature for one hour before 20 µl diluted streptavidin-MBs (1:5 v/v, 10mM HEPBS with 40mM MgCl$_2$) were added to the mixture and incubated for another hour. Similarly, 40 µl fluorescent-labeled P4-CA (200 nM) and 40 µl biotinylated Antisense-CA (200 nM) were pre-incubated for one hour and mixed with streptavidin-MBs for another hour. Afterwards, the beads were washed three times and re-suspended in 200 µl 10 mM HEPES buffer and measured by FLUOstar as described above. As negative controls, fluorescent-labeled Antisense-CA or fluorescent-labeled P4-CA was incubated with the buffer before being mixed with streptavidin-MBs respectively as negative controls.

Further, 40 µl fluorescent-labeled Antisense-CA of various concentrations (0-1 µM) were mixed with 40 µl biotinylated P4-CA of various concentrations (0-1 µM) respectively and incubated for one hour before being added to 20 µl streptavidin-MBs to optimize the concentrations used in the binding of biotinylated P4-CA and fluorescent-labeled Antisense-CA. Each data point was repeated in duplicates.

5.2.3.6   The effect of P4 on the binding of Antisense-CA and P4-CA (Scheme 5.2b)

A serial dilution of P4 was prepared by diluting the P4 stock solution (10 mg/ml, methanol) in 10 mM HEPES buffer containing 40 mM MgCl$_2$. 20 µl of each P4 dilution (0-100 µg/ml) was incubated with

20 µl fluorescent-labeled Antisense-CA (400 nM) and 40 µl biotinylated P4-CA (200 nM) respectively at room temperature for one hour before 20 µl diluted streptavidin-MBs (1:5 v/v) were added to each mixture for another hour. After three washes, the beads were re-suspended in 200 µl 10mM HEPES buffer with 40 mM $MgCl_2$ and the fluorescence was measured as described above. Each data point was repeated in duplicates.

5.2.4   Colorimetric assay

5.2.4.1 Prepare the Antisense-CA plates

100 µl avidin (0.1 mg/ml, PBS) or streptavidin (0.01 mg/ml, PBS) was added to the wells of the 96 well microplates for at least one hour at room temperature, or at 4°C overnight, before the plate was washed three times with PBS with 0.05% Tween20. The plates coated with avidin or streptavidin were sealed and stored dry at 4°C or used immediately. To immobilize Antisense-CA, 100 µl biotinylated Antisense-CA (10 nM) was added to the wells of the plates coated with avidin or streptavidin, or Pierce neutravidin plates for one hour at room temperature before being washed three times. The Antisense-CA plates were used immediately.

5.2.4.2   P4-CA binding to the Antisense-CA plates (Scheme 5.3 a and b)

The binding of P4-CA to the Antisense-CA plates was detected in two manners as illustrated in Scheme 5.3. In Scheme 5.3a, 10 µl biotinylated P4-CA (100 µM, PBS) and 10 µl HRP-avidin (5 mg/ml, PBS) were diluted in 980 µl PBS and the mixture was incubated at room temperature for one hour to form conjugates (P4-CA-HRP). 100 µl diluted P4-CA-HRP (1:400, PBS with 0.05% Tween20) was added to each well for one hour at room temperature under constant shaking. After the plates were washed six times with PBS with 0.05% Tween20, 100 µl substrate solution (1mg/ml TMB and 0.2% concentrated H_2O_2, 10% Ethanol) was added at room temperature for no longer than 20 mins under constant shaking in the dark. The enzymatic reaction was stopped by adding 20 µl H_2SO_4 (2 M) to each well and the plates were read and recorded at 450nm by an Epoch 2-plate reader. In Scheme 5.3b, 100 µl P4-CA (2.5 nM, PBS) was added to each well for one hour at room temperature, under constant shaking, before being washed three times. Then 100 µl diluted HRP-avidin (1:40000 v/v, PBS with 0.05% Tween20) was added to each well for one hour before the plates were washed six times and the enzymatic reaction was performed, and the plates were read as described above. The wells of the

protein coated plates where no Antisense-CA was immobilized, and the Antisense-CA immobilized wells where no biotinylated P4-CA was added were used as negative controls. Each data point was repeated in triplicates.

5.2.4.3 The effect of P4 on the binding of P4-CA to the Antisense-CA plates

To test the effect of P4 on the binding of P4-CA to the Antisense-CA plates, the same procedures as that of the binding of P4-CA were followed except that: (1) in Scheme 5.3a, diluted P4-CA-HRP (1:200) and P4 solutions (0, 50 µg/ml) were mixed (1:1 v/v) respectively and incubated at room temperature for one hour, before 100 µl of the mixture was added to the wells for one hour instead of 100 µl diluted P4-CA-HRP (1:400); (2) in Scheme 5.3b, biotinylated P4-CA (5 nM) and P4 solution (0, 50 µg/ml) was mixed (1:1 v/v) respectively and incubated at room temperature for one hour, before 100 µl of the mixture was added to the wells for one hour instead of 100 µl biotinylated P4-CA (2.5 nM). Each data point was repeated in triplicates.

To optimize the condition for P4 inhibition, the Antisense-CA plates were prepared by adding biotinylated Antisense-CA of various concentrations (0.2 nM, 1 nM and 10 nM) and added to the streptavidin plates, and P4 solution (0 and 50 µg/ml) was mixed with biotinylated P4-CA of various concentrations (0.2, 1 and 5 nM) was mixed (1:1 v/v) before being added to each Antisense-CA surface respectively. Each data point was repeated in duplicates.

5.3   Results and Discussions

5.3.1   Selection, design and analysis of P4-CA and Antisense-CA by Neoventures

The P4-CA aptamer was selected *via* a process called FRELEX [199]. In brief, an aptamer library is first blocked at primer sequences, before it is hybridized to an 'immobilization field' which is a solid support immobilized with random oligomers. The unbound portion of the library is washed away from the immobilization field, while the bounded portion is eluted and incubated with a selection target. After incubation, the mixture of the eluted library and the target is added to the 'immobilization field' again and the unbound portion of the library is kept, as it is assumed that this portion of the library fails to bind the 'immobilization field' due to binding to the targets. The unbounded sequences are then enriched by

PCR before the next round of selection and enrichment. After a few rounds of selection, the enriched sequences are analyzed by next generation sequencing and further verified for the target binding.

The binding of P4-CA and P4 was verified by Neoventures using GNP analysis. Aptamers can bind GNPs and then disperse GNPs, but the binding of aptamers to their targets cause their dissociation from GNPs and GNPs aggregate. The aggregation of GNPs can be measured by the change of the absorbance of GNP suspension at 520 nm and 620 nm. To verify the binding of P4-CA and P4, P4-CA (12.5 pmoles) and P4 (0-2 µM) was mixed respectively and added to GNPs (diameter=5 nm) in 10 mM HEPES buffer before the absorbance of the GNPs at 520 and 620 nm was measured over 30 min. The results were provided by Neoventures as Figure 5.3. They concluded: there was a clear binding curve of P4-CA and P4, though the curve did slope upwards at the concentrations of P4 above 1 µM, possibly due to multiple binding sites of P4-CA. Except for this GNP analysis, no information on the binding affinity of P4 and P4-CA, on the folding structure or binding sequences of P4-CA were provided or investigated by Neoventures.
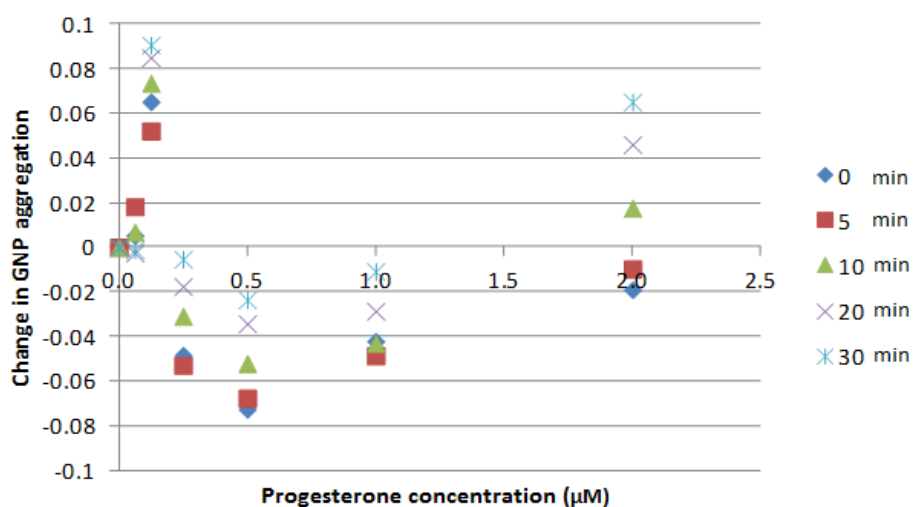
Figure 5.3 The results of GNP analysis of P4-CA and P4 provided by Neoventures Biotechnology. The legend (0-30 min) refers to the time expired before measurement of GNP aggregation.

Also, an antisense probe of P4-CA, and Antisense-CA was designed by Neoventures. The hybridization complex of P4-CA and P4 was predicted using the DINAMelt web server [200] (Figure 5.4). According to Neoventures, antisense probes are designed by covering two or three discrete regions of homology

that are at least four nucleotides each, and the binding affinities of aptamers and their antisense probes are subtly affected by the symmetry and sizes of the gaps between these regions so that the affinities of aptamers and their antisense probes can be fine-tuned to match those of aptamers and their targets.
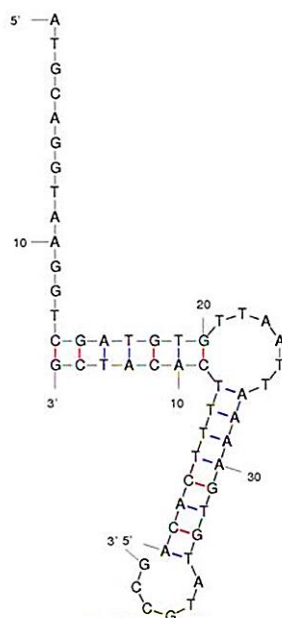
Figure 5.4 The hybridization of P4-CA aptamer and its antisense ssDNA Antisense-CA predicted by the DINAMelt web server in the conditions of the aptamer selection buffer.

The effect of P4 on the binding of P4-CA and Antisense-CA was investigated by Neoventures using SPRi assays, where P4-CA (500 nM) was mixed with P4 of various concentrations respectively before the mixture was injected for 4 min at 50 µl/min over the SPR gold surface immobilized with Antisense-CA *via* a thiol group on its 3' end. The analysis was performed in 10 mM HEPES buffer (pH 7.4) containing 120 mM NaCl, 5 mM KCl and 20mM $MgCl_2$. The sensorgram of binding during SPRi assays and the binding coefficients of P4-CA and Antisense-CA with and without P4 were provided by Neoventures (Figure 5.5 and Table 5.3). Neoventures concluded: in the presence of P4 the binding between P4-CA and Antisense-CA was higher and the curve of disassociation was steeper, so that P4 appeared to potentially enhance binding of P4-CA and Antisense-CA and also led to higher rates of disassociation of P4-CA from Antisense-CA. Also, they mentioned that this effect of P4 did not titrate well between 0 and 1 µM of P4.
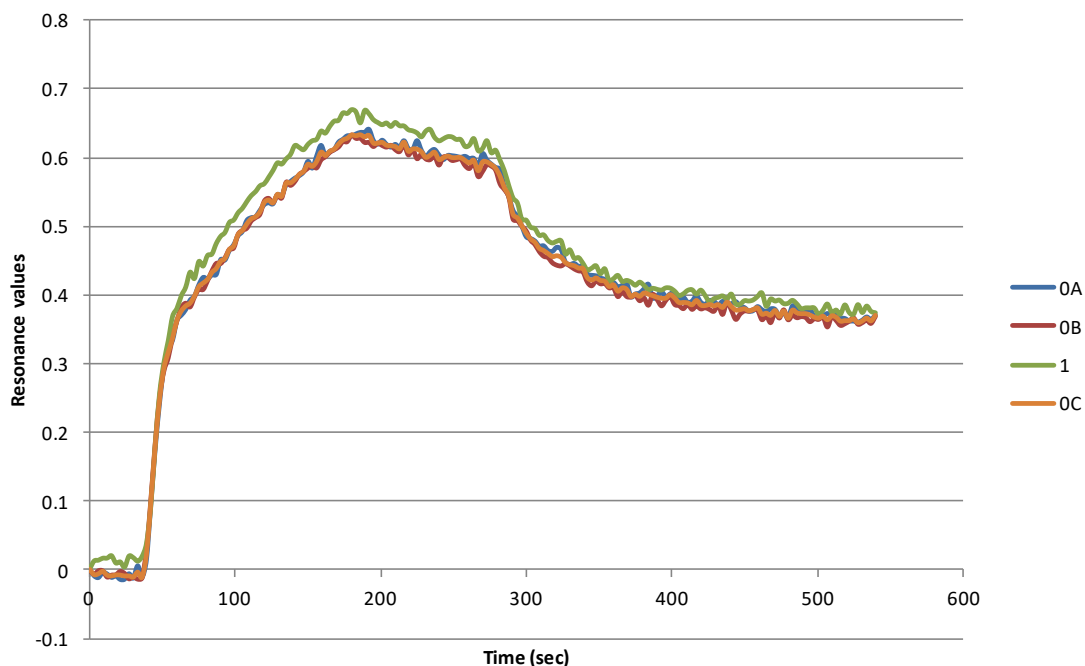
Figure 5.5 The results of SPRi analysis on the binding kinetics of P4-CA to Antisense-CA with P4 provided by Neoventures Biotechnology. The legend (0 and 1 µM) refers to the concentration of P4, in which three trials with 0 µM P4 were labeled as '0A', '0B' and '0C' and one trial of 1 µM P4 as '1'.

Table 5.3 The binding coefficients between P4-CA and Antisense-CA, with or without P4, obtained from SPRi analysis provided by Neoventures.

P4 concentration (µM)	K_d	K_a	K_D
0	6.85 E -03	1.96 E +05	3.05 E -08
1	1.02 E -02	1.91 E +05	5.32 E -08
Standard Deviation (P4 concentration = 0)	1.70 E -05	6.12 E +03	1.18 E -09

5.3.2 SPR aptasensors

5.3.2.1 SPR detection of P4-CA binding on the P4-OVA surface

Biotinylated P4-CA (0-1 µM) showed slightly increased binding signals with the increase of P4-CA concentration on P4-OVA SPR surfaces (Figure 5.6a). However, overall, the binding signals were very low (13-20 RU). Since the molecular weight of P4-CA is about 1/10 to those of antibodies, P4-CA was less effective in stimulating SPR signals. Thus, streptavidin-MBs were used to amplify SPR signals. The sequential injection of streptavidin-MBs resulted in higher SPR responses, but the SPR responses showed poor correlation (R=0.52) with the concentrations of biotinylated P4-CA (Figure 5.6a). The

injection of the pre-formed P4-CA-MB conjugates prepared by incubating different concentrations of biotinylated P4-CA with streptavidin-MBs showed an increase in the binding signals with the increase of biotinylated P4-CA concentrations from 0 to 100 nM, but the binding signal of P4-CA-MBs prepared by 250 nM biotinylated P4-CA dropped (Figure 5.6b). The increased binding of P4-CA-MBs may result from the increased P4-CA on MB surfaces using 0 to 100 nM biotinylated P4-CA concentrations, but 250 nM biotinylated P4-CA might result in overcrowded P4-CA on MB surfaces, which caused steric hindrance of binding to P4-OVA SPR surfaces.
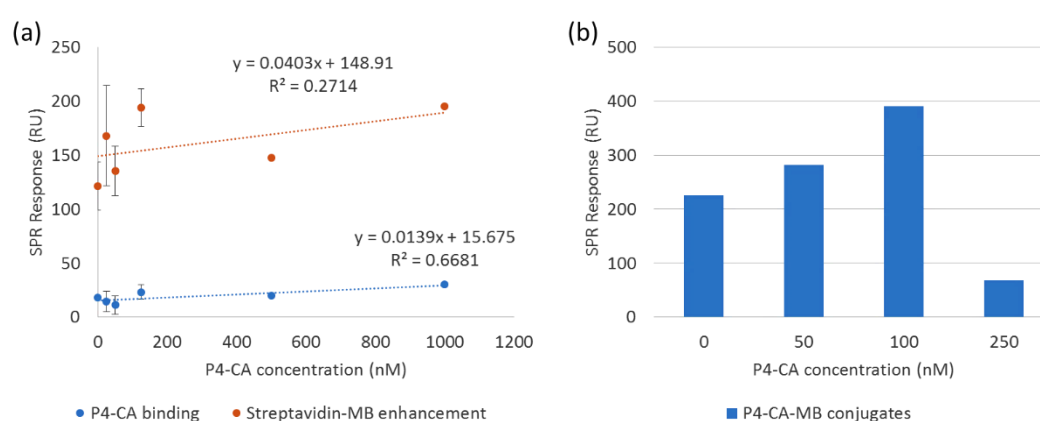
Figure 5.6 SPR detection of P4-CA binding on the P4-OVA surface: (a) the results of sequential injection of biotinylated P4-CA and streptavidin-MBs; (b) the results of injection of P4-CA-MB conjugates. The data points with error bar were repeated in duplicates.

However, compared with the binding of *anti*-P4 mAb on the same P4-OVA surface (170 RU by 6.6 nM mAbs), the binding of concentrated P4-CA (20 RU by 1 µM P4-CA) was much less and it was suspected that the binding affinity of P4-CA to the P4-OVA surface was lower than that of *anti*-P4 mAbs. The binding affinities of small molecules and aptamers are often in the nanomolar to low micromolar range [201]. P4 as a hydrophobic molecule may be less attractive to the strongly hydrophilic aptamers [41] and more likely to have a relatively low binding affinity due to a lack of hydrophobic interaction by natural nucleotides [202]. In comparison, the binding affinities of antibody and antigen can be in the picomolar, even femtomolar range.

The limited binding of P4-CA to the P4-OVA surface may also result from a relatively short interaction time between P4-CA and the P4-OVA surface (10 min). A longer injection time was not attempted since

it would require a large amount of P4-CA, especially when high concentrations of P4-CA are used. In contrast, other reported P4 aptasensors used longer interaction times of aptamers and P4 (up to 2 hours) [97, 100-102, 104]. Also, the immobilization of P4 on the SPR surface may cause the steric hindrance of binding, or the loss of the aptamer binding site, depending on where P4-CA binds P4, yet such information of P4-CA was not available. In general, direct detection of binding of small molecules and aptamers on SPR seems to be difficult due to low molecular weight.

In addition, high non-specific binding (>100 RU) of streptavidin-MBs (1:100 v/v) was observed on the P4-OVA surface, compared to the experiments in Chapter 4 where they barely bound P4-OVA surfaces (<20 RU). Surface regeneration was also very difficult even with harsh regeneration reagents such as SDS and strong bases and acids as described in Section 5.2.2.1. During some cycles, the binding of streptavidin-MBs were not completely removed and therefore it left about 70-150 RU SPR responses after surface regeneration. The reason was not clear. It may be related to biotinylated aptamers of high concentrations used here that may contaminate the Biacore fluidic system. The poor surface regeneration affected the binding in the following cycles; the repeatability of results and the stability of the P4-OVA surface. In fact, this may account for the poor correlation between P4-CA concentrations and SPR responses, as part of SPR responses could indeed be non-specific binding, and streptavidin-MBs that were not removed from the SPR surfaces after previous cycles may lead to non-specific binding of biotinylated P4-CA in the following cycles.

5.3.2.2 SPR detection of P4-CA and Antisense-CA binding on the SPR surfaces

The P4-CA surface and the Antisense-CA surface were prepared by injection of biotinylated P4-CA and biotinylated Antisense-CA of the same concentration over two SPR surfaces where similar amounts of streptavidin were immobilized (10923 RU and 10902.2 RU). Based on the molecular weights of P4-CA and Antisense-CA, more Antisense-CA was immobilized (1666.7 RU) than P4-CA (2874.5 RU) on the SPR surfaces, possibly because the smaller Antisense-CA can form a more densely packed surface.

The binding of Antisense-CA to the P4-CA surface was detected when Antisense-CA of different concentrations was injected over the P4-CA surface in 10mM HEPES buffer (Figure 5.7a). The binding was relatively stable according to the sensorgrams, though some dissociation was observed after finishing the injection of Antisense-CA at high concentrations (50–200 nM). Antisense-CA dissociated

from the P4-CA surface faster at high concentrations, possibly due to the increased electrostatic repulsion when more negatively charged Antisense-CA bound to the negatively charged P4-CA surface and the negative charges could not be neutralized by the salts of 10 mM HEPES buffer. The binding curve (Figure 5.7b) showed a good linear relation between SPR responses and Antisense-CA concentrations (0-50 nM), and 20 nM Antisense-CA had about 100 RU SPR responses on the P4-CA surface, which was sufficient to test the effect of P4 on the binding.
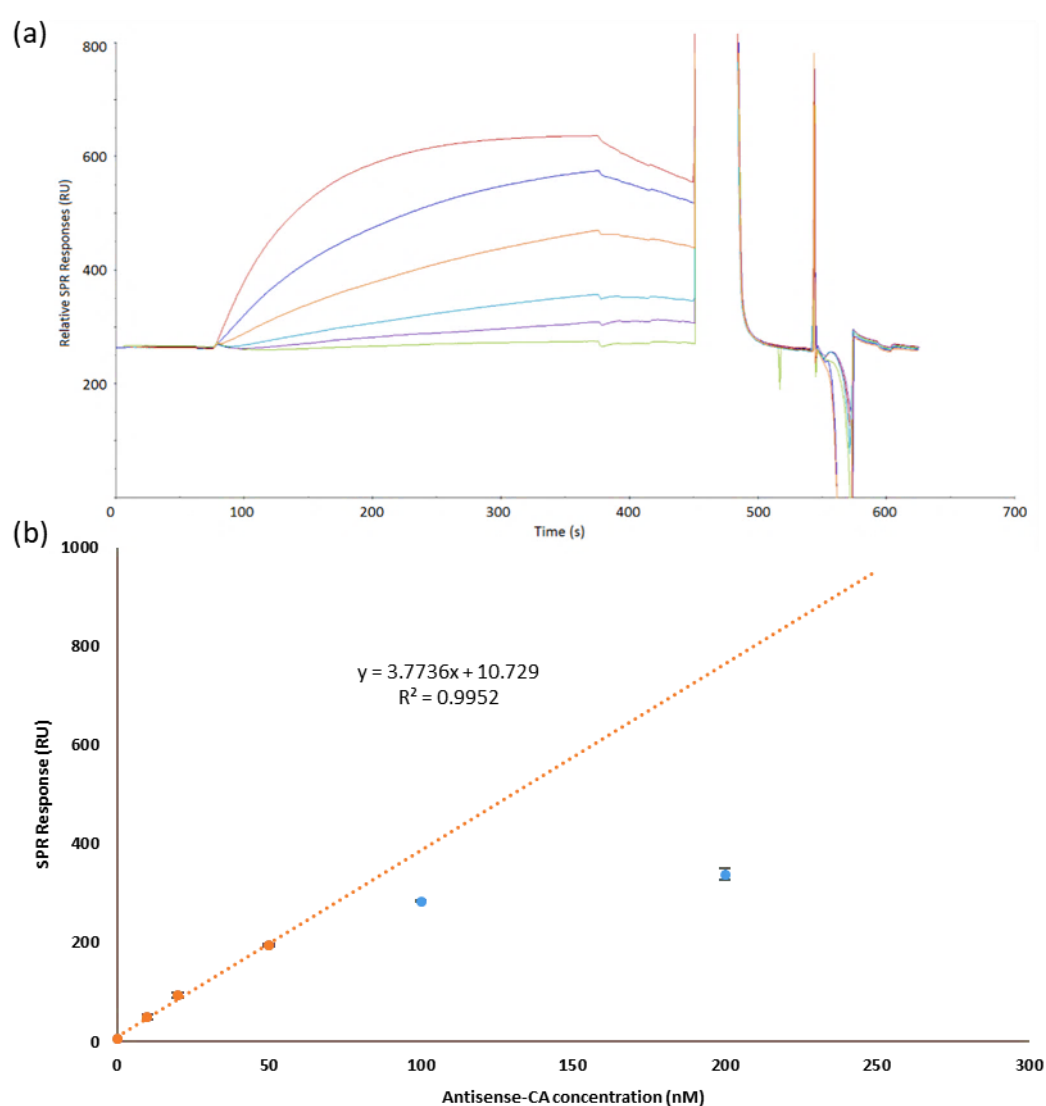
Figure 5.7 SPR detection of Antisense-CA binding on the P4-CA surface: (a) overlapped SPR sensorgrams of injection of Antisense-CA (0, 10, 20, 50. 100 and 200nM); (b) binding curve of Antisense-CA. Each data point was repeated in duplicates.

However, when P4-CA of different concentrations was injected over the Antisense-CA surface in 10 mM HEPES buffer, much lower binding was detected (Figure 5.8b) compared to Antisense-CA of the same concentrations on the P4-CA surface (Figure 5.7b). The sensorgrams (Figure 5.8a) showed rapid dissociation of P4-CA from the Antisense-CA surface at all the concentrations.
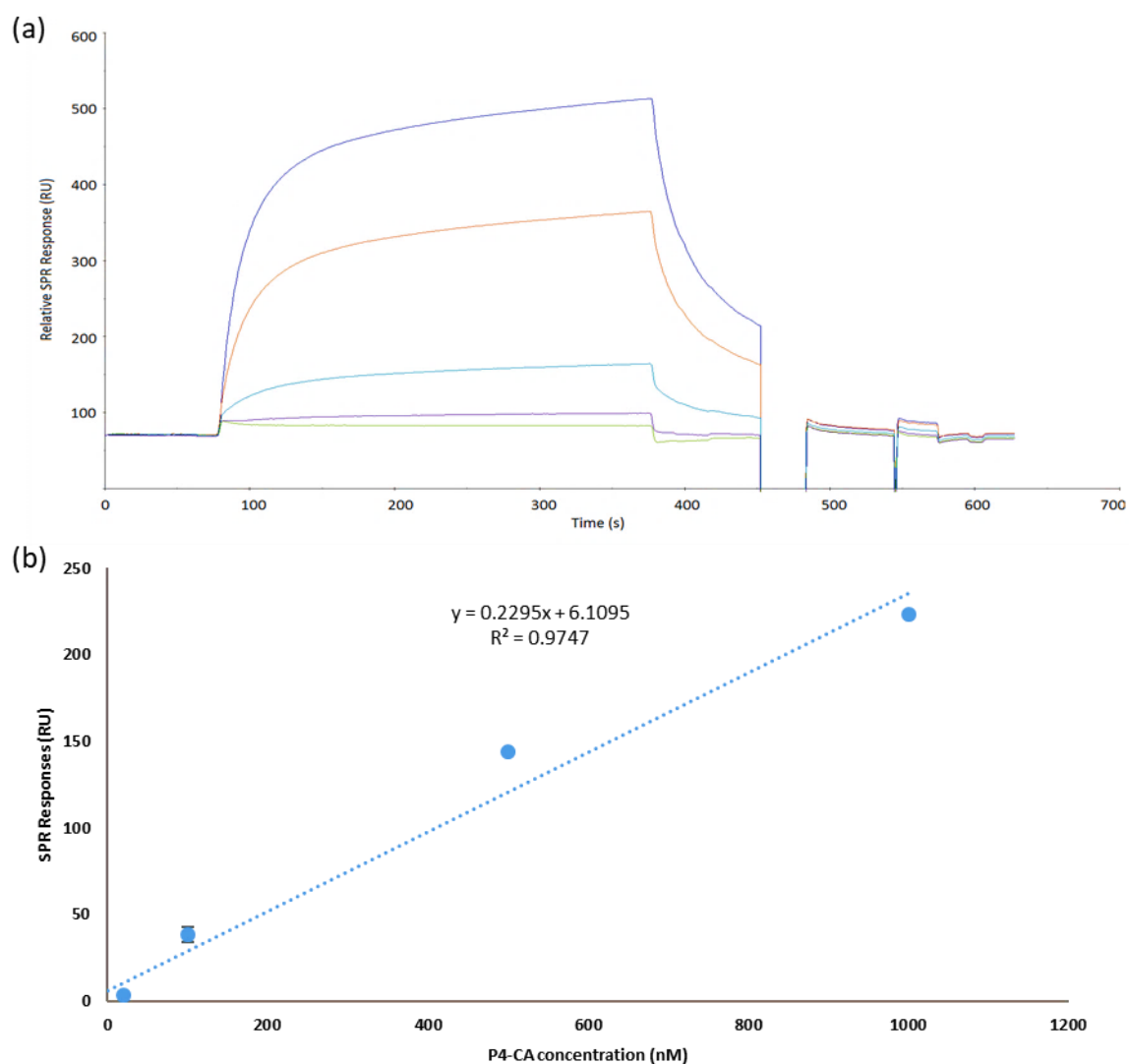
Figure 5.8 SPR detection of P4-CA binding on the Antisense-CA surface in 10 mM HEPES buffer: (a) overlapped SPR sensorgrams of injection of Antisense-CA (0, 100, 500 and 1000 nM); (b) the binding curve. Each data point was repeated in duplicates.

The effect of the flow rates of the binding of P4-CA on the Antisense-CA surface was investigated. The sensorgrams showed that higher flow rates increased both association rates and dissociation rates

(Figure 5.9a), but there was no difference in SPR responses which measured 30 seconds after the end of injection of P4-CA (Figure 5.9b). The binding of P4-CA to the Antisense-CA surface was found unstable in 10 mM HEPES buffer.
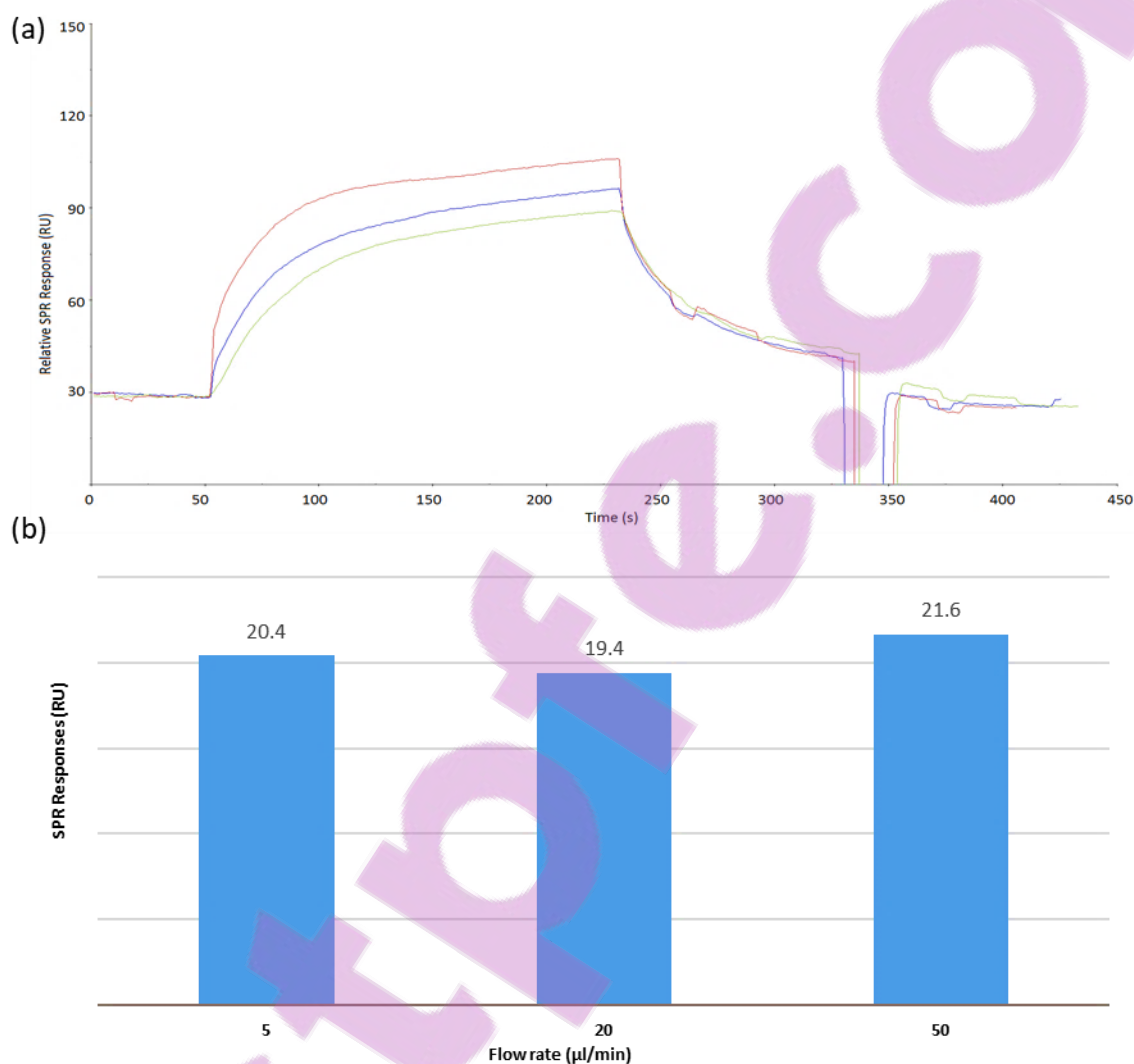
Figure 5.9 The effect of injection rates on P4-CA (100 nM) binding to the Antisense-CA surface in 10 mM HEPES buffer: (a) overlapped SPR sensorgrams of the injection rates as 5 μl/ml (green), 10 μl/ml (blue) and 20 μl/ml (red) respectively; (b) SPR responses measured 30 seconds after the finish of injection at different rates.

Increasing ion concentrations stabilizes DNA hybridization complexes in solution [203] and on solid supports [204]. Thus, $MgCl_2$ was added to 10 mM HEPES buffer at various concentrations (0-15 mM). With the increase of $MgCl_2$ concentration, the binding of P4-CA to the Antisense-CA surface increased

and became more stable (Figure 5.10). Divalent magnesium ions were found much more efficient in stabilization of DNA duplexes than monovalent sodium ions during ssDNA binding events on the SPR surfaces, as Mg^{2+} is more efficient in neutralizing negative charges of ssDNA in restricted spaces such as SPR surfaces [204]. Mg^{2+} stabilized the binding of P4-CA on the Antisense-CA surface by neutralizing the negative charges, reducing the electrostatic repulsion and slowing down the dissociation of the hybridization complexes. Interestingly, Mg^{2+} appeared more important in the binding of P4-CA to the Antisense-CA surface than that of Antisense-CA to the P4-CA surface. The size and the surface density of the molecules immobilized on the SPR surface may also play roles in determining the binding kinetics: first, the short Antisense-CA immobilized *via* the biotin at its 3' end on the SPR surface may cause more steric hindrance of binding than the long P4-CA immobilized *via* the biotin at its 5' end, as indicated by the structure of hybridization complexes in Figure 5.4; second, the hybridization complexes formed on the Antisense-CA surface were closer to the negatively charged CM5 dextran surface than those formed on the P4-CA surfaces, which lead to more electrostatic repulsion; third, the Antisense-CA surface had more ssDNA immobilized than the P4-CA surface as discussed before, and a densely packed ssDNA surface was found to lower the hybridization efficiency and kinetics due to repulsive force by a more negatively charged surface and steric hindrance [205]; and last, the long P4-CA may need more energy to refold its conformation to hybridize with the short Antisense-CA on the surface, which affected the hybridization kinetics [206].
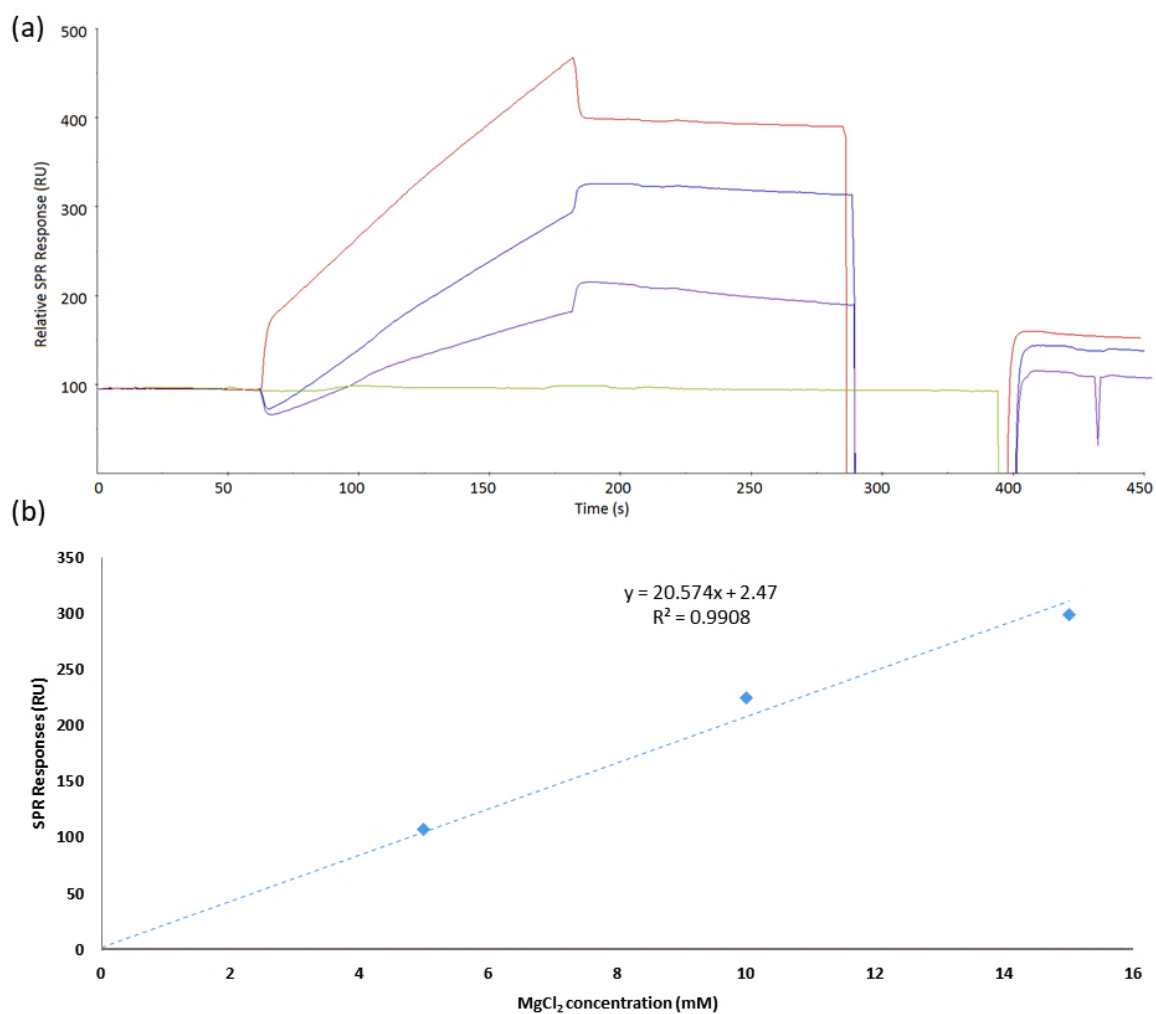
Figure 5.10 The effect of $MgCl_2$ on P4-CA binding to the Antisense-CA surface: (a) overlapped SPR sensorgrams in 10 mM HEPES buffer with various concentrations of $MgCl_2$: 15 mM (red), 10 mM (blue), 5 mM (purple) and 0 (green); (b) the relation between the P4-CA binding and the concentration of $MgCl_2$ in the buffer.

According to the sensorgrams in Figure 5.10a, 10 mM $MgCl_2$ in 10mM HEPES buffer was enough to stabilize the binding of P4-CA on the Antisense-CA surface. The binding assay (Figure 5.11) performed in this buffer showed that 10nM P4-CA had about 100 RU SPR responses, which was sufficient to test the effect of P4 on the binding.
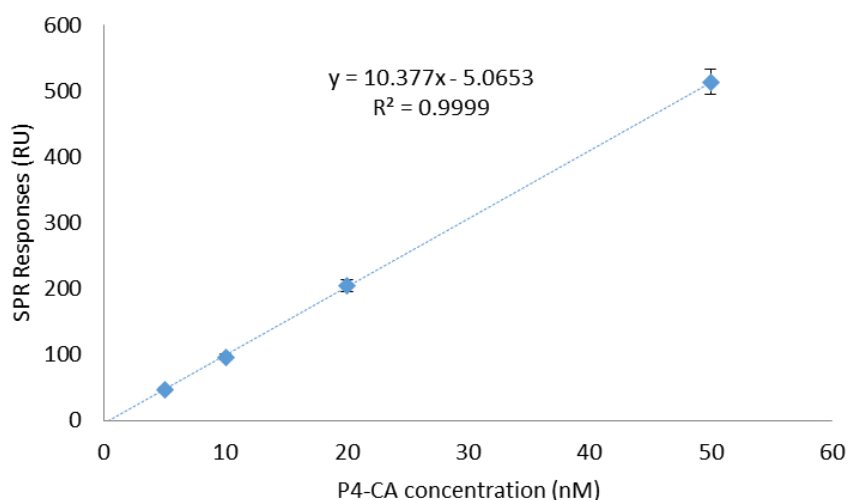
Figure 5.11 The binding curve of P4-CA on the Antisense-CA surface measured by SPR using 10 mM HEPES buffer containing 10 mM $MgCl_2$. Each data point was repeated in duplicate.

5.3.2.3 The effect of P4 on P4-CA and Antisense-CA binding

The effect of P4 on the binding of P4-CA and Antisense-CA on the SPR surfaces was tested by: (1) sequentially injecting P4 and Antisense-CA on the P4-CA surface (Figure 12a and b) or sequentially injecting P4-CA and P4 on the Antisense-CA surface (Figure 13a); (2) injecting the mixture of P4 and Antisense-CA on the P4-CA surface (Figure 12c) or the mixture of P4 and P4-CA on the Antisense-CA surface (Figure 13b). Sequential injections resulted in 2.2% inhibition on the binding of Antisense-CA (20 nM) onto the P4-CA surface (Figure 12b) and 4.1% inhibition on the binding of P4-CA (10 nM) onto the Antisense-CA surfaces (Figure 13a) by 50 ng/ml of P4 respectively, but no significant difference was found by t-tests ($P > 0.05$) when comparing the signals obtained by 0 and 50 ng/ml of P4. Pre-mixing of P4 and P4-CA or Antisense-CA showed no obvious inhibition effect on the binding of P4-CA and Antisense-CA on the two SPR surfaces (Figure 12c and Figure 13b). To be noted, when P4-CA (10 nM) was incubated with P4 (50 ng/ml or 50 µg/ml) in solution for an hour before injection, there was sufficient interaction of P4 and P4-CA and there was no steric hindrance of the binding since P4 was not immobilized or bounded to any molecules or surfaces. Thus, P4 showed no obvious inhibition effect on the binding of P4-CA and Antisense-CA in any of these SPR assays. The reasons for the limited inhibition effect of P4 on the binding of P4-CA and Antisense-CA may be: (1) P4-CA bound P4 with a low affinity so that very little P4-CA was bounded by P4; (2) the binding sequences of P4-CA to P4 did

not overlap the sequences of P4-CA binding to Antisense-CA so that the P4-CA bound P4 and Antisense-CA simultaneously; or (3) the binding affinity of P4-CA and Antisense-CA was higher than that of P4-CA and P4 so that P4-CA dissociated from P4 and bound Antisense-CA. However, there is a lack of information on the binding sequence of P4-CA and the binding affinity between P4-CA and P4 or Antisense-CA, so it is difficult to diagnose the problem to improve the design and performance of the SPR aptasensors.
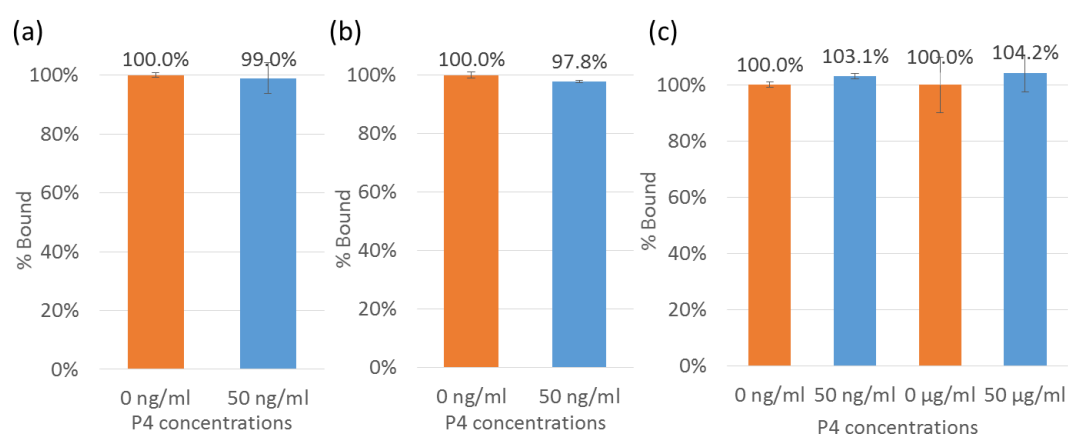
Figure 5.12 The effect of P4 on the binding of Antisense-CA to the P4-CA surface detected by SPR: (a) sequential injection of P4 followed by Antisense-CA on the P4-CA surface; (b) sequential injection of Antisense-CA followed by P4 on the P4-CA surface, and (c) injection of the pre-mixed Antisense-CA and P4 on the P4-CA surface. Each data point was repeated in duplicates.
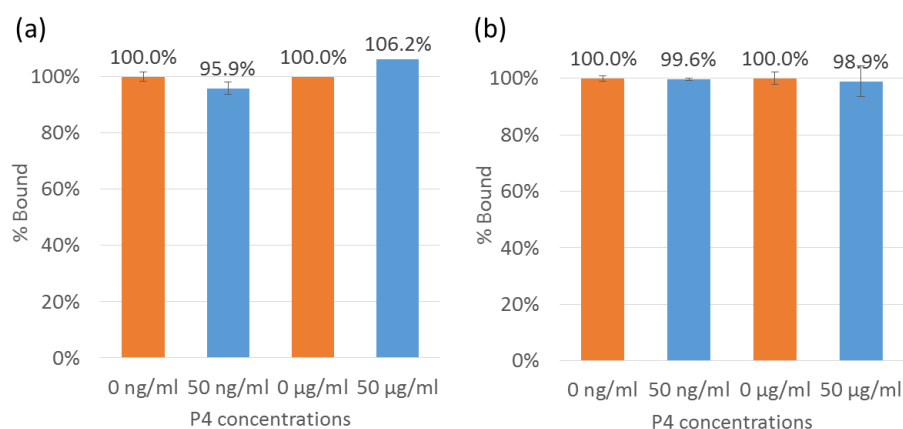
Figure 5.13 The effect of P4 on the binding of P4-CA to the Antisense-CA surface detected by SPR: (a) sequential injection of P4-CA followed by P4 on the Antisense-CA surface; (b) injection of the pre-incubated P4-CA and P4 on the Antisense-CA surface. Each data point was repeated in duplicates.

5.3.3   Fluorescent aptasensors

5.3.3.1 Synthesis and evaluation of P4-OVA/P4 and MB conjugates

Three different P4/P4-OVA and MB conjugates, P4-NH$_2$-MBs, P4-OVA-NH$_2$-MBs and P4-OVA-COOH-MBs were synthesized and evaluated using *anti*-P4 mAbs and F-sAbs. All the conjugates showed higher fluorescence signals than the unmodified MBs after incubation with the antibodies (Figure 5.14), indicating P4 and P4-OVA were conjugated to MBs successfully. Among the three, P4-NH$_2$-MBs showed the highest binding with antibodies, likely due to the high surface density of P4. The other two conjugates may have a lower surface density of P4 due to the limited conjugation ratio of P4 to OVA in P4-OVA (3.3:1), although it was expected that OVA could extend P4 away from the MB surfaces to reduce the steric hindrance of binding and increase antibody binding. Therefore, P4-NH$_2$-MBs were used to test the binding of P4-CA.
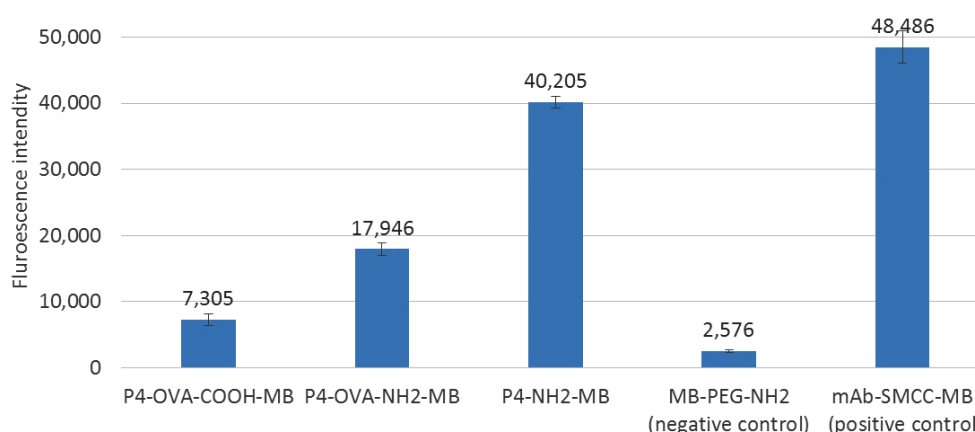
Figure 5.14 Evaluation of P4/P4-OVA and MB conjugates using fluorescent antibodies. Each data point was repeated in duplicates.

5.3.3.2 Fluorescence detection of P4-CA binding to P4-NH$_2$-MBs

P4-NH$_2$-MBs incubated with either fluorescent P4-CA (1 µM) or with biotinylated P4-CA (1 µM) and F-streptavidin had slightly higher fluorescence signals than P4-NH$_2$-MBs incubated with the buffer or F-streptavidin (Figure 5.15); and the fluorescence signals of P4-NH$_2$-MBs incubated in biotinylated P4-CA and F-streptavidin were significantly different ($P<0.01$) from those incubated with the buffer and F-streptavidin (Figure 5.15b). These indicated the binding of P4-CA to P4-NH$_2$-MBs. Unexpectedly, the

111

unmodified PEG-NH$_2$-MBs incubated with P4-CA showed high fluorescence signals, even higher than P4-NH$_2$-MBs. Negatively charged P4-CA may bind PEG-NH$_2$-MBs non-specifically *via* the NH$_2$ groups which may have positive charges. However, there were fewer NH$_2$ groups on the surfaces of P4-NH$_2$-MBs. Also, unmodified MBs used as controls were likely of higher bead concentration than P4-NH$_2$-MBs, since some beads may be lost in the separation and wash steps during the synthesis process of P4-NH$_2$-MBs. Thus, these unmodified beads may not provide a very relevant control. A better control would be a random ssDNA incubated with P4-NH$_2$-MBs.

Although there was an increase in fluorescence after P4-NH$_2$-MBs were incubated with fluorescent-labeled P4-CA (1 µM), the increase was much smaller than those incubated with *anti*-P4 mAbs (1 µg/ml, 6.6 nM) using the same amount of P4-NH$_2$-MBs (Figure 5.14). It indicated that the binding of P4-CA to P4-NH$_2$-MBs was much lower than that of *anti*-P4 mAbs, similar to what was found by the SPR aptasensor where P4-CA was injected over the P4-OVA surface. Since in this fluorescent aptasensor the interaction of P4-CA and P4 took place in solution for one hour, which should have allowed sufficient interaction between them, the low binding may be the result of the low binding affinity of P4-CA and P4, unless the binding was affected by the conjugation of P4 to MBs due to the loss of binding sites or steric hindrance.
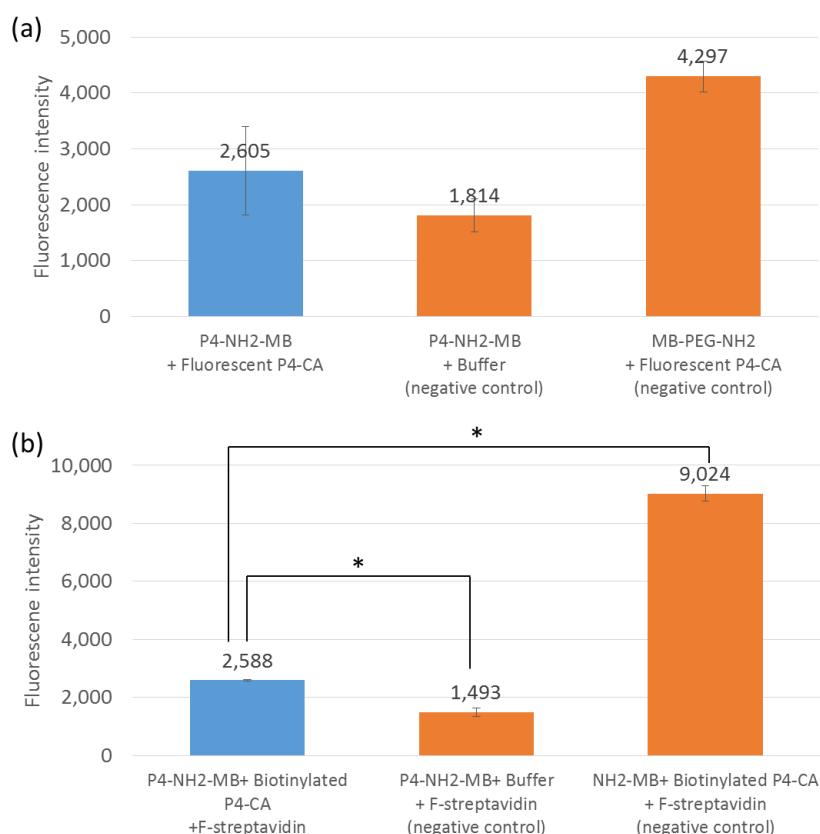
Figure 5.15 Fluorescent detection of P4-CA binding to P4-NH₂-MBs. (a) MBs incubated with fluorescent-labeled P4-CA; (b) MBs incubated with biotinylated P4-CAs and F-streptavidin. Each data point was repeated in duplicates. *Significant difference at t-test p<0.01 levels.

5.3.3.3 Fluorescence detection of Antisense-CA and P4-CA on streptavidin-MBs

The streptavidin-MBs incubated with the mixture of biotinylated P4-CA and fluorescent-labeled Antisense-CA, or the mixture of fluorescent-labeled P4-CA and biotinylated Antisense-CA showed much higher fluorescence signals than all the negative controls (Figure 5.16). T-tests showed a significant difference between the fluorescence of these beads compared to the controls (P<0.01), indicating that the hybridization complexes of P4-CA and Antisense-CA bound streptavidin-MBs. The mixture of biotinylated P4-CA and fluorescent Antisense-CA resulted in slightly higher fluorescence signals than that of biotinylated Antisense-CA and fluorescent P4-CA, possibly due to a relatively low steric hindrance in the binding of the hybridization complexes to streptavidin-MBs as illustrated in Figure 5.17. The biotin at 5' end of the long P4-CA was more accessible to streptavidin-MBs, and extended the hybridization complexes away from the streptavidin-MBs surface, so that more hybridization complexes could bind streptavidin-MBs.
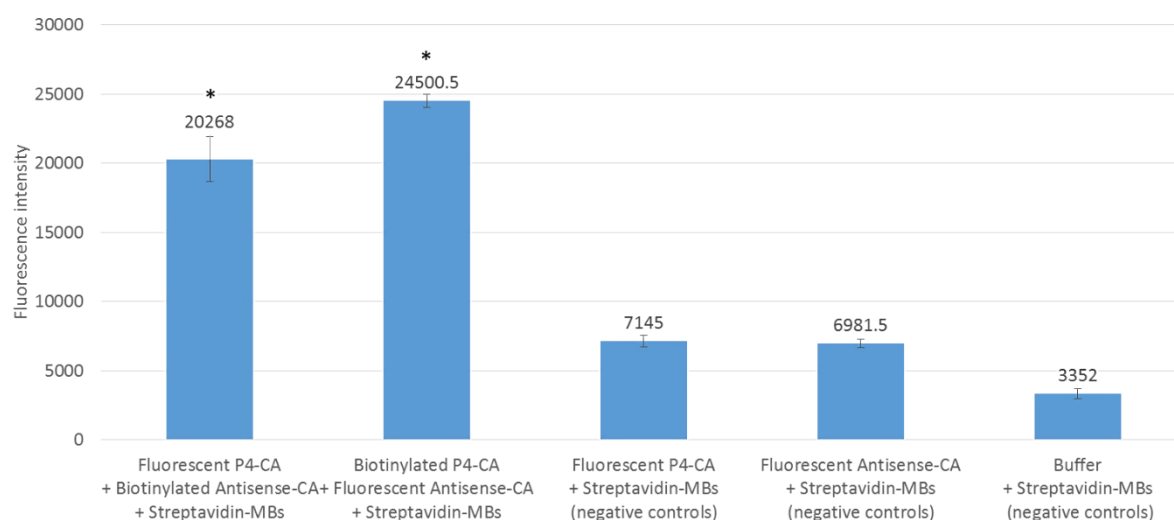
Figure 5.16 Antisense-CA and P4-CA binding to Streptavidin-MBs. Each data point was repeated in duplicates. *Significant difference at t-test $p<0.01$ levels compared with all the control groups.
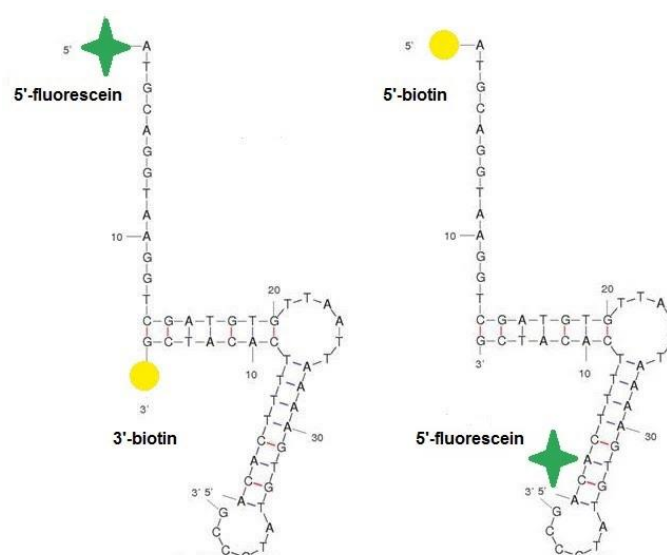
Figure 5.17 Structures of the hybridization complex of fluorescent P4-CA and biotinylated Antisense-CA (left) and that of fluorescent Antisense-CA and biotinylated P4-CA (right).

Further, the concentrations of biotinylated P4-CA and fluorescent Antisense-CA was optimized. Firstly, when the concentration of biotinylated P4-CA was fixed at 200 nM, increasing the concentration of fluorescent Antisense-CA increased the fluorescence signals and the signal-to-noise ratios (Figure 5.18a), as more hybridization complexes were formed and bound to streptavidin-MBs. Since Antisense-CA and P4 compete in binding to P4-CA, less Antisense-CA is preferred. Compared with 1 µM

fluorescent Antisense-CA, 200 nM fluorescent Antisense-CA showed enough fluorescence signals and signal-to-noise ratios. Then, when the concentration of fluorescent Antisense-CA was fixed at 200 nM, increasing the concentration of biotinylated P4-CA from 0 to 200 nM increased the fluorescence signals and signal-to-noise ratios, but a further increase of the concentration to 1000 nM lead to a lower fluorescence signal (Figure 5.18b). According the manufacturer of streptavidin-MBs, there are 15-20 µg streptavidin per ml MBs and therefore 200 nM biotinylated P4-CA saturated the binding capacity of streptavidin-MBs. When 200 nM fluorescent Antisense-CA and 1000 nM biotinylated P4-CA were used, almost all fluorescent Antisense-CA hybridized with biotinylated P4-CA, but only a portion (~20%) of the formed hybridization complexes could bind to streptavidin-MBs. In comparison, when 200 nM fluorescent Antisense-CA and 200 nM biotinylated P4-CA were used, a similar amount of fluorescent hybridization complexes formed but almost all of the hybridization complexes were bound to streptavidin-MB surfaces. Thus, 1000 nM biotinylated P4-CA resulted in lower fluorescence than 200 nM biotinylated P4-CA when the concentration of fluorescent Antisense-CA was fixed at 200 nM. Therefore, the optimized concentrations of both biotinylated P4-CA and fluorescent Antisense-CA were 200 nM.
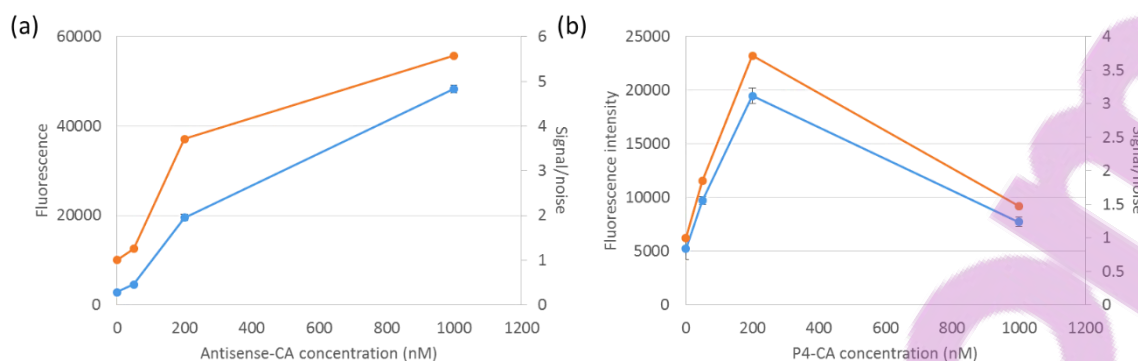
Figure 5.18 Optimization of the concentrations of fluorescent Antisense-CA and biotinylated P4-CA on streptavidin-MBs: (a) the fluorescence intensity (blue) and signal to noise ratio (orange) of the beads when 0-1000 nM fluorescent Antisense-CA incubated with 200 nM biotinylated P4-CA respectively; (b) the fluorescence intensity (blue) and signal to noise ratio (orange) of the beads when 0-1000 nM biotinylated P4-CA incubated with 200 nM fluorescent Antisense-CA respectively. The data points with error bar were repeated in duplicates.

5.3.3.4 The effect of P4 on the binding of P4-CA and Antisense-CA

When the mixture of biotinylated P4-CA and fluorescence Antisense-CA were incubated with 0-100 µg/ml of P4 respectively before streptavidin-MBs were added, the fluorescence signals from the beads decreased with the increase of P4 concentration, indicating that P4 could inhibit the binding of P4-CA and Antisense-CA (Figure 5.19). ~10% of inhibition was observed by 10 or 100 µg/ml of P4. P4 solubility in aqueous media is about 15-16 µg/ml [207], which may explain why 10 and 100 µg/ml of P4 have a similar inhibition effect. T-tests showed that only the assay using 100 µg/ml P4 was significantly different in fluorescence compared to the control (P4=0). The fluorescent aptasensor showed more inhibition effect of P4 on P4-CA and Antisense-CA binding than the SPR aptasensors (Figure 5.12 and 5.13), but the inhibition effect was still very limited. The reasons for the limited inhibition effect of P4 on the binding of P4-CA and Antisense-CA on the fluorescent aptasensors may be similar to those of the SPR aptasensors as discussed in Section 5.3.2.3.
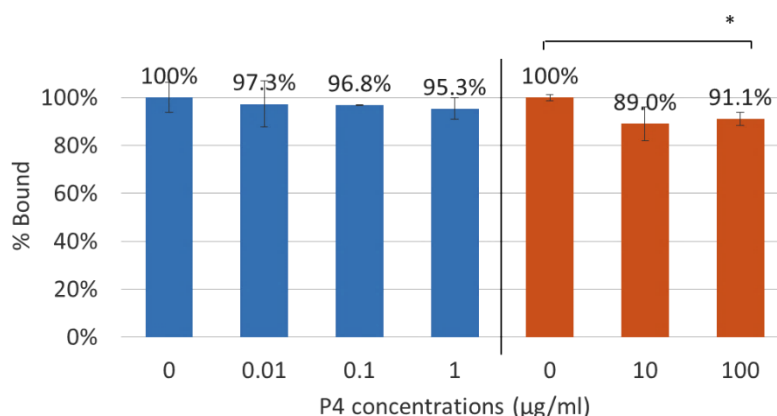
Figure 5.19 P4 inhibition on fluorescent Antisense-CA binding to biotinylated P4-CA and streptavidin-MBs. Each data point was repeated in duplicates. *Significant difference at t-test $p<0.05$ levels.

It was possible to improve the inhibition effect of P4 on P4-CA and Antisense-CA binding by decreasing the binding of P4-CA and Antisense-CA or increasing the binding of P4 and P4-CA. For example, decreasing the ion concentrations may affect the stability of DNA hybridization complexes as shown in Table 5.4, or pre-incubation of P4 and P4-CA before mixing with Antisense-CA may increase the binding of P4 and P4-CA. Also, reducing the concentrations of P4-CA/Antisense-CA may improve the inhibition effect of P4 by increasing the molar ratio of P4 and P4-CA/Antisense-CA. However, further decreasing the binding stability or concentrations of fluorescent Antisense-CA or biotinylated P4-CA will lead to low fluorescence signals and signal/noise ratio (Figure 5.18) on the fluorescence aptasensors. It was attempted to use lower ion concentrations, pre-incubate P4 and P4-CA, and lower P4-CA and Antisense-CA concentrations on colorimetric aptasensors based on enzymatic reactions, which are more efficient in signal transduction.

Table 5.4 The stability (energy) of P4-CA and Antisense-CA depending on the concentrations of Mg2+calculated by DINAMelt web server ([Na+] = 125 mM, [P4-CA] =200 nM).

Concentration of Mg^{2+} (mM)	ΔG (kcal/mol)	ΔH (kcal/mol)	ΔS (cal/mol/K)	Tm (°C)
0	-14.1	-108.3	-321.3	32.2
2	-15.1	-108.3	-316.3	36.5
10	-16.6	-108.3	-313.0	39.5
40	-17.6	-108.3	-309.5	42.7

5.3.4   Colorimetric aptasensors

5.3.4.1 Colorimetric detection of P4-CA binding on the Antisense-CA plates

The Antisense-CA plates were prepared by adding biotinylated Antisense-CA to the plates coated with three different biotin binding proteins, avidin, streptavidin and neutravidin respectively. The high colorimetric signals were detected from the wells where pre-formed P4-CA-HRP conjugates were added (Figure 5.20), indicating the binding of P4-CA to the Antisense-CA plates. Among all the three Antisense-CA plates, non-specific binding of P4-CA-HRP was found from the wells of the plate coated with avidin when no biotinylated Antisense-CA was added (Figure 5.20). The non-specific binding was likely due to the electrostatic attraction of positively charged avidin and the negatively charged P4-CA in P4-CA-HRP conjugates [208]. Therefore, the plates coated with avidin were omitted from further experiments.
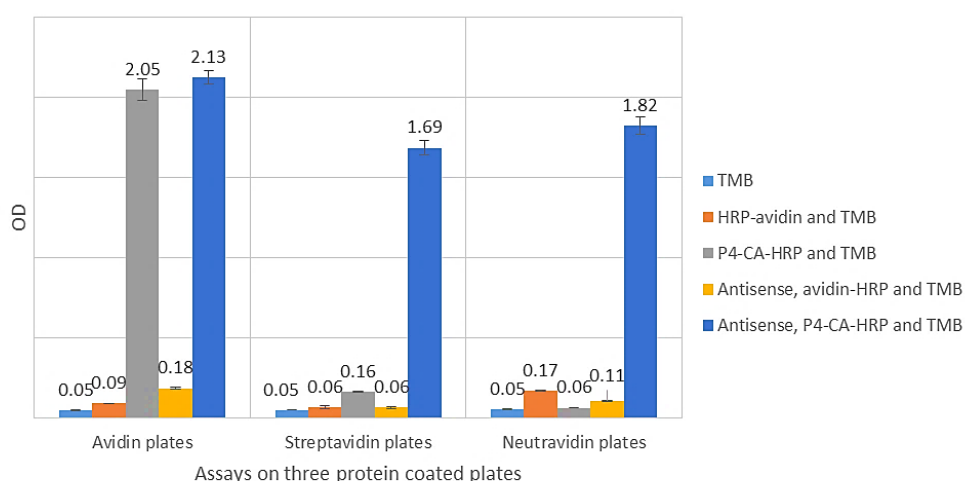
Figure 5.20 P4-CA binding on the protein coated plates immobilized with Antisense-CA using pre-formed P4-CA-HRP complexes. Each data point was repeated in triplicates.

Similarly, on the Antisense-CA plates, colorimetric signals were detected from the wells where biotinylated P4-CA and avidin-HRP were sequentially added and no obvious non-specific binding of biotinylated P4-CA or avidin-HRP was observed (Figure 5.21). However, the colorimetric signals developed on the Antisense-CA plates, which were prepared using the plate coated with neutravidin, appeared to be much lower than those on the Antisense-CA plates coated with streptavidin (Figure

5.21). The reason was not clear. The neutravidin plates were purchased from Thermo Fisher and pre-blocked by a SuperBlock™ buffer by the manufacturer. It was suspected that the blocking may affect the binding of biotinylated P4-CA to Antisense-CA on the surface. Thus, sequential binding of biotinylated P4-CA and HRP-avidin on the Neutravidin plate was not used in further experiments.
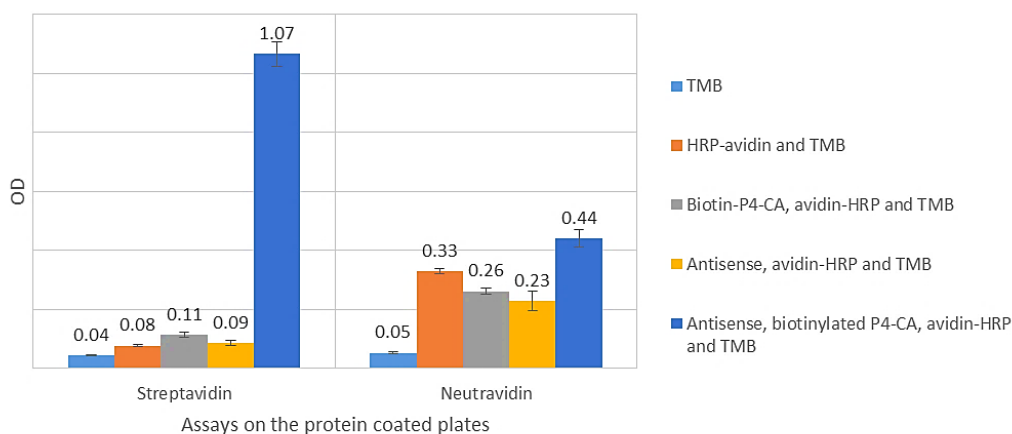
Figure 5.21 P4-CA binding on the protein-coated plates immobilized with Antisense-CA using sequential binding of biotinylated P4-CA and avidin-HRP. Each data point was repeated in triplicates.

Comparing the colorimetric signals developed by pre-formed P4-CA-HRP conjugates, and those by sequentially adding biotinylated P4-CA and HRP-avidin, the former resulted in relatively high signals in general, possibly due to fewer wash steps or more stable binding of P4-CA-HRP conjugates to the Antisense-CA surface than P4-CA ssDNA alone. Possibly, by forming P4-CA-HRP conjugates, the negative charge of P4-CA was partially neutralized and therefore bound the negatively charged Antisense-CA more stably. Also, there were two P4-CA molecules per P4-CA-HRP that may have enhanced the binding of P4-CA-HRP and Antisense-CA.

5.3.4.2 The effect of P4 on the binding of P4-CA to the Antisense-CA plates

When P4-CA-HRP or biotinylated P4-CA was incubated with 50 µg/ml P4 before being added to the Antisense plates, no inhibition of P4 on the binding of pre-formed P4-CA-HRP to the Antisense-CA plates was observed (Figure 5.22a), but the binding of biotinylated P4-CA to the Antisense-CA plates was reduced by about 14% (Figure 5.22b). The conjugation with avidin-HRP may account for the difference in the effects of P4: firstly, the conjugation of P4-CA to avidin-HRP may affect the interaction

of P4-CA to P4 due to the steric hindrance of binding, or change the folding of P4-CA due to the surface charges of avidin-HRP; secondly, there were two P4-CA molecules in each pre-formed P4-CA-HRP-avidin and thus it may require both P4-CA to bind to P4 in order to inhibit the binding of P4-CA-HRP to the Antisense plates, which would be more difficult; thirdly, P4-CA-HRP may bind the Antisense-CA plates more stably as discussed above.
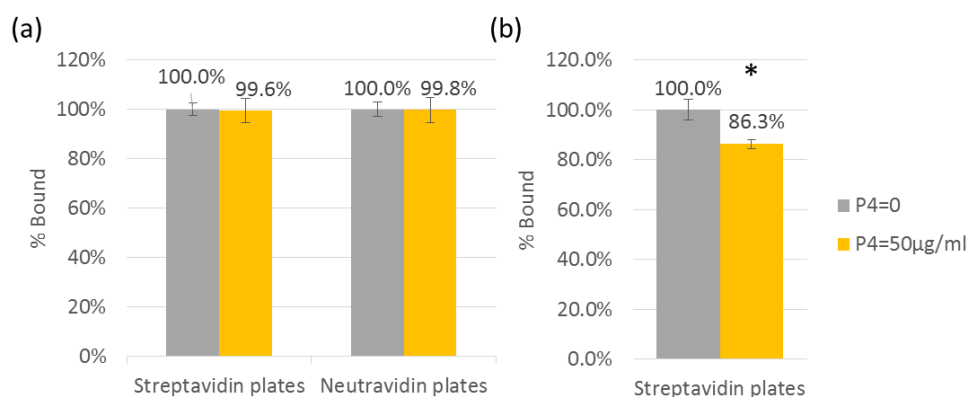
Figure 5.22 The effect of P4 (50 µg/ml) on the binding of P4-CA to the Antisense-CA plates: (a) pre-formed P4-CA-HRP was incubated with P4 before being added to the Antisense-CA plates; (b) biotinylated P4-CA was incubated with P4 before being added to the Antisense-CA plates followed by avidin-HRP. Each data point was repeated in triplicates. * Significant difference at t-test $p<0.05$ levels compared with P4 = 0.

5.3.4.3 Optimization of the sequential binding assays

To further improve the inhibition effect of P4 on the binding of biotinylated P4-CA to the Antisense surface, it was attempted to increase the molar ratio of P4 to P4-CA/Antisense-CA by decreasing the concentration of Antisense-CA and P4-CA. On the streptavidin plates, decreasing the concentrations of either biotinylated Antisense-CA (0-10 nM) or biotinylated P4-CA (0-5 nM) decreased the colorimetric signals (Figure 5.23a) and more than 1 nM of both biotinylated Antisense-CA and P4-CA were necessary to maintain enough signal-to-noise ratios. The effect of P4 (50 µg/ml) on the binding of biotinylated P4-CA (1 or 5 nM) on the Antisense-CA plates prepared with 1 or 10 nM Antisense-CA was measured (Figure 5.23b). The highest inhibition of P4 (~18%) was observed, when 1 nM biotinylated P4-CA was incubated with 50 µg/ml P4 before being added on the Antisense-CA plates prepared by 10 nM biotinylated Antisense-CA. Although the inhibition effect of P4 demonstrated by the colorimetric

aptasensors was higher than the SPR and fluorescent aptasensors, it was still limited, given the high concentration of P4 used and the high molar ratio of P4 to P4-CA/Antisense-CA. It was suspected that P4-CA may bind P4 at a low binding affinity or the binding of P4 and P4-CA had limited inhibition effect on the binding of P4-CA and Antisense-CA as discussed previously.
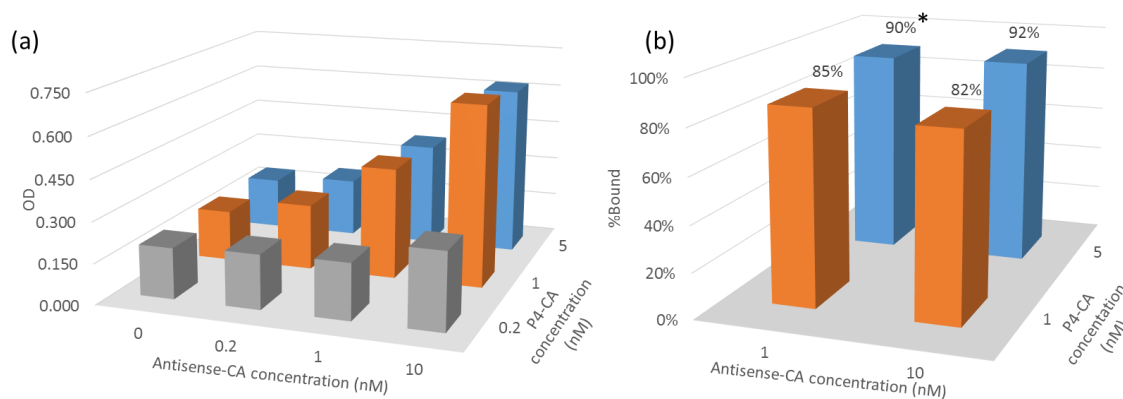
Figure 5.23 Optimization of the concentrations of Antisense-CA and P4-CA on the streptavidin plates: (a) colorimetric signals developed using Antisense-CA and P4-CA of various concentrations; (b) the inhibition effect of P4 (50 µg/ml) on the binding of biotinylated P4-CA (1 or 5 nM) to the Antisense-CA plates prepared by 1 or 10 nM biotinylated Antisense-CA. Each data point was repeated in duplicates. * Significant difference at t-test $p < 0.05$ levels compared with P4 = 0.

5.3.5 The binding of P4-CA to P4

Little direct binding of P4 and the aptamer P4-CA was detected using either the SPR or fluorescent aptasensor developed here, while P4 showed limited inhibition on the binding of P4-CA and Antisense-CA on the SPR, fluorescent and colorimetric aptasensors. It was difficult to diagnose the problems and improve the sensor performance since P4-CA is not well characterized, lacking the information on the binding affinity, binding sequence, folding structure, specificity, and selectivity, *etc.*.

The binding constant of P4-CA to P4 was not determined, although Neoventures showed the binding of P4 and P4-CA using GNP analysis. The binding affinities as well as the specificities of the same aptamers can vary depending on the methods, e.g. K_D values of P4-G13 and P4-G11 listed in Table 5.1 and found by other researchers [104, 198, 209]. The status of the target or the aptamer (in solution or on a solid support), the modification of them and the sensitivity of detection technology all play some role in determining the binding affinity. P4-CA was selected *via* FRELEX and evaluated *via* GNP

analysis by Neoventures, where neither P4-CA, nor P4 was attached to a surface or modified with labels (*e.g.* fluorophore or biotin). Yet, both our SPR and fluorescent aptasensors designed to detect direct binding between P4 and P4-CA involved immobilizing P4 on a surface and used fluorescent-labeled P4-CA, which was different from how P4 and P4-CA were used FRELEX and GNP analysis, and may affect the binding affinity by causing steric hindrance of binding, covering the binding sites, or affecting the folding of the aptamer [198, 209]. The other difference laid in the signal transduction.

During FRELEX, the bindings of P4-CA and P4 were followed by PCR, which efficiently amplified the binding event, while the signal transduction in the aptasensors here such as SPR, fluorescence and colorimetric signals was less efficient in amplifying the binding effect. Interestingly, the enzymatic reactions used in the colorimetric aptasensor usually efficiently improve detection sensitivity in immunosensors, but they showed limited improvement on the aptasensors developed here and similar results were found in other aptasensors [210]. Indeed, the choice of signal transduction and detection techniques for small molecules aptamers is limited by the low molecular weight of the small molecule [209]. These may be some of the reasons why limited, direct binding of P4 and P4-CA was detected or the binding affinity was found low.

Besides the affinity, the information on the binding sequences is important for the design of the aptasensors using antisense probes. Not only does the binding affinity of the aptamer and the antisense probe influence the performance of these aptasensors [211], but also does the sequence of the antisense probe. Munzar *et al.* designed two antisense probes of the same sequence lengths and the similar binding affinities to an ATP aptamer, but they resulted in a 55-fold difference in LODs in detection of ATP, where higher detection sensitivity was achieved by the antisense probe that hybridizes to part of the binding sequences of the aptamer to ATP [212]. However, the binding sequences of P4-CA to P4 is not available, which made it difficult to improve the aptasensors designed here using P4-CA and an antisense probe.

Another important aspect is the folding of the aptamer. The consensus of the folded structures is suggested to be more important than the consensus of the sequences of the aptamers that bind the same target molecule [190]. Some aptamer protocols emphasize preheating aptamers and cooling them down to room temperature in the buffers containing Mg^{2+}, to help the aptamers fold into proper

122

conformation before target binding [197]. However, in our experiments, no difference in P4-CA and P4 binding was observed using pre-heated P4-CA or different binding buffers. It is suggested that similar to the other ligand-binder systems there may exist two binding pathways of aptamers, the confirmation selection model [213] and induced fit model [214].

As illustrated by Munzar *et al*. in Figure 5.24, aptamers can pre-fold into the conformations that bind the target, or they can fold into a specific conformation only upon binding to the target. In the conformational selection model, it is important to pre-fold aptamers into certain conformations before target binding so that the preheating of the aptamers and the choice of the buffers (*i.e.* buffer components, ionic strength, pH and temperature) are important, especially when one aptamer sequence may have many possible secondary structural variants whose thermodynamic stabilities are affected by the buffer conditions [192]. However, *in silico* folding analysis by DINAMelt and GRS Mapper [215] showed limited secondary structures in P4-CA without P4, suggesting P4-CA is unlikely to fold into a specific conformation before binding. Meanwhile, many aptasensors operate based on the induced fit model, where the conformations of the aptamer change before and after binding the target [216-218]. Chushak and Stone used *in silico* methods to show that (1) the free energy of secondary structure formation of some RNA aptamers is significantly lower than the median same-length random sequence value; and (2) some RNA aptamers undergo conformation change upon target binding to rest in a conformation of lower free energy [219], which indicates the thermos-stability of the secondary structures of RNA aptamers lies in both the sequence and the binding to its target. Also, it indicated that the binding complex of the aptamer and its target likely has lower energy after all, so it may not be necessary (or sometime even impossible) for the aptamer to fold into a certain conformation favored by target binding beforehand. However, it may be more efficient (shorter incubation time) for the aptamer to bind to its target if a target-binding conformation can be formed in advance.

It is also possible that the binding pathway is determined by the type of interaction between the aptamer and its target. It is not clear how P4-CA interacts with P4, but often the aptamers that bind small molecules of aromatic rings fold into binding pockets to stack the target coplanarly with an adjacent base to form intermolecular hydrogen bonds [91, 218-220]. Similarly, a P4 aptamer was found to interact with an A-ring of P4 with the formation of a hydrogen bond with C17 group to stabilize the binding [195]. In such folding structures, the small molecule targets are usually buried within the small binding pocket

[218]. Therefore, the aptamers more likely fold into a certain conformation with the presence of small molecules rather than beforehand. That may also explain why pre-heating P4-CA did not make any difference in P4 binding. Metal ions in the buffers are suggested to be important for the binding of aptamers, as they can stabilize the folding structure by neutralizing the high density of negative charge created by multiple phosphate groups [221] and increase the binding of the aptamer to their target [221-224]. However, the metal ions were also found to decrease the binding, especially if electrostatic attraction is involved in the interaction [225-227]. The importance of different ions or buffers may differ between individual aptamers, and some aptamers can bind their targets in different buffers [97, 100, 194]. Thus, it is not surprising that different buffers had no effect on P4-CA.
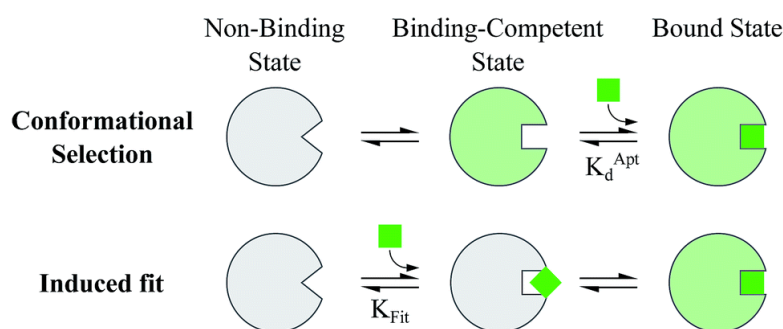
Figure 5.24 The two binding pathways of ligand and binder systems [212].

All the above fundamental biological questions of P4-CA are indeed important for the design, troubleshooting and improvement of the aptasensors. However, unfortunately due to the limited laboratory resources, skills and time, the experiments to answer these questions were not conducted.

5.4   Conclusions

In this chapter, a newly selected P4 aptamer – P4-CA – was investigated for its potential in replacing *anti*-P4 mAbs as the recognition molecules of biosensors. However, P4-CA showed very limited binding to P4 on either the SPR aptasensors or the fluorescent aptasensors, even when 1 µM P4-CA was used to bind the P4 immobilized sensor surfaces. Also, P4 showed limited inhibition on the binding of P4-CA and its antisense probe, Antisense-CA, on the SPR, and fluorescent and colorimetric aptasensors. The

maximum inhibition effect was only about 18% when 50 µg/ml P4 was used to inhibit the binding of 1 nM P4-CA to the Antisense-CA surface of the colorimetric aptasensor.

The performance of P4-CA was not as good as *anti*-P4 mAbs on these biosensors. It was suspected that the binding affinity of P4-CA and P4 was much lower than that of *anti*-P4 mAbs. Different buffer conditions and preheating P4-CA showed no effect on the performance of these aptasensors. It was possible that the immobilization of P4 on the sensor surfaces and labeling P4-CA affected the binding of P4-CA and P4, as free P4 and unlabeled P4-CA were used during the selection process and initial verification assays of P4-CA. Further, the inhibition effect of P4 on the binding of P4-CA and its antisense probe might be improved by re-designing of antisense probes. Yet, since the information of P4-CA such as the binding affinity, binding sequence, target interaction and folding structure was not available, it is difficult to diagnose the problems and improve the design of P4-CA aptasensors.

In the future, it would be helpful to develop evaluation methods to determine the binding affinity of P4-CA and the methods could be used to determine the binding sequences of P4-CA using truncated sequences. During the development of evaluation methods, it is important to align the aptamer assay formats of evaluation methods with those of the final applications, as the status of targets or aptamers (in solution or on a solid support), the modification of them and the sensitivity of detection technologies all play roles in determining the binding affinity. Once the evaluation methods and aptamer information are available, it is possible to optimize P4-CA sequences for higher P4 binding affinity and design of new antisense probes for better performances of aptasensors, which may lead to more sensitive P4 detection. A workflow of evaluating and optimizing aptamers is provided by McKeague *et al.* [198], which would be a good guide for future work on aptamers. Alternatively, one can investigate other P4 aptamers from literatures or select new P4 aptamers for the potential of replacing *anti-P4* mAbs in P4 detection as well as

Last, but not least, aptamers have many advantages over antibodies as summarized previously, but they are still relatively new in research and application. Biological fundamental questions such as binding affinities, binding sequences, folding structures and target interaction are not completely understood. Also, although some aptamers show binding affinities as high as antibodies, this is not necessarily the case of all aptamers. For example, Piro *et al.* compared electrochemical

immunosensors and aptasensors for small organic molecule detection and concluded that immunosensors are more sensitive than aptasensors due to higher affinities of antibodies [210]. Other problems related to the selection and application of small molecule aptamers can be found in the review by Pfeiffer and Mayer [197]. Nevertheless, with steady progress in research and application of aptamers, it is expected to obtain a better understanding in biological fundaments of aptamers and design new chemically modified nucleic acids for synthesis of aptamers with a higher binding affinity and stability, which will overcome current limitations in selection and application of aptamers.

6   Chapter 6: Conclusions and Future Perspectives

A milk P4 test was developed using mAb and MB conjugates on an SPR platform, where the MB conjugates were used to separate P4 from milk before measurement by SPR to reduce milk matrix effects. The assay achieved an LOD of 0.020 ± 0.006 ng/ml P4 in the buffer and 0.036 ± 0.010 ng/ml P4 in diluted raw milk. The P4 concentrations in the cow's milk collected on dairy farms measured by this SPR assay showed good correlation with those measured by a commercial ELISA kit and exhibited expected patterns of P4 levels during the estrous cycles, although there were differences between the P4 concentrations determined by the two methods. Nevertheless, the SPR responses obtained during the SPR tests of the milk samples correlated well with the estrous cycles of the cows and could be used to directly predict the onset of estrus. Thus, this test showed potential in monitoring the estrous cycles of cows to aid in the reproductive management for dairy farms. In the future, it may be transferred to a low cost sensor platform to realize cost-effective milk P4 tests for routine uses on dairy farms.

During the development of the test, there were two major obstacles in using relatively big MBs (100 nm in diameter): the restrained distance (300 nm from the gold surface), where the evanescent wave travels and SPR signals can be stimulated effectively upon the binding of MBs to the surface; and the steric hindrance, which prevents the binding of the antibodies conjugated to MBs and the small molecule (P4) immobilized on the sensor surface. To overcome these obstacles, two strategies were employed. Firstly, a low molecular weight of gold coating agent - a new carboxylated terthiophene molecule - was used to functionalize the SPR gold surface. The self-assembled monolayer of this molecule is in the order of nanometers thick, which is thin enough to allow the large MB to effectively stimulate SPR signals upon binding to the sensing surface by bringing the binding site closer to the SPR gold surface. Secondly, to reduce the steric hindrance of binding, P4 was immobilized *via* a long linker to pre-immobilized OVA on the SPR surface, while mAb was conjugated to MBs *via* maleimide coupling using a bifunctional crosslinker. The long linker between P4 and OVA extended P4 away from the SPR surface and increased the flexibility of its movement so that P4 was more accessible to the MB conjugates. The maleimide coupling, *via* the reduced disulfide bond in mAbs improved the specificity of the conjugation and potentially resulted in better orientation and uniformity of mAbs on the MB surfaces. The increased accessibility of P4 and the improved orientation of mAb aided the binding of MB conjugates to the SPR sensor surfaces, which led to more sensitive P4 detection.

It is worth mentioning that the application of new materials as well as the new methods developed here are not limited to P4 tests in milk. For example, the new carboxylated terthiophene forms stable SAMs on gold surfaces and provides well-organized anchors for molecule immobilization, which can be used in other SPR sensors, or other sensors based on gold surfaces with the potential of multiple reuses in general. The *in situ* conjugation approach of synthesizing P4 and OVA on the sensing surface is much quicker, easier and more environmentally-friendly than the conventional approach of synthesizing conjugates in solution before immobilization. This could be extended to prepare conjugates of other small molecules, peptides or even proteins on sensor surfaces. Furthermore, the method of synthesizing antibody and magnetic particle conjugates are easy and versatile, with potential application in biosensors for food safety, environmental monitoring, and disease diagnostics, *etc.* where the matrix interferes with sample measurements.

A newly selected P4 aptamer was investigated for its potential in replacing mAb as the recognition molecules of P4, however, it showed a low binding ability to P4 in several optical biosensors designed in this thesis, much lower than mAb used. Thus, this aptamer is not a suitable replacement for mAbs at present. More research on the binding affinity, binding sequences, and folding structure of this aptamer may provide more information to improve the binding affinity of this aptamer and the design of biosensors in the future. Alternatively, other P4 aptamers from literatures or new selection processes can be investigated for the potential of replacing *anti-P4* antibodies in P4 detection. In general, although aptamers have some advantages over antibodies and their research and application progresses rapidly, they are still relatively new. Some biological fundamental questions are to be answered and some limitations in selection and application of aptamers are to be overcome, before they can be extensively used in biosensors and other fields to replace antibodies.

Appendices

Table A1 Summary of P4 inhibition assays performed on T3C SAM surfaces and CM5 surfaces. The standard curves of these assays were plotted in Figure A1 in the Appendices.

Assay No.	1	2	3	4	5	6
Surface Type	T3C SAM	T3C SAM	T3C SAM	CM5	CM5	CM5
mAb concentration used (µg/ml)	1	0.8	0.5	3	4	4
Buffer used	HBS	PBST	HBS	HBS	PBST	HBS
Four parameters regression results						
min	-0.63	0.00	9.54	0.58	-6.58	-12.70
max	197.16	214.72	218.03	163.87	188.59	205.68
EC50 (ng/ml)	1.61	1.64	0.93	5.19	8.28	4.37
Hillslope	-1.71	-2.12	-2.55	-1.80	-2.10	-1.62
LOD (ng/ml)	0.42	0.82	0.18	1.17	2.11	0.45
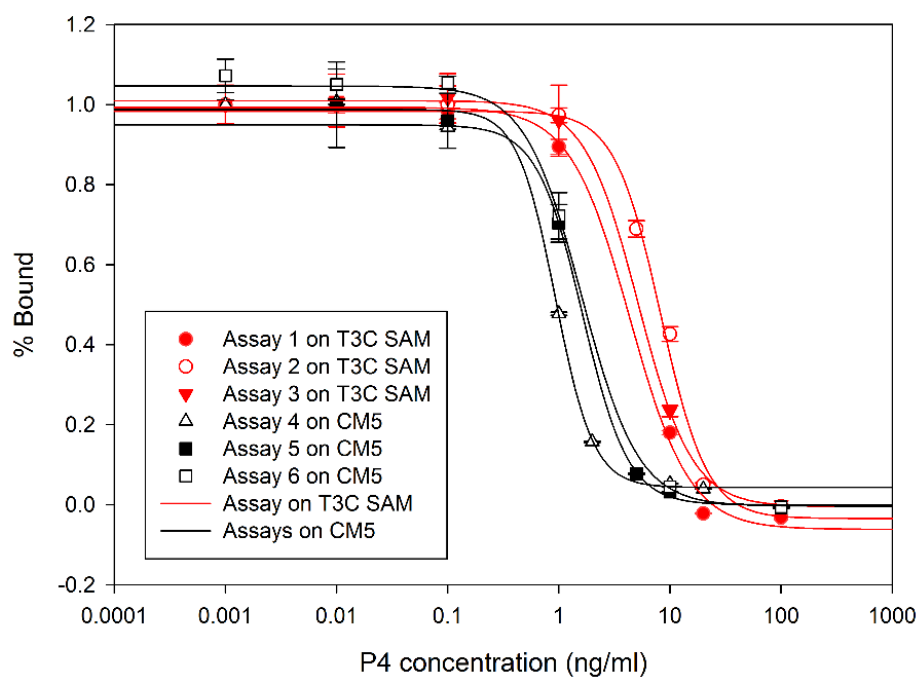
Figure A1 P4 inhibition assays on T3C SAM surfaces and CM5 surfaces immobilized with P4-OVA. Each data point was repeated in triplicates. The assay results are summarized in Table A1 in the Appendices.

Table A2 Summary of four *in situ* synthesis experiments

Synthesis Experiment	OVA and linker immobilization	OVA immobilization level	P4 activation	P4 attachment	Observation after P4 attachment	Synthesized conjugates
1	OVA was immobilized and the linkers were extended as described in Section 3.2.2 in Chapter 3.	20156.2±223.9 (n=4)	P4 3-CMO (19.4 mg in 0.2 ml DMF) was activated using DCC (41.27 mg in 0.15 ml DMF) and NHS (23.02 mg in 0.15 ml DMF). After 3 hours incubation at room temperature under constant stirring, the mixture was centrifuged at 1000 rpm for 2 min and the supernatant was reserved.	30 µl of the supernatant containing reactive P4 NHS-ester was dropped on the CM5 chip where OVA and linkers had been immobilized. After one hour incubation at room temperature, the chip was rinsed by ethanol and water and air-dried.	The entire gold chip surface was covered by some white substance, suspected to be DCC. Washing with ethanol helped to remove some of it but the final chip appeared to have a layer of white substance on top.	P4-3 atoms-OVA, P4-19 atoms-OVA, P4-26 atoms PEG-OVA, P4-26 atoms-OVA
2		22344.3±586.9 (n=4)	P4 3-CMO (9.7 mg in 0.2 ml DMF) was activated using DCC (10.32 mg in 0.15 ml DMF) and NHS (5.8 mg in 0.15 ml DMF). After 3 hours incubation at room temperature under constant stirring, the mixture was centrifuged, and the supernatant was reserved.	50 µl of the supernatant containing reactive P4 NHS-ester was diluted with 350 µl DMF and 100 µl water. Using Biacrore, 200 µl of diluted P4 NHS ester was injected for 20 min over the CM5 chip surface where the OVA and linker had been immobilized, followed by injection of ethanol and water immediately. Finally, the chip was taken out of Biacore and rinsed by DMF, ethanol and water before being air-dried.	The chip surface where flow cells were located appeared covered by some white substance, less than what was observed in Experiment 1, while the rest of the chip surface remained a gold colour. All the flow cells had a big shift in baselines and the baselines reached maximum RU of Biacore detection limit. Washing with DMF helped to remove some of the white substance and the baselines dropped back. Biacore was desorbed. Later, a System check test showed blockage in the fluidic system, which was replaced by a Service Engineer. Likely the blockage was due to injection of P4 NHS-ester in DMF.	P4-3 atoms-OVA, P4-19 atoms-OVA, P4-26 atoms PEG-OVA, P4-26 atoms-OVA

Synthesis Experiment	OVA and linker immobilization	OVA immobilization level	P4 activation	P4 attachment	Observation after P4 attachment	Synthesized conjugates
3	OVA was immobilized and the linkers were extended as described in Section 3.2.2 in Chapter 3.	16067.0±61.8 (n=2)	P4 3-CMO (4 mg in 0.6 ml ethanol) was activated using EDC (37.5 mg in 0.2 ml ethanol) and NHS (22.5 mg in 0.2 ml ethanol) as described in Section 3.2.2 in Chapter 3.	Reactive P4 NHS-ester in ethanol was injected over CM5 chip surfaces where OVA and linker had been immobilized using Biacore as described in Section 3.2.2 in Chapter 3. Finally, the chip surfaces were rinsed by ethanol and water, and air-dried.	The chip surfaces remained a gold colour although where flow cells were located it appeared less shinny. Biacore system was desorbed immediately after P4 attachment experiments and worked fine.	P4-26 atoms PEG-OVA, P4-26 atoms-OVA
4		16636.3±380.5 (n=5)				P4-3 atoms-OVA, P4-19 atoms-OVA, P4-26 atoms-OVA, P4-33 atoms-OVA, P4-32 atoms PEG-OVA
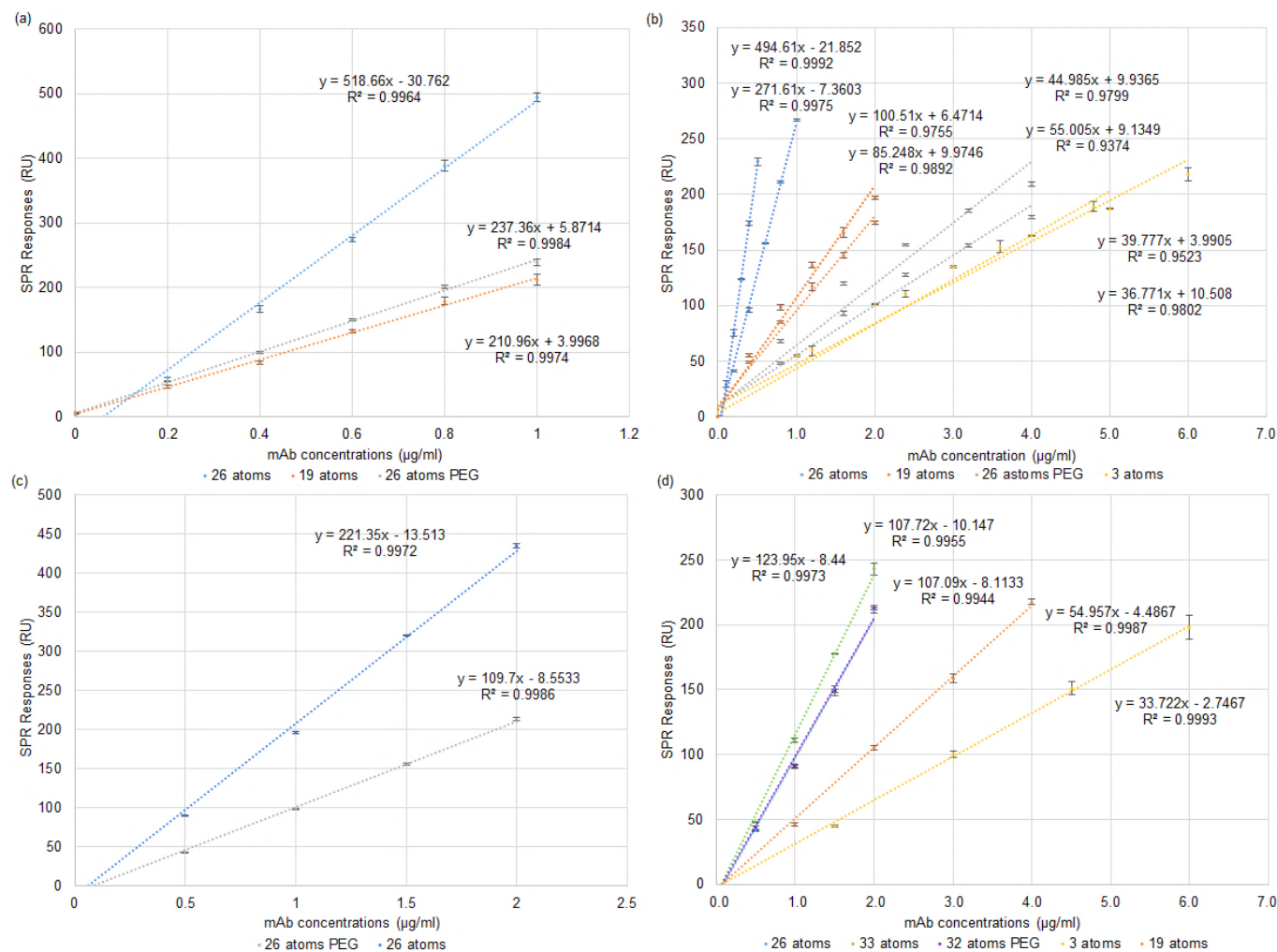
Figure A2 mAb binding assays on P4-linker-OVA surfaces prepared using *in situ* synthesis approach. (a)~(d) are four separate *in situ* synthesis experiments when different P4-linker-OVA conjugates were synthesized as described in Table A2. P4-OVA conjugates are described using their linker lengths in the legends. Each data point was repeated in triplicates.
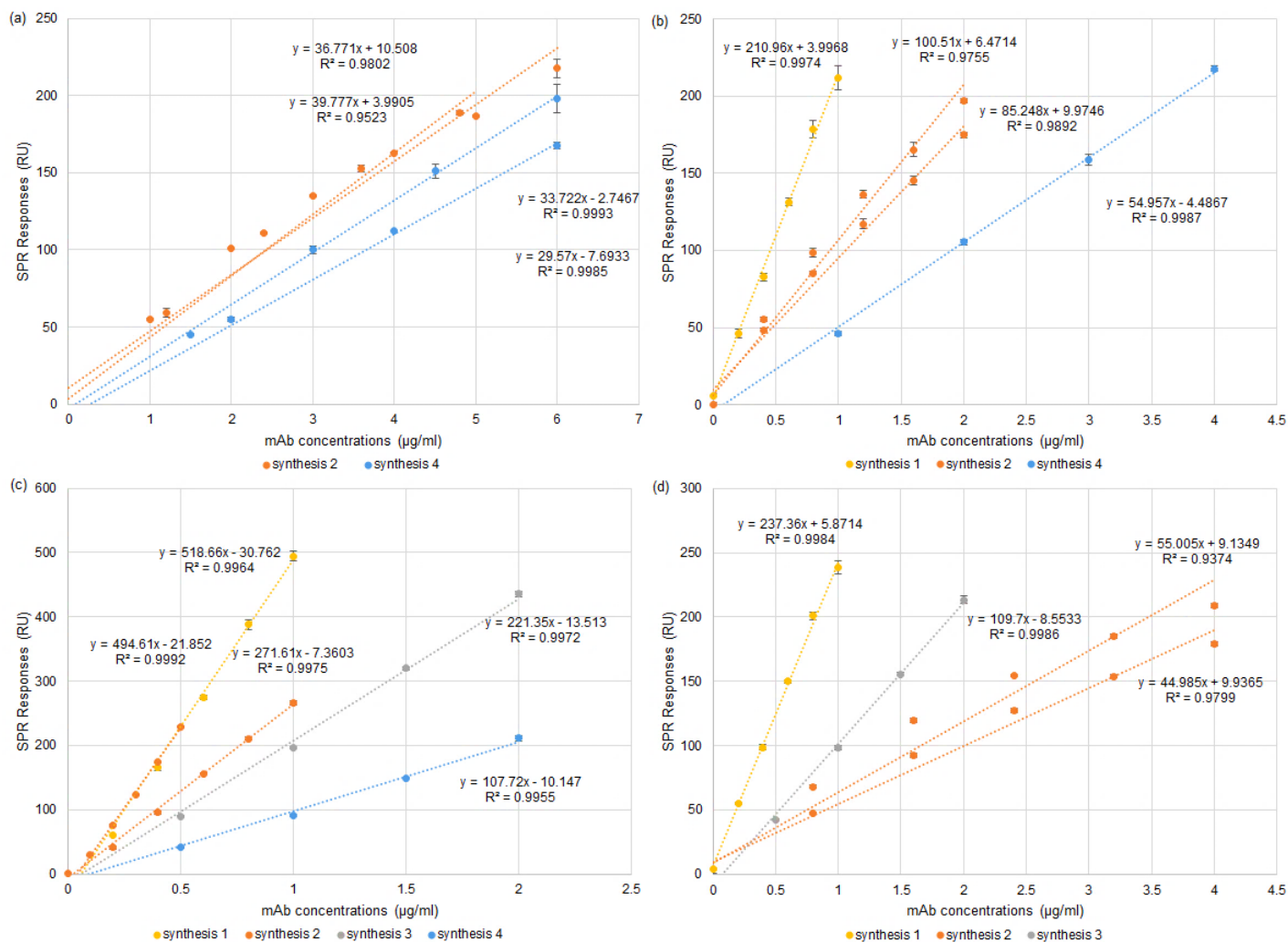
Figure A3 mAb binding assay on CM5 surfaces immobilized with four different P4-linker-OVAs synthesized *in situ*. The conjugates were synthesized in different experiments as described by the legends. (a) P4-3 atoms-OVA, (b) P4-19 atoms-OVA, (c) P4-26 atoms-OVA and (d) P4-26 atoms PEG-OVA. Each data point was repeated in triplicates.

Table A3 Summary of P4 standard curves obtained on CM5 surfaces immobilized with different P4-linker-OVA conjugates using the *in situ* synthesis method.

Conjugates	P4-3 atoms-OVA			
Synthesis experiment [+]	Synthesis 2 ^			Synthesis 4
mAb concentration (µg/ml) [#]	3.6	4	5	4.8
min	-0.04	-0.02	-0.06	-0.04
max	0.99	0.99	0.98	1.00
EC50 (ng/ml)	7.82	6.11	11.24	1.78
Hillslope	-2.11	-2.38	-1.92	-2.03
R	0.9962	0.9987	0.9968	0.9996
LOD (ng/ml)	-*	0.98	1.07	0.33

Conjugates	P4-19 atoms-OVA	
Synthesis experiment [+]	Synthesis 2 ^	
mAb concentration (µg/ml) [#]	1.6	2
Min	-0.03	0.01
Max	0.97	0.98
EC50 (ng/ml)	4.50	4.88
Hillslope	-2.92	-3.28
R	0.9970	0.9976
LOD (ng/ml)	1.43	1.7

Conjugates	P4-26 atoms-OVA		P4-26 atoms PEG-OVA	
Synthesis experiment [+]	Synthesis 2 ^		Synthesis 2 ^	
mAb concentration (µg/ml) [#]	0.3	0.6	2.4	3.2
Min	-0.10	0.04	-0.022	-0.02
Max	1.00	0.99	0.98	0.99
EC50 (ng/ml)	0.65	1.26	4.99	7.30
Hillslope	-1.84	-1.97	-3.45	-2.19
R	0.9996	0.9995	0.9983	0.9975
LOD (ng/ml)	0.06	0.29	-*	-*

Conjugates	P4-32 atoms PEG-OVA	P4-33 atoms-OVA
Synthesis experiment [+]	Synthesis 4	Synthesis 4
mAb concentration (µg/ml) [#]	1.5	1.25
Min	20.44	17.82
Max	163.91	152.07
EC50 (ng/ml)	0.86	0.63
Hillslope	-2.26	-2.49
R	0.9992	0.9996
LOD (ng/ml)	0.18	0.15

+ The *in situ* synthesis experiments (Table A2) when the conjugates were immobilized
# The concentrations of mAb used in P4 inhibition assays
* LOD were not available when calculated as the concentrations corresponding to the blank signals less two standard deviations of the blank signals
^ Standard curves were shown in Figure A4 in the Appendices.
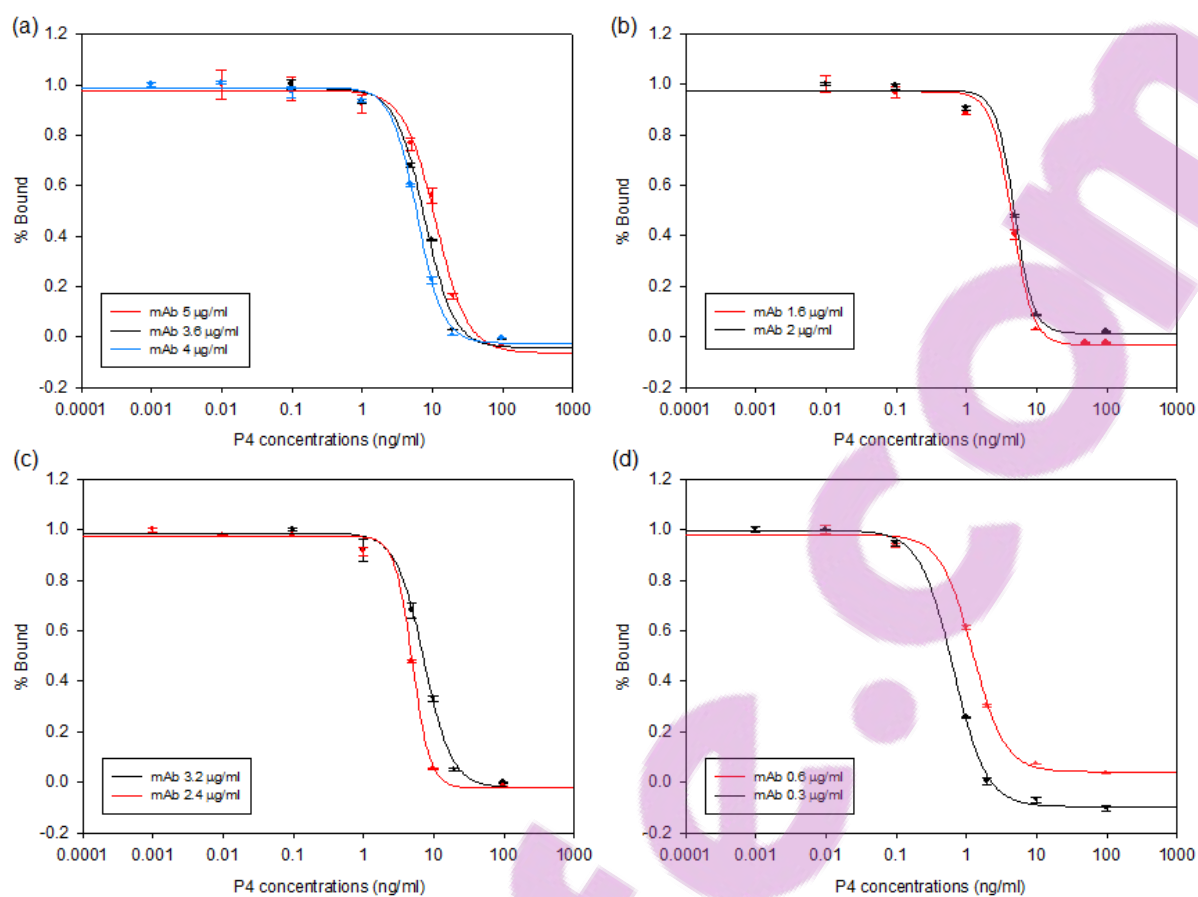
Figure A4 P4 standard curves obtained on four P4-linker-OVA surfaces prepared in one *in situ* synthesis experiment (Experiment #2 in Table A2). (a) P4-3 atoms-OVA, (b) P4-19 atoms-OVA, (c) P4-26 atoms PEG-OVA and (d) P4-26 atoms-OVA. mAb concentrations used in the assays were indicated in the legend. Each data point was repeated in triplicates. The assays results were listed in Table A2 in Appendices.

Table A4 The stability of mAb and sAb-MB/ Protein A coated MB complexes.

Effect of wash [a]		
	SPR responses (RU)	
	Before wash	After wash
mAb and sAb-MB complex 1 [d]	175.9	90.5
mAb and sAb-MB complex 2 [d]	223.8	133.7
Effect of incubation [b]		
	SPR responses (RU)	
	Before incubation	After incubation
mAb and Protein A-MB complex	208.8 (60 µl/ 3 min)	57.7 (40 µl/ 2 min)
Effect of delayed injection [c]		
	SPR responses (RU)	
	before	after
mAb and sAb-MB complex 3 [d]	243.6	108.5
mAb and sAb-MB complex 4 [d]	264.7	126.0

a. mAbs and sAb-MBs were incubated at room temperature for 30 mins and the formed mAb and sAb-MB complexes were separated on a magnet and washed 3 times by HBS-EP buffer. Then, the complexes were re-suspended in HBS-EP buffer and injected over P4-OVA surfaces (60 µl / 3 min). The complexes were washed three more times and the binding was tested and compared.
b. Protein A coated MBs and mAb were incubated overnight under agitation to form mAb bounded Protein A coated MBs. The binding of these MBs were tested after the supernatant was removed and the MBs re-suspended in the buffer. The MBs were then incubated in HBS-EP buffer under constant shaking for 30 mins and the binding was tested again after the supernatant was removed and the MBs re-suspended
c. mAb and sAb-MBs were formed as described above. The binding was tested directly, then the complexes were left on the bench for 3 hours without shaking and the binding was tested again.
d. mAb and sAb-MB complexes 1-4 were prepared using different concentrations of antibodies.
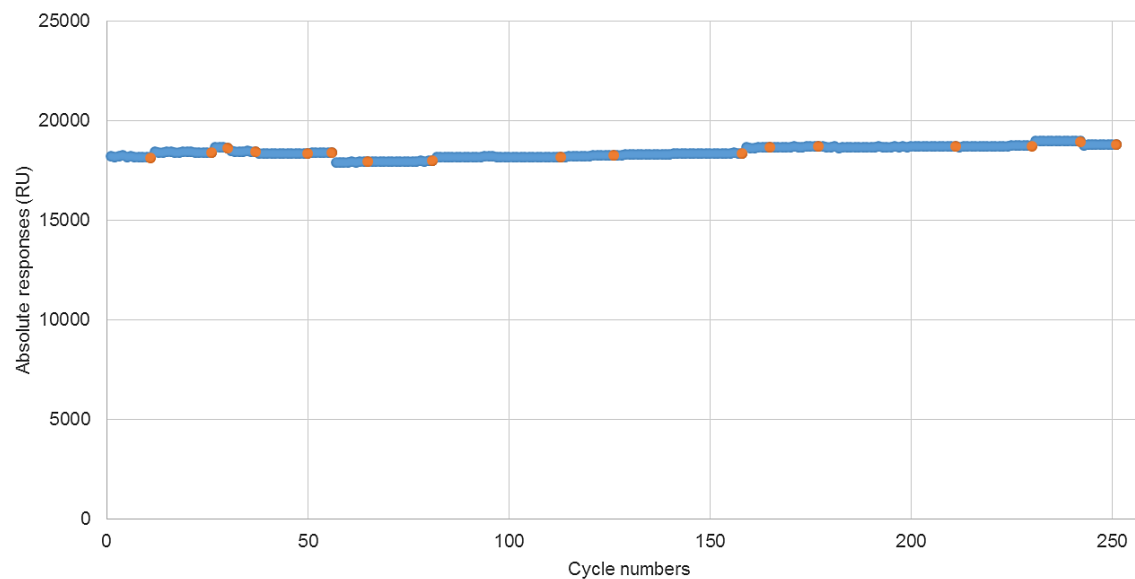
Figure A5 The baseline responses of a T3C SAM surface immobilized with P4-32 atoms PEG linker-OVA over multiple mAb-MB binding/regeneration cycles on different days over a two month period. The blue dots show absolute responses of the baselines. The red dots showed the last baseline response of each day. The baselines remained reasonably stable within each day. The fluctuation between days resulted from re-docking the chip or using different running buffers.

Table A5 LODs of P4 inhibition assays using mAb-SMCC-MBs with P4 standards prepared in the buffer or milk P4 standards and comparison by t-tests.

LODs of P4 inhibition assays using P4 standards prepared in the buffer			
	LOD (ng/ml)	Average (n=4)	SD (n=5)
1	0.013	0.020	0.006
2	0.026		
3	0.017		
4	0.023		

LODs of P4 inhibition assays using diluted milk P4 standards			
	LOD (ng/ml)	Average (n=6)	SD (n=6)
1	0.044	0.036	0.01
2	0.039		
3	0.032		
4	0.027		
5	0.050		
6	0.024		

Group Name	N	Missing	Mean	Std Dev	SEM
Buffer standards	4	0	0.0198	0.00585	0.00293
Milk standards	6	0	0.0360	0.0101	0.00412

Difference   -0.0162

$t = -2.876$ with 8 degrees of freedom.

95 percent two-tailed confidence interval for difference of means: -0.0293 to -0.00322

Two-tailed P-value = 0.0206

The difference in the mean values of the two groups is greater than would be expected by chance; there is a statistically significant difference between the input groups ($P = 0.021$).

One-tailed P-value = 0.0103

The sample mean of group LODs of P4 inhibition assays u exceeds the sample mean of group LODs of P4 inhibition assays u by an amount that is greater than would be expected by chance, rejecting the hypothesis that the population mean of group LODs of P4 inhibition assays u is greater than, or equal to, the population mean of group LODs of P4 inhibition assays u. ($P = 0.010$).

Power of performed two-tailed test with alpha = 0.050: 0.713

Power of performed one-tailed test with alpha = 0.050: 0.836

Table A6 EC50s of P4 inhibition assays using mAb-SMCC-MBs with P4 standards prepared in the buffer or milk P4 standards and comparison by t-tests.

EC50s of P4 inhibition assays using P4 standards prepared in the buffer			
	EC50 (ng/ml)	Average (n=4)	SD (n=4)
1	0.0346	0.056	0.022
2	0.0598		
3	0.0857		
4	0.0455		

LODs of P4 inhibition assays using diluted milk P4 standards			
	EC50 (ng/ml)	Average (n=6)	SD (n=6)
1	0.046	0.058	0.017
2	0.066		
3	0.040		
4	0.067		
5	0.083		
6	0.045		

Group Name	N	Missing	Mean	Std Dev	SEM
Buffer standards	4	0	0.0564	0.0221	0.0110
Milk standards	6	0	0.0578	0.0168	0.00685

Difference   -0.00143

$t = -0.117$ with 8 degrees of freedom.

95 percent two-tailed confidence interval for difference of means: -0.0296 to 0.0268

Two-tailed P-value = 0.910

The difference in the mean values of the two groups is not great enough to reject the possibility that the difference is due to random sampling variability. There is not a statistically significant difference between the input groups (P = 0.910).

One-tailed P-value = 0.455

The sample mean of group milk standards does not exceed the sample mean of the group buffer by an amount great enough to exclude the possibility that the difference is due to random sampling variability. The hypothesis that the population mean of group buffer is greater than, or equal to, the population mean of group milk standards cannot be rejected. (P = 0.455).

Power of performed two-tailed test with alpha = 0.050: 0.051

The power of the performed test (0.051) is below the desired power of 0.800.
Less than desired power indicates you are less likely to detect a difference when one actually exists.
Negative results should be interpreted cautiously.

Power of performed one-tailed test with alpha = 0.050: 0.062

The power of the performed test (0.062) is below the desired power of 0.800.
Less than desired power indicates you are less likely to detect a difference when one actually exists.
Negative results should be interpreted cautiously.
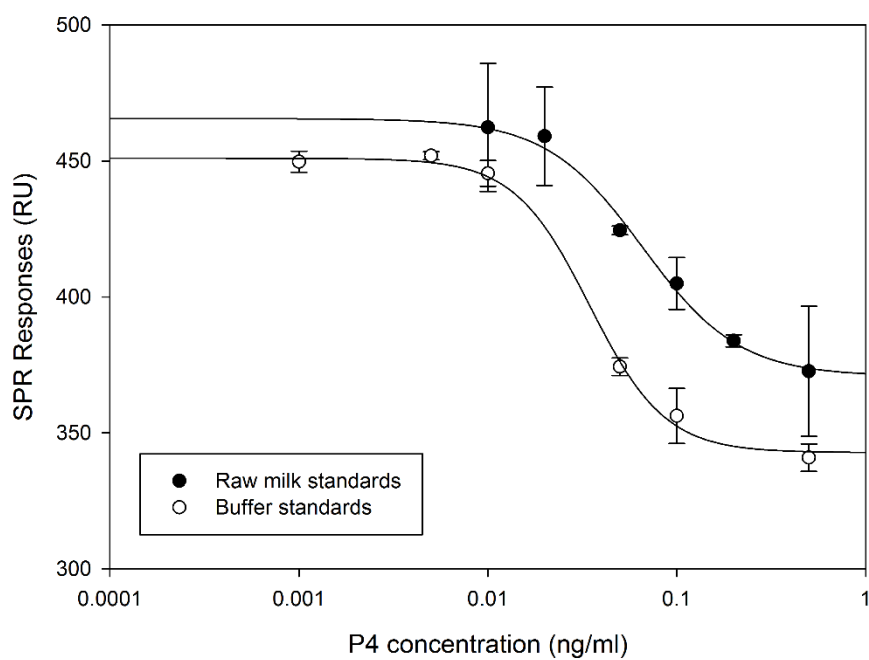
Figure A6 P4 inhibition assays using P4 standards prepared in the buffer and in diluted raw milk.

References

[1] D. Berry, N. C. Friggens, M. Lucy *et al.*, "Milk production and fertility in cattle," *Annu. Review of Animal Biosciences,* vol. 4, pp. 269-290, 2016.

[2] M. L. O'Connor, "Milk progesterone analysis for determining reproductive status," *The Pennsywania State University Publication DAS*, pp. 98-95, 1998.

[3] C. Inchaisri, R. Jorritsma, P. L. A. M. Vos *et al.*, "Economic consequences of reproductive performance in dairy cattle," *Theriogenology,* vol. 74, no. 5, pp. 835-846, 2010.

[4] E. Homer, Y. Gao, X. Meng *et al.*, "Technical note: A novel approach to the detection of estrus in dairy cows using ultra-wideband technology," *J. of Dairy Sci.,* vol. 96, no. 10, pp. 6529-6534, 2013.

[5] A. Chanvallon, S. Coyral-Castel, J. Gatien *et al.*, "Comparison of three devices for the automated detection of estrus in dairy cows," *Theriogenology,* vol. 82, no. 5, pp. 734-741, 2014.

[6] I. Michaelis, E. Hasenpusch, and W. Heuwieser, "Estrus detection in dairy cattle: Changes after the introduction of an automated activity monitoring system?," *Tierärztliche Praxis Großtiere,* vol. 41, no. 3, pp. 159-165, 2013.

[7] C. S. Mayne, D. R. Mackey, M. Verner *et al.*, "Fertility of dairy cows in Northern Ireland," *Veterinary Record,* vol. 150, no. 23, pp. 707-713, 2002.

[8] L. Ingenhoff, E. Hall, and J. House, "Evaluation of a cow-side milk progesterone assay and assessment of the positive predictive value of oestrus diagnosis by dairy farmers in New South Wales," *Australian Veterinary J.,* vol. 94, no. 12, pp. 445-451, 2016.

[9] J. A. Laing, and R. B. Heap, "The concentration of progesterone in the milk of cows during the reproductive cycle," *The British Veterinary J.,* vol. 127, no. 8, pp. xix-xxii, 1971.

[10] G. Gumauskas, V. Žilaitis, and J. Rudejevienė, "The dairy cows heat ability assessment by changes of progesterone concentration at postpartum," *Veterinarija ir Zootechnika,* vol. 68, no. 90, 2014.

[11] Y. Oku, T. Osawa, T.-I. Hirata *et al.*, "Validation of a direct time-resolved fluoroimmunoassay for progesterone in milk from dairy and beef cows," *The Veterinary J.,* vol. 190, no. 2, pp. 244-248, 2011.

[12] T. J. Reimers, R. D. Smith, and S. K. Newman, "Management factors affecting reproductive performance of dairy cows in the northeastern United States," *J. of Dairy Sci.,* vol. 68, no. 4, pp. 963-972, 1985.

[13] R. von Leesen, J. Tetens, W. Junge *et al.*, "Mathematical approaches to detect low concentrations in progesterone profiles," *animal,* vol. 7, no. 12, pp. 2008-2015, 2013.

[14] R. L. Nebel, "On-farm milk progesterone tests," *J. of Dairy Sci,* vol. 71, no. 6, pp. 1682-90, Jun, 1988.

[15] S. G. Moore, S. Scully, J. A. Browne *et al.*, "Genetic merit for fertility traits in Holstein cows: V. Factors affecting circulating progesterone concentrations," *J. of Dairy Sci.,* vol. 97, no. 9, pp. 5543-5557, 2014.

[16] G. A. Posthuma-Trumpie, A. van Amerongen, J. Korf *et al.*, "Perspectives for on-site monitoring of progesterone," *Trends in Biotechnology,* vol. 27, no. 11, pp. 652-660, 2009.

[17] Dairy Cattle Reproduction Council. (2012). *Back to the basics: explaining the estrous cycle* [Online]. Available: http://www.dcrcouncil.org/wp-content/uploads/2017/04/Back-to-the-Basics_Explaining-the-Estrous-Cycle.pdf.

[18] W. W. Thatcher, A. Guzeloglu, A. Meikle *et al.*, "Regulation of embryo survival in cattle," *Reproduction (Cambridge, England) Supplement,* vol. 61, pp. 253-266, 2003.

[19] P. Blavy, M. Derks, O. Martin *et al.*, "Overview of progesterone profiles in dairy cows," *Theriogenology,* vol. 86, no. 4, pp. 1061-1071, 2016.

[20] A. Dharap, "Effect of Season on pregnancy rates, milk progesterone, and milk melatonin profiles in water buffalo reared in Canada," M.S. thesis, Dept. Biomedical Sci., The Univ. of Guelph, Guelph, Canada, 2016.

[21] Y. Gao, R.V. Short, T.P. Fletcher, "Progesterone concentrations in plasma, saliva and milk of cows in different reproductive states," *British Veterinary J.,* vol. 144, no. 3, pp. 262-268, 1988.

[22] H. A. Robertson, "Sequential changes in plasma progesterone in the cow during the estrous cycle, pregnancy, at parturition, and post-partum," *Canadian J. of Animal Sci.,Science,* vol. 52, no. 4, pp. 645-658, 1972.

[23] J. A. McCracken, "The distribution of progesterone in body fluids and tissues of the dairy cow," Ph.D. dissertation, Endocrinology, Univ. of Glasgow, Glasgow , UK, 1964.

[24]   R. A. Harkness, and J. A. B. Darling, "Steroid levels in milk," *Acta Endocrinologica,* vol. 68, no. 1 Supplb, pp. S92-S92, 1971.

[25]   R. C. Rhodes. *The use of milk progesterone assays for reproductive management* [Online]. Accessed in 2014 from https://www.wvu.edu/~agexten/forglvst/Dairy/dirm9.pdf.

[26]   D. C. Bulman, and G. E. Lamming, "Milk progesterone levels in relation to conception, repeat breeding and factors influencing acyclicity in dairy cows," *J. of Reproduction and Fertility,* vol. 54, no. 2, pp. 447-458, 1978.

[27]   M. Delwiche, X. Tang, R. BonDurant *et al.*, "Estrus detection with a progesterone biosensor," *Transctions-Amer. Soc. of Agricultural Engineers,* vol. 44, no. 6, pp. 2003-2008, 2001.

[28]   J. B. Roelofs, F. J. C. M. Van Eerdenburg, W. Hazeleger *et al.*, "Relationship between progesterone concentrations in milk and blood and time of ovulation in dairy cattle," *Animal Reproduction Sci.,* vol. 91, no. 3-4, pp. 337-343, 2006.

[29]   R. B. Heap, M. Gwyn, J. A. Laing *et al.*, "Pregnancy diagnosis in cows: changes in milk progesterone concentration during the oestrous cycle and pregnancy measured by a rapid radioimmunoassay," *J. of Agricultural Sci.,* vol. 81, no. 01, pp. 151-157, 1973.

[30]   R. Haimov-Kochman, L. S. Shore, and N. Laufer, "The milk we drink, food for thought," *Fertility and Sterility,* vol. 106, no. 6, pp. 1310-1311, 2016.

[31]   G. Humbert, M.-F. Guingamp, G. Linden *et al.*, "The Clarifying Reagent, or how to make the analysis of milk and dairy products easier," *J. of Dairy Research,* vol. 73, no. 04, pp. 464-471, 2006.

[32]   I. Heertje, "Structure and function of food products: a review," *Food Structure,* vol. 1, no. 1, pp. 3-23, 2014.

[33]   E. H. Gillis, I. Traynor, J. P. Gosling *et al.*, "Improvements to a surface plasmon resonance-based immunoassay for the steroid hormone progesterone," *J. of AOAC International,* vol. 89, no. 3, pp. 838-842, 2006.

[34]   K. Sananikone, M. J. Delwiche, R. H. BonDurant *et al.*, "Quantitative lateral flow immunoassay for measuring progesterone in bovine milk," *Transctions-Amer. Soc. of Agricultural Engineers,* vol. 47, no. 4, pp. 1357-1365, 2004.

[35]   R. M. Pemberton, J. P. Hart, and J. A. Foulkes, "Development of a sensitive, selective electrochemical immunoassay for progesterone in cow's milk based on a disposable screen-printed amperometric biosensor," *Electrochimica Acta,* vol. 43, no. 23, pp. 3567-3574, 1998.

[36]   M. Tudorache, I. A. Zdrojewska, and J. Emnéus, "Evaluation of progesterone content in saliva using magnetic particle-based immuno supported liquid membrane assay (m-ISLMA)," *Biosensors and Bioelectronics,* vol. 22, no. 2, pp. 241-246, 2006.

[37]   C. Basheer, and H. K. Lee, "Hollow fiber membrane-protected solid-phase microextraction of triazine herbicides in bovine milk and sewage sludge samples," *J. of Chromatography A,* vol. 1047, no. 2, pp. 189-194, 2004.

[38]   B. Shao, H. Han, X. Tu *et al.*, "Analysis of alkylphenol and bisphenol A in eggs and milk by matrix solid phase dispersion extraction and liquid chromatography with tandem mass spectrometry," *J. of Chromatography B,* vol. 850, no. 1, pp. 412-416, 2007.

[39]   S. Bogialli, R. Curini, A. Di Corcia *et al.*, "Simple and rapid assay for analyzing residues of carbamate insecticides in bovine milk: hot water extraction followed by liquid chromatography–mass spectrometry," *J. of Chromatography A,* vol. 1054, no. 1, pp. 351-357, 2004.

[40]   D. K. Alexiadou, N. C. Maragou, N. S. Thomaidis *et al.*, "Molecularly imprinted polymers for bisphenol A for HPLC and SPE from water and milk," *J. of Separation sci.,* vol. 31, no. 12, pp. 2272-2282, 2008.

[41]   Y. Hu, Y. Wang, Y. Hu *et al.*, "Liquid–liquid–solid microextraction based on membrane-protected molecularly imprinted polymer fiber for trace analysis of triazines in complex aqueous samples," *J. of Chromatography A,* vol. 1216, no. 47, pp. 8304-8311, 2009.

[42]   W. Yan, Y. Li, L. Zhao *et al.*, "Determination of estrogens and bisphenol A in bovine milk by automated on-line C 30 solid-phase extraction coupled with high-performance liquid chromatography–mass spectrometry," *J. of Chromatography A,* vol. 1216, no. 44, pp. 7539-7545, 2009.

[43]   L. Yang, C. Lan, H. Liu *et al.*, "Full automation of solid-phase microextraction/on-fiber derivatization for simultaneous determination of endocrine-disrupting chemicals and steroid hormones by gas chromatography–mass spectrometry," *Analytical and Bioanalytical Chemistry,* vol. 386, no. 2, pp. 391-397, 2006.

[44]   Y. S. Li, X. Y. Meng, Y. Zhou *et al.*, "Magnetic bead and gold nanoparticle probes based immunoassay for β-casein detection in bovine milk samples," *Biosensors and Bioelectronics,* vol. 66, pp. 559-564, 2015.

[45]   M. Wang, Y.-x. She, X.-w. Du *et al.*, "Determination of melamine using magnetic molecular imprinted polymers and high performance liquid chromatography," *Analytical Letters,* vol. 46, no. 1, pp. 120-130, 2013.

[46]   F. Conzuelo, V. R.-V. Montiel, S. Campuzano *et al.*, "Rapid screening of multiple antibiotic residues in milk using disposable amperometric magnetosensors," *Analytica Chimica Acta,* vol. 820, pp. 32-38, 2014.

[47]   D. Liu, Y. Huang, S. Wang *et al.*, "A modified lateral flow immunoassay for the detection of trace aflatoxin M1 based on immunomagnetic nanobeads with different antibody concentrations," *Food Control,* vol. 51, pp. 218-224, 2015.

[48]   H. Lan, N. Gan, D. Pan *et al.*, "An automated solid-phase microextraction method based on magnetic molecularly imprinted polymer as fiber coating for detection of trace estrogens in milk powder," *J. of Chromatography A,* vol. 1331, pp. 10-18, 2014.

[49]   S. P. Yazdankhah, A.-L. Hellemann, K. Rønningen *et al.*, "Rapid and sensitive detection of Staphylococcus species in milk by ELISA based on monodisperse magnetic particles," *Veterinary Microbiology,* vol. 62, no. 1, pp. 17-26, 1998.

[50]   S. Liébana, A. Lermo, S. Campoy *et al.*, "Rapid detection of Salmonella in milk by electrochemical magneto-immunosensing," *Biosensors and Bioelectronics,* vol. 25, no. 2, pp. 510-513, 2009.

[51]   C. M. Duarte, A. C. Fernandes, F. A. Cardoso *et al.*, "Magnetic counter for Group B streptococci detection in milk," *IEEE Trans. Magn.,* vol. 51, no. 1, pp. 1-4, 2015.

[52]   T. Ivanova, and T. Godjevargova, "Sensitive progesterone determination using a magnetic particle-based enzyme-linked immunosorbent assay," *Analytical Letters,* vol. 48, no. 5, pp. 843-860, 2015.

[53]   H. A. Robertson, and I. R. Sarda, "A very early pregnancy test for mammals: its application to the cow, ewe and sow," *The J. of endocrinology,* vol. 49, no. 3, pp. 407-419, 1971.

[54]   J. A. Darling, A. H. Laing, and R. A. Harkness, "A survey of the steroids in cows' milk," *J. of Endocrinology,* vol. 62, no. 2, pp. 291-297, 1974.

[55]   L. Siekmann, "Determination of steroid hormones by the use of isotope dilution-mass spectrometry: a definitive method in clinical chemistry," *J. of Steroid Biochemistry,* vol. 11, no. 1, pp. 117-123, 1979.

[56]   R. H. Purdy, C. K. Durocher, P. H. Moore *et al.*, "Analysis of metabolites of progesterone in bovine liver, kidney, kidney fat, and milk by high performance liquid chromatography," *J. of Steroid Biochemistry,* vol. 13, no. 11, pp. 1307-1315, 1980.

[57]   M. S. Díaz-Cruz, M. J. López de Alda, R. López *et al.*, "Determination of estrogens and progestogens by mass spectrometric techniques (GC/MS, LC/MS and LC/MS/MS)," *J. of Mass Spectrometry,* vol. 38, no. 9, pp. 917-923, 2003.

[58]   C. Munro, and G. Stabenfeldt, "Development of a microtitre plate enzyme immunoassay for the determination of progesterone," *J. of endocrinology,* vol. 101, no. 1, pp. 41-49, 1984.

[59]   R. L. Nebel, D. L. Altemose, T. W. Munkittrick *et al.*, "Comparisons of eight commercial on-farm milk progesterone tests," *Theriogenology,* vol. 31, no. 4, pp. 753-764, 1989.

[60]   J. V. Samsonova, A. P. Osipov, and S. E. Kondakov, "A new dried milk sampling technique and its application for progesterone detection in cows," *The Veterinary J.,* vol. 199, no. 3, pp. 471-472, 2014.

[61]   M. P. Laitinen, and M. Vuento, "Immunochromatographic assay for quantitation of milk progesterone," *Acta Chemica Scandinavica,* vol. 50, no. 2, pp. 141-145, 1996.

[62]   J. V. Samsonova, V. A. Safronova, and A. P. Osipov, "Pretreatment-free lateral flow enzyme immunoassay for progesterone detection in whole cows' milk," *Talanta,* vol. 132, pp. 685-689, 2015.

[63]   T. Asmussen, E. Kujina, E. Galvanoska *et al.*, "Herd Navigator or how to benefit from frequent measurements," *ICAR Technical Series*, no. 14, pp. 291-293, 2010.

[64]   M. Saint-Dizier, and S. Chastant-Maillard, "Towards an automated detection of oestrus in dairy cattle," *Reproduction in Domestic Animals,* vol. 47, no. 6, pp. 1056-1061, 2012.

[65]   N. C. Friggens, M. Bjerring, C. Ridder *et al.*, "Improved detection of reproductive status in dairy cows using milk progesterone measurements," *Reproduction in Domestic Animals,* vol. 43 Suppl 2, pp. 113-121, 2008.

[66]   R. K. Koelsch, D. J. Aneshansley, and W. R. Butler, "Milk progesterone sensor for application with dairy cattle," *J. of Agricultural Eng. Research,* vol. 58, no. 2-3, pp. 115-120, 1994.

[67]   E. H. Gillis, J. P. Gosling, J. M. Sreenan *et al.*, "Development and validation of a biosensor-based immunoassay for progesterone in bovine milk," *J. of Immunological Methods,* vol. 267, no. 2, pp. 131-138, 2002.

[68]   J. S. Mitchell, Y. Wu, C. J. Cook *et al.*, "Sensitivity enhancement of surface plasmon resonance biosensing of small molecules," *Analytical Biochemistry,* vol. 343, no. 1, pp. 125-135, 2005.

[69]   J. Yuan, R. Oliver, J. Li *et al.*, "Sensitivity enhancement of SPR assay of progesterone based on mixed self-assembled monolayers using nanogold particles," *Biosensors and Bioelectronics,* vol. 23, no. 1, pp. 144-148, 2007.

[70]   S. C. Huang, G. B. Lee, F. C. Chien *et al.*, "A microfluidic system with integrated molecular imprinting polymer films for surface plasmon resonance detection," *J. of Micromechanics and Microengineering,* vol. 16, no. 7, pp. 1251-1257, 2006.

[71]   D. Daems, J. Lu, F. Delport *et al.*, "Competitive inhibition assay for the detection of progesterone in dairy milk using a fiber optic SPR biosensor," *Analytica Chimica Acta,* vol. 950, pp. 1-6, 1/15/, 2017.

[72]   M. P. Kreuzer, R. McCarthy, M. Pravda *et al.*, "Development of electrochemical immunosensor for progesterone analysis in milk," *Analytical Letters,* vol. 37, no. 5, pp. 943-956, 2004.

[73]   R. M. Pemberton, J. P. Hart, and T. T. Mottram, "An electrochemical immunosensor for milk progesterone using a continuous flow system," *Biosensors and Bioelectronics,* vol. 16, no. 9-12, pp. 715-723, 2001.

[74]   J. P. Hart, R. M. Pemberton, R. Luxton *et al.*, "Studies towards a disposable screen-printed amperometric biosensor for progesterone," *Biosensors and Bioelectronics,* vol. 12, no. 11, pp. 1113-1121, 1997.

[75]   H. Y. Zhang, X. Y. Du, Q. Liu *et al.*, "Detection of progesterone in bovine milk using an electrochemical immunosensor," *International J. of Dairy Technology,* vol. 66, no. 4, pp. 461-467, 2013.

[76]   V. Carralero, A. Gonzalez-Cortes, P. Yanez-Sedeno *et al.*, "Nanostructured progesterone immunosensor using a tyrosinase-colloidal gold-graphite-Teflon biosensor as amperometric transducer," *Analytica Chimica Acta,* vol. 596, no. 1, pp. 86-91, 2007.

[77]   F. J. Arevalo, G. A. Messina, P. G. Molina *et al.*, "Determination of progesterone from bovine serum samples using a microfluidic immunosensor system," *Talanta,* vol. 80, no. 5, pp. 1986-1992, 2010.

[78]   K. Kaneko, and N. Takagi, "Accurate ultrasonographic prediction of progesterone concentrations greater than 1 ng/ml in Holstein lactating dairy cows," *Reproduction in Domestic Animals,* vol. 49, no. 6, pp. 985-988, 2014.

[79]   A. D. McNaught, and A. Wilkinson, *IUPAC Compendium of Chemical Terminology*. Oxford, UK: Generic, Blackwell Scientific Publications, 1997.

[80]   L. C. Clark, Jr., and C. Lyons, "Electrode systems for continuous monitoring in cardiovascular surgery," *Ann. of the New York Academy of Sciences,* vol. 102, pp. 29-45, 1962.

[81]   J. S. Mitchell, Y. Wu, C. J. Cook *et al.*, "Estrogen conjugation and antibody binding interactions in surface plasmon resonance biosensing," *Steroids,* vol. 71, no. 7, pp. 618-631, 2006.

[82]   G. S. Dombroski, "Enhancing sensitivity in the analysis of small biomolecules by surface plasmon resonance," Ph.D. dissertation, Dept. Chemistry, Massey Univ., Manawatu, New Zealand, 2012.

[83]   R. S. Yalow, and S. A. Berson, "Assay of plasma insulin in human subjects by immunological methods," *Nature,* vol. 184, no. 4699, pp. 1648-1649, 1959.

[84]   M. M. L. M. Vareiro, J. Liu, W. Knoll *et al.*, "Surface plasmon fluorescence measurements of human chorionic gonadotrophin: Role of antibody orientation in obtaining enhanced sensitivity and limit of detection," *Analytical Chemistry,* vol. 77, no. 8, pp. 2426-2431, 2005.

[85]   J. Zhang, Y. Sun, Q. Wu *et al.*, "A protein A modified Au-graphene oxide composite as an enhanced sensing platform for SPR-based immunoassay," *Analyst,* vol. 138, no. 23, pp. 7175-7181, 2013.

[86]   A. D. Ellington, and J. W. Szostak, "In vitro selection of RNA molecules that bind specific ligands," *Nature,* vol. 346, no. 6287, pp. 818-822, 1990.

[87]   D. E. Andrew, and W. S. Jack, "Selection in vitro of single-stranded DNA molecules that fold into specific ligand-binding structures," *Nature,* vol. 355, no. 6363, pp. 850, 1992.

[88] D. Mann, C. Reinemann, R. Stoltenburg *et al.*, "In vitro selection of DNA aptamers binding ethanolamine," *Biochemical and Biophysical Research Commun.,* vol. 338, no. 4, pp. 1928-1934, 2005.

[89] D. A. Daniels, H. Chen, B. J. Hicke *et al.*, "A tenascin-C aptamer identified by tumor cell SELEX: Systematic evolution of ligands by exponential enrichment," *Proc. of the National Academy of Sciences,* vol. 100, no. 26, pp. 15416-15421, 2003.

[90] S. Li, H. Xu, H. Ding *et al.*, "Identification of an aptamer targeting hnRNP A1 by tissue slide-based SELEX," *J. of Pathology,* vol. 218, no. 3, pp. 327-336, 2009.

[91] T. Hermann, and D. J. Patel, "Adaptive recognition by nucleic acid aptamers," *Science,* vol. 287, no. 5454, pp. 820-825, 2000.

[92] R. Stoltenburg, C. Reinemann, and B. Strehlitz, "SELEX-A (r)evolutionary method to generate high-affinity nucleic acid ligands," *Biomolecular Eng.,* vol. 24, no. 4, pp. 381-403, 2007.

[93] E. S. Gragoudas, A. P. Adamis, E. T. Cunningham Jr *et al.*, "Pegaptanib for neovascular age-related macular degeneration," *Amer. J. of Ophthalmology,* vol. 139, no. 4, pp. 761-762, 2005.

[94] R. Stoltenburg, C. Reinemann, and B. Strehlitz, "FluMag-SELEX as an advantageous method for DNA aptamer selection," *Analytical and Bioanalytical Chemistry,* vol. 383, no. 1, pp. 83-91, 2005.

[95] K. M. Song, S. Lee, and C. Ban, "Aptamers and their biological applications," *Sensors,* vol. 12, no. 1, pp. 612-631, 2012.

[96] A. D. Keefe, and S. T. Cload, "SELEX with modified nucleotides," *Current Opinion in Chemical Biology,* vol. 12, no. 4, pp. 448-456, 2008.

[97] G. Contreras Jiménez, S. Eissa, A. Ng *et al.*, "Aptamer-based label-free impedimetric biosensor for detection of progesterone," *Analytical Chemistry,* vol. 87, no. 2, pp. 1075-1082, 2015.

[98] G. B. John, A. Z. Miguel, P. C. Maria *et al.*, "Development of naturally selected and molecularly engineered intrachain and competitive FRET-aptamers and aptamer beacons," *Combinatorial Chemistry & High Throughput Screening,* vol. 14, no. 7, pp. 622-630, 2011.

[99] J. W. Guthrie, C. L. A. Hamula, H. Zhang *et al.*, "Assays for cytokines using aptamers," *Methods,* vol. 38, no. 4, pp. 324-330, 2006.

[100] G. Du, L. Wang, D. Zhang *et al.*, "Colorimetric aptasensor for progesterone detection based on surfactant-induced aggregation of gold nanoparticles," *Analytical Biochemistry,* vol. 514, pp. 2-7, 2016.

[101] G. Du, D. Zhang, B. Xia *et al.*, "A label-free colorimetric progesterone aptasensor based on the aggregation of gold nanoparticles," *Microchimica Acta,* vol. 183, no. 7, pp. 2251-2258, 2016.

[102] E. Zeidan, R. Shivaji, V. C. Henrich *et al.*, "Nano-SPRi aptasensor for the detection of progesterone in the buffer," *Scientific Reports,* vol. 6, pp. 26714, 2016.

[103] B. Strehlitz, C. Reinemann, S. Linkorn *et al.*, "Aptamers for pharmaceuticals and their application in environmental analytics," *Bioanalytical Reviews,* vol. 4, no. 1, pp. 1-30, 2012.

[104] H. A. Alhadrami, R. Chinnappan, S. Eissa *et al.*, "High affinity truncated DNA aptamers for the development of fluorescence based progesterone biosensors," *Analytical Biochemistry,* vol. 525, pp. 78-84, 2017.

[105] Y. Tan, X. Hu, M. Liu *et al.*, "Simultaneous visualization and quantitation of multiple steroid hormones based on signal-amplified biosensing with duplex molecular recognition," *Chemistry-A European J.,* vol. 23, no. 44, pp. 10683-10689, 2017.

[106] S. Nara, V. Tripathi, S. K. Chaube *et al.*, "Influence of hydrophobic and hydrophilic spacer-containing enzyme conjugates on functional parameters of steroid immunoassay," *Analytical Biochemistry,* vol. 373, no. 1, pp. 18-25, 2008.

[107] Y. Wu, J. Mitchell, C. Cook *et al.*, "Evaluation of progesterone-ovalbumin conjugates with different length linkers in enzyme-linked immunosorbant assay and surface plasmon resonance-based immunoassay," *Steroids,* vol. 67, no. 7, pp. 565-572, 2002.

[108] GE Healthcare. (2008) *Biacore sensor surface handbook* [Online]. Available: http://proteins.gelifesciences.com/~/media/protein-purification-ib/documents/handbooks/biacore_sensor_surface_handbook.pdf?la=en.

[109] S. Löfås, and B. Johnsson, "A novel hydrogel matrix on gold surfaces in surface plasmon resonance sensors for fast and efficient covalent immobilization of ligands," *J. of the Chemical Soc., Chemical Commun.*, no. 21, pp. 1526-1528, 1990.

[110] S. Baker, M. C. Petty, G. G. Roberts *et al.*, "The preparation and properties of stable metal-free phthalocyanine Langmuir-Blodgett films," *Thin Solid Films,* vol. 99, no. 1, pp. 53-59, 1983.

[111] R. G. Nuzzo, and D. L. Allara, "Adsorption of bifunctional organic disulfides on gold surfaces," *J. of the Amer. Chemical Soc.,* vol. 105, no. 13, pp. 4481-4483, 1983.

[112] T. Wink, S. J. Van Zuilen, A. Bult *et al.*, "Self-assembled monolayers for biosensors," *Analyst,* vol. 122, no. 4, pp. 43R-50R, 1997.

[113] N. Stephanopoulos, and M. B. Francis, "Choosing an effective protein bioconjugation strategy," *Nature Chemical Biology,* vol. 7, no. 12, pp. 876-884, 2011.

[114] G. T. Hermanson, *Bioconjugate techniques, 3*rd ed. Academic press, 2013.

[115] N. Tort, J.-P. Salvador, A. Aviñó *et al.*, "Synthesis of Steroid–Oligonucleotide Conjugates for a DNA Site-Encoded SPR Immunosensor," *Bioconjugate Chemistry,* vol. 23, no. 11, pp. 2183-2191, 2012.

[116] G. Houen, D. Olsen, P. Hansen *et al.*, "Preparation of bioconjugates by solid-phase conjugation to ion exchange matrix-adsorbed carrier proteins," *Bioconjugate Chemistry,* vol. 14, no. 1, pp. 75-79, 2003.

[117] B. Merrifield, "Solid phase synthesis," *Science,* vol. 232, no. 4748, pp. 341-347, 1986.

[118] B. Liedberg, I. Lundström, and E. Stenberg, "Principles of biosensing with an extended coupling matrix and surface plasmon resonance," *Sensors and Actuators B: Chemical,* vol. 11, no. 1, pp. 63-72, 1993.

[119] J. R. Lakowicz, *Principles of fluorescence spectroscopy, 3*rd ed. Springer Science & Business Media, 2007.

[120] R. Y. Tsien, "The green fluorescent protein," *Annu. Review of Biochemistry,* vol. 67, no. 1, pp. 509-544, 1998.

[121] I. L. Medintz, H. T. Uyeda, E. R. Goldman *et al.*, "Quantum dot bioconjugates for imaging, labelling and sensing," *Nature materials,* vol. 4, no. 6, pp. 435-446, 2005.

[122] N. Raghavachari, Y. P. Bao, G. Li *et al.*, "Reduction of autofluorescence on DNA microarrays and slide surfaces by treatment with sodium borohydride," *Analytical Biochemistry,* vol. 312, no. 2, pp. 101-105, 2003/01/15/, 2003.

[123] P. Ihalainen, and J. Peltonen, "Covalent immobilization of antibody fragments onto Langmuir-Schaefer binary monolayers chemisorbed on gold," *Langmuir,* vol. 18, no. 12, pp. 4953-4962, 2002.

[124] N. Soh, T. Tokuda, T. Watanabe *et al.*, "A surface plasmon resonance immunosensor for detecting a dioxin precursor using a gold binding polypeptide," *Talanta,* vol. 60, no. 4, pp. 733-745, 2003.

[125] J. S. Mitchell, "Spin-coated methacrylic acid copolymer thin films for covalent immobilization of small molecules on surface plasmon resonance substrates," *European Polymer J.,* vol. 47, no. 1, pp. 16-23, 2011.

[126] A. Murata, T. Ooya, and T. Takeuchi, "Simple immobilization of antibody in organic/inorganic hybrid thin films for immunosensing," *Biosensors and Bioelectronics,* vol. 43, pp. 45-49, 2013.

[127] S. Szunerits, N. Maalouli, E. Wijaya *et al.*, "Recent advances in the development of graphene-based surface plasmon resonance (SPR) interfaces," *Analytical and Bioanalytical Chemistry,* vol. 405, no. 5, pp. 1435-1443, 2013.

[128] C. Situ, A. R. Wylie, A. Douglas *et al.*, "Reduction of severe bovine serum associated matrix effects on carboxymethylated dextran coated biosensor surfaces," *Talanta,* vol. 76, no. 4, pp. 832-836, 2008.

[129] C.-C. Fong, M.-S. Wong, W.-F. Fong *et al.*, "Effect of hydrogel matrix on binding kinetics of protein–protein interactions on sensor surface," *Analytica Chimica Acta,* vol. 456, no. 2, pp. 201-208, 2002.

[130] E. Stenberg, B. Persson, H. Roos *et al.*, "Quantitative determination of surface concentration of protein with surface plasmon resonance using radiolabeled proteins," *J. of Colloid and Interface Sci.,* vol. 143, no. 2, pp. 513-526, 1991.

[131] J. Roncali, "Conjugated poly (thiophenes): synthesis, functionalization, and applications," *Chemical Reviews,* vol. 92, no. 4, pp. 711-738, 1992.

[132] A. A. Abdelwahab, M. S. Won, and Y. B. Shim, "Direct electrochemistry of cholesterol oxidase immobilized on a conducting polymer: application for a cholesterol biosensor," *Electroanalysis,* vol. 22, no. 1, pp. 21-25, 2010.

[133] K. Singh, M. A. Rahman, J. I. Son *et al.*, "An amperometric immunosensor for osteoproteogerin based on gold nanoparticles deposited conducting polymer," *Biosensors and Bioelectronics,* vol. 23, no. 11, pp. 1595-1601, 2008.

[134] F. Darain, S.-U. Park, and Y.-B. Shim, "Disposable amperometric immunosensor system for rabbit IgG using a conducting polymer modified screen-printed electrode," *Biosensors and Bioelectronics,* vol. 18, no. 5, pp. 773-780, 2003.

[135] T.-Y. Lee, and Y.-B. Shim, "Direct DNA hybridization detection based on the oligonucleotide-functionalized conductive polymer," *Analytical chemistry,* vol. 73, no. 22, pp. 5629-5632, 2001.

[136] Y.-T. Kong, M. Boopathi, and Y.-B. Shim, "Direct electrochemistry of horseradish peroxidase bonded on a conducting polymer modified glassy carbon electrode," *Biosensors and Bioelectronics,* vol. 19, no. 3, pp. 227-232, 2003.

[137] R. Pernites, R. Ponnapati, M. J. Felipe *et al.*, "Electropolymerization molecularly imprinted polymer (E-MIP) SPR sensing of drug molecules: Pre-polymerization complexed terthiophene and carbazole electroactive monomers," *Biosensors and Bioelectronics,* vol. 26, no. 5, pp. 2766-2771, 2011.

[138] M. Ocafrain, T. K. Tran, P. Blanchard *et al.*, "Electropolymerized Self‐assembled monolayers of a 3, 4‐ethylenedioxythiophene‐thiophene hybrid system," *Advanced Functional Materials,* vol. 18, no. 15, pp. 2163-2171, 2008.

[139] T. Matsuura, and Y. Shimoyama, "Growth kinetics of self-assembled monolayers of thiophene and terthiophene on Au (111): An infrared spectroscopic study," *The European Physical J. E,* vol. 7, no. 3, pp. 233-240, 2002.

[140] T. G. Edwardson, K. L. Lau, D. Bousmail *et al.*, "Transfer of molecular recognition information from DNA nanostructures to gold nanoparticles," *Nature chemistry,* vol. 8, no. 2, pp. 162-170, 2016.

[141] H. Zhao, I. I. Gorshkova, G. L. Fu *et al.*, "A comparison of binding surfaces for SPR biosensing using an antibody–antigen system and affinity distribution analysis," *Methods,* vol. 59, no. 3, pp. 328-335, 2013.

[142] J. Yuan, R. Oliver, M.-I. Aguilar *et al.*, "Surface plasmon resonance assay for chloramphenicol," *Analytical chemistry,* vol. 80, no. 21, pp. 8329-8333, 2008.

[143] S. A. Fernando, J. R. Sportsman, and G. S. Wilson, "Studies of the low dose 'hook'effect in a competitive homogeneous immunoassay," *J. of Immunological Methods,* vol. 151, no. 1, pp. 27-46, 1992.

[144] D. R. Shankaran, K. V. Gobi, and N. Miura, "Recent advancements in surface plasmon resonance immunosensors for detection of small molecules of biomedical, food and environmental interest," *Sensors and Actuators B: Chemical,* vol. 121, no. 1, pp. 158-177, 2007/01/30/, 2007.

[145] J. Kalia, and R. T. Raines, "Advances in bioconjugation," *Current Organic Chemistry,* vol. 14, no. 2, pp. 138, 2010.

[146] J. Mitchell, Y. Wu, C. Cook *et al.*, "Technical note: protein conjugate-based immunoassay of whole milk progesterone," *J. of Dairy Science,* vol. 87, no. 9, pp. 2864-2867, 2004.

[147] C. Bieniarz, M. Husain, G. Barnes *et al.*, "Extended length heterobifunctional coupling agents for protein conjugations," *Bioconjugate Chemistry,* vol. 7, no. 1, pp. 88-95, 1996.

[148] P. Luppa, C. Brückner, I. Schwab *et al.*, "7α-biotinylated testosterone derivatives as tracers for a competitive chemiluminescence immunoassay of testosterone in serum," *Clinical Chemistry,* vol. 43, no. 12, pp. 2345-2352, 1997.

[149] S. Martić, M. Labib, D. Freeman *et al.*, "Probing the role of the linker in ferrocene–ATP conjugates: Monitoring protein kinase catalyzed phosphorylations electrochemically," *Chemistry-A European Journal,* vol. 17, no. 24, pp. 6744-6752, 2011.

[150] S. J. Attwood, A. Simpson, R. Stone *et al.*, "A simple bioconjugate attachment protocol for use in single molecule force spectroscopy experiments based on mixed self-assembled monolayers," *International J. of Molecular Sciences,* vol. 13, no. 10, pp. 13521-13541, 2012.

[151] X. Gao, Y. Cui, R. M. Levenson *et al.*, "In vivo cancer targeting and imaging with semiconductor quantum dots," *Nature Biotechnology,* vol. 22, no. 8, pp. 969-976, 2004.

[152] C. Boozer, J. Ladd, S. Chen *et al.*, "DNA directed protein immobilization on mixed ssDNA/oligo (ethylene glycol) self-assembled monolayers for sensitive biosensors," *Analytical Chemistry,* vol. 76, no. 23, pp. 6967-6972, 2004.

[153] L. Li, S. Chen, J. Zheng *et al.*, "Protein adsorption on oligo (ethylene glycol)-terminated alkanethiolate self-assembled monolayers: the molecular basis for nonfouling behavior," *J. of Physical Chemistry B,* vol. 109, no. 7, pp. 2934-2941, 2005.

[154] A. Warnecke, and F. Kratz, "Maleimide-oligo (ethylene glycol) derivatives of camptothecin as albumin-binding prodrugs: synthesis and antitumor efficacy," *Bioconjugate Chemistry,* vol. 14, no. 2, pp. 377-387, 2003.

[155] G. Liu, and J. J. Gooding, "An interface comprising molecular wires and poly (ethylene glycol) spacer units self-assembled on carbon electrodes for studies of protein electrochemistry," *Langmuir,* vol. 22, no. 17, pp. 7421-7430, 2006.

[156] O. McCarthy, and H. Singh, "Physico-chemical properties of milk," *Advanced Dairy Chemistry*, vol. 3, pp. 691-758, 2009.

[157] Y. Wang, A. Partridge, and Y. Wu, "Comparison of a carboxylated terthiophene surface with carboxymethylated dextran layer for SPR detection of progesterone," *Analytical Biochemistry*, vol. 508, pp. 46-49, 2016.

[158] S. D. Soelberg, T. Chinowsky, G. Geiss *et al.*, "A portable surface plasmon resonance sensor system for real-time monitoring of small to large analytes," *Journal of industrial microbiology and biotechnology,* vol. 32, no. 11-12, pp. 669-674, 2005.

[159] E. Mauriz, A. Calle, A. Montoya *et al.*, "Determination of environmental organic pollutants with a portable optical immunosensor," *Talanta,* vol. 69, no. 2, pp. 359-364, 2006.

[160] B. Feltis, B. Sexton, F. Glenn *et al.*, "A hand-held surface plasmon resonance biosensor for the detection of ricin and other biological agents," *Biosensors and Bioelectronics,* vol. 23, no. 7, pp. 1131-1136, 2008.

[161] H. Kawazumi, K. V. Gobi, K. Ogino *et al.*, "Compact surface plasmon resonance (SPR) immunosensor using multichannel for simultaneous detection of small molecule compounds," *Sensors and Actuators B: Chemical,* vol. 108, no. 1-2, pp. 791-796, 2005.

[162] S. J. Kim, K. V. Gobi, H. Iwasaka *et al.*, "Novel miniature SPR immunosensor equipped with all-in-one multi-microchannel sensor chip for detecting low-molecular-weight analytes," *Biosensors and Bioelectronics,* vol. 23, no. 5, pp. 701-707, 2007.

[163] B. Lu, M. R. Smyth, and R. O'Kennedy, "Tutorial review. Oriented immobilization of antibodies and its applications in immunoassays and immunosensors," *Analyst,* vol. 121, no. 3, pp. 29R-32R, 1996.

[164] L. Tang, J. Casas, and M. Venkataramasubramani, "Magnetic nanoparticle mediated enhancement of localized surface plasmon resonance for ultrasensitive bioanalytical assay in human blood plasma," *Analytical Chemistry,* vol. 85, no. 3, pp. 1431-1439, 2013.

[165] J. Wang, A. Munir, Z. Zhu *et al.*, "Magnetic nanoparticle enhanced surface plasmon resonance sensing and its application for the ultrasensitive detection of magnetic nanoparticle-enriched small molecules," *Analytical Chemistry,* vol. 82, no. 16, pp. 6782-6789, 2010.

[166] K. Saha, F. Bender, and E. Gizeli, "Comparative study of IgG binding to proteins G and A: nonequilibrium kinetic and binding constant determination with the acoustic waveguide device," *Analytical chemistry,* vol. 75, no. 4, pp. 835-842, 2003.

[167] W. Choe, T. A. Durgannavar, and S. J. Chung, "Fc-binding ligands of immunoglobulin G: an overview of high affinity proteins and peptides," *Materials,* vol. 9, no. 12, pp. 994, 2016.

[168] Abcam. *KD value: a quantitative measurement of antibody affinity* [Online]. Available: http://www.abcam.com/primary-antibodies/kd-value-a quantitative measurement of antibody affinity.

[169] N. M. Green, "Avidin and streptavidin," *Methods in enzymology,* vol. 184, pp. 51-67, 1990.

[170] G. T. Hermanson, *Bioconjugate Techniques: Third Edition*, 2013.

[171] H. Bagçi, F. Kohen, U. Kusçuoglu *et al.*, "Monoclonal anti-biotin antibodies simulate avidin m the recognition of biotin," *FEBS Letters,* vol. 322, no. 1, pp. 47-50, 1993.

[172] K. K. Caswell, J. N. Wilson, U. H. F. Bunz *et al.*, "Preferential end-to-end assembly of gold nanorods by biotin−streptavidin connectors," *J. of the Amer. Chemical Soc.,* vol. 125, no. 46, pp. 13914-13915, 2003.

[173] C. O. Parker, and I. E. Tothill, "Development of an electrochemical immunosensor for aflatoxin M 1 in milk with focus on matrix interference," *Biosensors and Bioelectronics,* vol. 24, no. 8, pp. 2452-2457, 2009.

[174] D. L. Brandon, and L. M. Adams, "Milk matrix effects on antibody binding analyzed by enzyme-linked immunosorbent assay and biolayer interferometry," *J. of Agricultural and Food Chemistry,* vol. 63, no. 13, pp. 3593-3598, 2015.

[175] R. V. Vogt, D. L. Phillips, L. Omar Henderson *et al.*, "Quantitative differences among various proteins as blocking agents for ELISA microtiter plates," *J. of Immunological Methods,* vol. 101, no. 1, pp. 43-50, 1987.

[176] M. Cassandro, A. Comin, M. Ojala *et al.*, "Genetic Parameters of Milk Coagulation Properties and Their Relationships with Milk Yield and Quality Traits in Italian Holstein Cows," *J. of Dairy Sci.,* vol. 91, no. 1, pp. 371-376, 2008.

[177]   F. Roca, and R. Gonzalez, "Effect of dietary and animal factors on milk fatty acids composition of grazing dairy cows: a review," *Iranian J. of Applied Animal Sci.,* vol. 2, no. 2, pp. 97-109, 2012.

[178]   A. Waldmann, E. Ropstad, K. Landsverk *et al.*, "Level and distribution of progesterone in bovine milk in relation to storage in the mammary gland," *Animal Reproduction Sci.,* vol. 56, no. 2, pp. 79-91, 1999.

[179]   G. Walker, F. Dunshea, and P. Doyle, "Effects of nutrition and management on the production and composition of milk fat and protein: a review," *Australian J. of Agricultural Research,* vol. 55, no. 10, pp. 1009-1028, 2004.

[180]   S. P. Oliver, K. J. Boor, S. C. Murphy *et al.*, "Food safety hazards associated with consumption of raw milk," *Foodborne Pathogens and Disease,* vol. 6, no. 7, pp. 793-806, 2009.

[181]   O. Ginther, L. Nuti, M. Garcia *et al.*, "Factors affecting progesterone concentration in cow's milk and dairy products," *J. of Animal Sci.,* vol. 42, no. 1, pp. 155-159, 1976.

[182]   R. Heap, A. Henville, and J. Linzell, "Metabolic clearance rate, production rate, and mammary uptake and metabolism of progesterone in cows," *J. of Endocrinology,* vol. 66, no. 2, pp. 239-247, 1975.

[183]   S. J. Lee, and J. W. Sherbon, "Chemical changes in bovine milk fat globule membrane caused by heat treatment and homogenization of whole milk," *J. of Dairy Research,* vol. 69, no. 4, pp. 555-567, 2002.

[184]   J. C. Kent, P. G. Arthur, and P. E. Hartmann, "Partitioning of calcium in human milk after freezing and thawing," *Dairy Sci. Technology,* vol. 89, no. 2, pp. 187-191, 2009.

[185]   K. Takahashi, K. Mizuno, and K. Itabashi, "The freeze–thaw process and long intervals after fortification denature human milk fat globules," *Amer. J. of Perinatology,* vol. 29, no. 04, pp. 283-288, 2012.

[186]   H. Eissa, R. Nachreiner, and K. Refsal, "Effects of sample handling temperatures on bovine skim milk progesterone concentrations," *Theriogenology,* vol. 43, no. 5, pp. 893-898, 1995.

[187]   R. Nachreiner, S. Oschmann, L. Edqvist *et al.*, "Factors affecting skim milk progesterone assay results," *Amer. J. of Veterinary Research,* vol. 53, no. 7, pp. 1085-1089, 1992.

[188]   P. Colas, B. Cohen, T. Jessen *et al.*, "Genetic selection of peptide aptamers that recognize and inhibit cyclin-dependent kinase 2," *Nature,* vol. 380, no. 6574, pp. 548, 1996.

[189]   B. Klevenz, K. Butz, and F. Hoppe-Seyler, "Peptide aptamers: exchange of the thioredoxin-A scaffold by alternative platform proteins and its influence on target protein binding," *Cellular and Molecular Life Sciences,* vol. 59, no. 11, pp. 1993-1998, 2002.

[190]   D. H. Bunka, and P. G. Stockley, "Aptamers come of age-at last," *Nature reviews. Microbiology,* vol. 4, no. 8, pp. 588, 2006.

[191]   M. Darmostuk, S. Rimpelova, H. Gbelcova *et al.*, "Current approaches in SELEX: an update to aptamer selection technology," *Biotechnology Advances,* vol. 33, no. 6, pp. 1141-1161, 2015.

[192]   S. D. Jayasena, "Aptamers: an emerging class of molecules that rival antibodies in diagnostics," *Clinical Chemistry,* vol. 45, no. 9, pp. 1628-1650, 1999.

[193]   R. Stoltenburg, C. Reinemann, and B. Strehlitz, "SELEX--a (r)evolutionary method to generate high-affinity nucleic acid ligands," *Biomolecular engineering,* vol. 24, no. 4, pp. 381-403, 2007.

[194]   H. Alhadrami, R. Chinnappan, S. Eissa *et al.*, "High affinity truncated DNA aptamers for the development of fluorescence based progesterone biosensors," *Analytical Biochemistry,* vol. 525, pp. 78-84, 2017.

[195]   V. Skouridou, T. Schubert, A. S. Bashammakh *et al.*, "Aptatope mapping of the binding site of a progesterone aptamer on the steroid ring structure," *Analytical Biochemistry,* vol. 531, pp. 8-11, 2017.

[196]   W. He, M.-A. Elizondo-Riojas, X. Li *et al.*, "X-Aptamers: a bead-based selection method for random incorporation of drug-like moieties onto next-generation aptamers for enhanced binding," *Biochemistry,* vol. 51, no. 42, pp. 8321-8323, 2012.

[197]   F. Pfeiffer, and G. Mayer, "Selection and biosensor application of aptamers for small molecules," *Frontiers in Chemistry,* vol. 4, pp. 25, 2016.

[198]   M. McKeague, A. De Girolamo, S. Valenzano *et al.*, "Comprehensive analytical comparison of strategies used for small molecule aptamer evaluation," *Analytical Chemistry,* vol. 87, no. 17, pp. 8608-8612, 2015.

[199]   G. Penner. (2015) *FRELEX: a new platform for aptamer discovery* [Online]. Available: https://www.linkedin.com/pulse/frelex-new-platform-aptamer-discovery-gregory-penner/.

[200] N. R. Markham, and M. Zuker, "DINAMelt web server for nucleic acid melting prediction," *Nucleic Acids Research,* vol. 33, no. suppl_2, pp. W577-W581, 2005.

[201] K. Vanschoenbeek, J. Vanbrabant, B. Hosseinkhani *et al.*, "Aptamers targeting different functional groups of 17β-estradiol," *The J. of Steroid Biochemistry and Molecular Biology,* vol. 147, pp. 10-16, 2015.

[202] M. Kimoto, R. Yamashige, K.-i. Matsunaga *et al.*, "Generation of high-affinity DNA aptamers using an expanded genetic alphabet," *Nature Biotechnology,* vol. 31, no. 5, pp. 453-457, 2013.

[203] R. Owczarzy, B. G. Moreira, Y. You *et al.*, "Predicting stability of DNA duplexes in solutions containing magnesium and monovalent cations," *Biochemistry,* vol. 47, no. 19, pp. 5336-5353, 2008.

[204] T. Šprinder, H. Šípová, H. Vaisocherová *et al.*, "Shielding effect of monovalent and divalent cations on solid-phase DNA hybridization: surface plasmon resonance biosensor study," *Nucleic Acids Research,* vol. 38, no. 20, pp. 7343-7351, 2010.

[205] A. W. Peterson, R. J. Heaton, and R. M. Georgiadis, "The effect of surface probe density on DNA hybridization," *Nucleic Acids Research,* vol. 29, no. 24, pp. 5163-5168, 2001.

[206] F. Yu, D. Yao, and W. Knoll, "Oligonucleotide hybridization studied by a surface plasmon diffraction sensor (SPDS)," *Nucleic Acids Research,* vol. 32, no. 9, pp. e75-e75, 2004.

[207] A. L. Haskins Jr, "Solubility of progesterone in sater and in saline," *Proc. of the Soc. for Experimental Biology and Medicine,* vol. 70, no. 2, pp. 228-229, 1949.

[208] A. T. Marttila, O. H. Laitinen, K. J. Airenne *et al.*, "Recombinant NeutraLite Avidin: a non‐glycosylated, acidic mutant of chicken avidin that exhibits high affinity for biotin and low non‐specific binding properties," *FEBS Letters,* vol. 467, no. 1, pp. 31-36, 2000.

[209] M. Svobodová, V. Skouridou, M. L. Botero *et al.*, "The characterization and validation of 17β-estradiol binding aptamers," *The J. of Steroid Biochemistry and Molecular Biology,* vol. 167, pp. 14-22, 2017.

[210] B. Piro, S. Shi, S. Reisberg *et al.*, "Comparison of electrochemical immunosensors and aptasensors for detection of small organic molecules in environment, food safety, clinical and public security," *Biosensors,* vol. 6, no. 1, pp. 7, 2016.

[211] A. Porchetta, A. Vallée-Bélisle, K. W. Plaxco *et al.*, "Using distal-site mutations and allosteric inhibition to tune, extend, and narrow the useful dynamic range of aptamer-based sensors," *J. of the Amer. Chemical Soc.,* vol. 134, no. 51, pp. 20601-20604, 2012.

[212] J. D. Munzar, A. Ng, M. Corrado *et al.*, "Complementary oligonucleotides regulate induced fit ligand binding in duplexed aptamers," *Chemical Sci.,* vol. 8, no. 3, pp. 2251-2256, 2017.

[213] J. Monod, J. Wyman, and J.-P. Changeux, "On the nature of allosteric transitions: a plausible model," *J. of Molecular Biology,* vol. 12, no. 1, pp. 88-118, 1965.

[214] D. E. Koshland, G. Némethy, and D. Filmer, "Comparison of experimental binding data and theoretical models in proteins containing subunits," *Biochemistry,* vol. 5, no. 1, pp. 365-385, 1966.

[215] O. Kikin, L. D'Antonio, and P. S. Bagga, "QGRS mapper: a web-based server for predicting G-quadruplexes in nucleotide sequences," *Nucleic Acids Research,* vol. 34, no. suppl_2, pp. W676-W682, 2006.

[216] J. J. Li, X. Fang, and W. Tan, "Molecular aptamer beacons for real-time protein recognition," *Biochemical and biophysical research communications,* vol. 292, no. 1, pp. 31-40, 2002.

[217] I. Nakamura, A.-C. Shi, R. Nutiu *et al.*, "Kinetics of signaling-DNA-aptamer–ATP binding," *Physical Review E,* vol. 79, no. 3, pp. 031906, 2009.

[218] K. Han, Z. Liang, and N. Zhou, "Design strategies for aptamer-based biosensors," *Sensors,* vol. 10, no. 5, pp. 4541, 2010.

[219] Y. Chushak, and M. O. Stone, "In silico selection of RNA aptamers," *Nucleic Acids Research,* vol. 37, no. 12, pp. e87-e87, 2009.

[220] J. Flinders, S. C. DeFina, D. M. Brackett *et al.*, "Recognition of planar and nonplanar ligands in the malachite green–RNA aptamer complex," *ChemBioChem,* vol. 5, no. 1, pp. 62-72, 2004.

[221] G. R. Zimmermann, C. L. Wick, T. P. Shields *et al.*, "Molecular interactions and metal binding in the theophylline-binding core of an RNA aptamer," *RNA,* vol. 6, no. 5, pp. 659-667, 2000.

[222] M. Sassanfar, and J. W. Szostak, "An RNA motif that binds ATP," *Nature,* vol. 364, no. 6437, pp. 550-553, 1993.

[223] M. N. Stojanovic, P. de Prada, and D. W. Landry, "Fluorescent sensors based on aptamer self-assembly," *J. of the Amer. Chemical Soc.,* vol. 122, no. 46, pp. 11547-11548, 2000.

[224] D. E. Huizenga, and J. W. Szostak, "A DNA aptamer that binds adenosine and ATP," *Biochemistry,* vol. 34, no. 2, pp. 656-665, 1995.

[225] Y. Jiang, C. Zhu, L. Ling *et al.*, "Specific aptamer− protein interaction studied by atomic force microscopy," *Analytical Chemistry,* vol. 75, no. 9, pp. 2112-2116, 2003.

[226] X. Fang, Z. Cao, T. Beck *et al.*, "Molecular aptamer for real-time oncoprotein platelet-derived growth factor monitoring by fluorescence anisotropy," *Analytical Chemistry,* vol. 73, no. 23, pp. 5752-5757, 2001.

[227] X. Fang, J. J. Li, and W. Tan, "Using molecular beacons to probe molecular interactions between lactate dehydrogenase and single-stranded DNA," *Analytical Chemistry,* vol. 72, no. 14, pp. 3280-3285, 2000.

THE UNIVERSITY OF AUCKLAND
SCHOOL OF GRADUATE STUDIES

Co-Authorship Form

This form is to accompany the submission of any PhD that contains published or unpublished co-authored work. **Please include one copy of this form for each co-authored work**. Completed forms should be included in all copies of your thesis submitted for examination and library deposit (including digital deposit), following your thesis Acknowledgements. Co-authored works may be included in a thesis if the candidate has written all or the majority of the text and had their contribution confirmed by all co-authors as not less than 65%.

Please indicate the chapter/section/pages of this thesis that are extracted from a co-authored work and give the title and publication details or details of submission of the co-authored work.	
Part of 'Chapter 2-investigating a carboxylated terthiophene surface for surface plasmon resonance detection of progesterone' was published in Analytical Biochemistry, vol. 508, pp. 46-49, Sep 2016.	
Nature of contribution by PhD candidate	Design and carrying out research, data anaylsis and writing
Extent of contribution by PhD candidate (%)	70%

CO-AUTHORS

Name	Nature of Contribution
Dr. Ashton Partridge	PI, funding, strategy, methodology, polishing
Dr. Yinqiu Wu	AI, strategy, methodology, guidance, editing

Certification by Co-Authors

The undersigned hereby certify that:
- the above statement correctly reflects the nature and extent of the PhD candidate's contribution to this work, and the nature of the contribution of each of the co-authors; and
- that the candidate wrote all or the majority of the text.

Name	Signature	Date
Dr. Ashton Partridge	*[signature]*	25/10/2017
Dr. Yinqiu Wu	*[signature]*	25/10/2017

Last updated: 19 October 2015

THE UNIVERSITY OF AUCKLAND
SCHOOL OF GRADUATE STUDIES

Co-Authorship Form

This form is to accompany the submission of any PhD that contains published or unpublished co-authored work. **Please include one copy of this form for each co-authored work.** Completed forms should be included in all copies of your thesis submitted for examination and library deposit (including digital deposit), following your thesis Acknowledgements. Co-authored works may be included in a thesis if the candidate has written all or the majority of the text and had their contribution confirmed by all co-authors as not less than 65%.

Please indicate the chapter/section/pages of this thesis that are extracted from a co-authored work and give the title and publication details or details of submission of the co-authored work.

Part of 'Chapter 2-investigating a carboxylated terthiophene surface for surface plasmon resonance detection of progesterone' was presented as a poster at the conference of Biosensor 2016 in Gothenburge, Sweden in May 2016.

Nature of contribution by PhD candidate	Carrying out research, data anaylsis and poster design
Extent of contribution by PhD candidate (%)	70%

CO-AUTHORS

Name	Nature of Contribution
Dr. Ashton Partridge	PI, funding, strategy, polishing
Dr. Yinqiu Wu	AI, strategy, guidance, editing

Certification by Co-Authors

The undersigned hereby certify that:
- ❖ the above statement correctly reflects the nature and extent of the PhD candidate's contribution to this work, and the nature of the contribution of each of the co-authors; and
- ❖ that the candidate wrote all or the majority of the text.

Name	Signature	Date
Dr. Ashton Partridge		25/10/2017
Dr. Yinqiu Wu		25/10/2017

Last updated: 19 October 2015

THE UNIVERSITY OF AUCKLAND
SCHOOL OF GRADUATE STUDIES
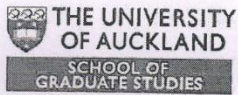
Co-Authorship Form

Graduate Centre
The ClockTower – East Wing
22 Princes Street, Auckland
Phone: +64 9 373 7599 ext 81321
Fax: +64 9 373 7610
Email: postgraduate@auckland.ac.nz
www.postgrad.auckland.ac.nz

This form is to accompany the submission of any PhD that contains published or unpublished co-authored work. **Please include one copy of this form for each co-authored work**. Completed forms should be included in all copies of your thesis submitted for examination and library deposit (including digital deposit), following your thesis Acknowledgements. Co-authored works may be included in a thesis if the candidate has written all or the majority of the text and had their contribution confirmed by all co-authors as not less than 65%.

Please indicate the chapter/section/pages of this thesis that are extracted from a co-authored work and give the title and publication details or details of submission of the co-authored work.

Part of 'Chapter 3-Functionalizing the sensor surfaces for progesterone detection by surface in situ synthesizing progesterone and ovalbumin conjugates' was published in Analytical Biochemistry (2017), doi: 10.1016/j.ab.2017.10.017.

Nature of contribution by PhD candidate	Design and carrying out research, design, data anaylsis and writing
Extent of contribution by PhD candidate (%)	70%

CO-AUTHORS

Name	Nature of Contribution
Dr. Ashton Partridge	PI, funding, strategy, polishing
Dr. Yinqiu Wu	AI, strategy, methodology, design, guidance, editing

Certification by Co-Authors

The undersigned hereby certify that:
- the above statement correctly reflects the nature and extent of the PhD candidate's contribution to this work, and the nature of the contribution of each of the co-authors; and
- that the candidate wrote all or the majority of the text.

Name	Signature	Date
Dr. Ashton Partridge	*[signature]*	25/10/2017
Dr. Yinqiu Wu	*[signature]*	25/10/2017

Last updated: 19 October 2015

155

THE UNIVERSITY OF AUCKLAND
SCHOOL OF GRADUATE STUDIES

Co-Authorship Form

This form is to accompany the submission of any PhD that contains published or unpublished co-authored work. **Please include one copy of this form for each co-authored work**. Completed forms should be included in all copies of your thesis submitted for examination and library deposit (including digital deposit), following your thesis Acknowledgements. Co-authored works may be included in a thesis if the candidate has written all or the majority of the text and had their contribution confirmed by all co-authors as not less than 65%.

Please indicate the chapter/section/pages of this thesis that are extracted from a co-authored work and give the title and publication details or details of submission of the co-authored work.

Part of 'Chapter 4-Developing antibody and magnetic bead conjugates based surface plasmon resonance assays for detecting milk progesterone' is in preparation for publication.

Nature of contribution by PhD candidate	Desgin, carrying out research, data anaylsis and writing
Extent of contribution by PhD candidate (%)	70%

CO-AUTHORS

Name	Nature of Contribution
Dr. Ashton Partridge	PI, funding, strategy, guidance, polishing
Dr. Yinqiu Wu	AI, strategy, methodology, guidance, editing

Certification by Co-Authors

The undersigned hereby certify that:
- ❖ the above statement correctly reflects the nature and extent of the PhD candidate's contribution to this work, and the nature of the contribution of each of the co-authors; and
- ❖ that the candidate wrote all or the majority of the text.

Name	Signature	Date
Dr. Ashton Partridge	*(signed)*	25/10/2017
Dr. Yinqiu Wu	*(signed)*	25/10/2017